Report

2005 Annual WAMIT Consortium Meeting

October 18-19, 2005

Woods Hole, Massachusetts

Agenda for 2005 Annual WAMIT Meeting
Room 310, Marine Resource Center, Swope Center, Woods Hole, MA

October 18:

9:00AM: Welcome

9:20AM: " Recent updates and preview of WAMIT V6.3"
C.-H. Lee, WAMIT

10:00AM: "Evaluation of quadratic forces using control surfaces"
C.-H. Lee, WAMIT

10:40AM: Break

11:00AM: "Effect of tanks or springs on mean drift forces"
J. N. Newman., WAMIT

11:30AM: "Notes on the use of artificial lid for the analysis of two-bodies interaction"
C.-H. Lee, WAMIT

12:00PM: Lunch

1:30PM: "Computational aspects of side by side offloading in waves"
P. Teigen, Statoil and J.M. Niedzwecki, OTRC

2:15PM: "Modelling problems related to the Snoehvit in-docking operation"
P. Teigen, Statoil

3:00 PM: Break

3:30 PM: "Summing linear and 2nd-order wave elevations using FS_ELV"
C.-H. Lee, WAMIT

5:30PM: Mixer and Dinner

October 19:

9:00AM: Technical discussion

10:30AM: Break

10:50AM: Business meeting

12:00AM: Lunch

Contents

Recent updates and preview of WAMIT V6.3

Updates in V6.3

- An option to accurate evaluation of the mean drift forces using control surface is added
- Any quadrants/halves of body geometry can be input when body has symmetric planes
- Thin flat elements can be specified at x=0 or y=0 plane without loosing symmetry.

Mean drift force by control surface

- The mean drift force/moment are evaluated by evaluating momentum flux on the control surface.

  The method provides as accurate results as far field momentum drift force (IOPTN.8). Thus the method can replace the pressure integration (IOPTN.9) when the latter must be used such as in the multiple body interaction.

  The control surface, CSF, should be specified as an input in the similar manner as GDF.

- Control surface encloses the body. It includes free surface portion if the vertical components is of interest

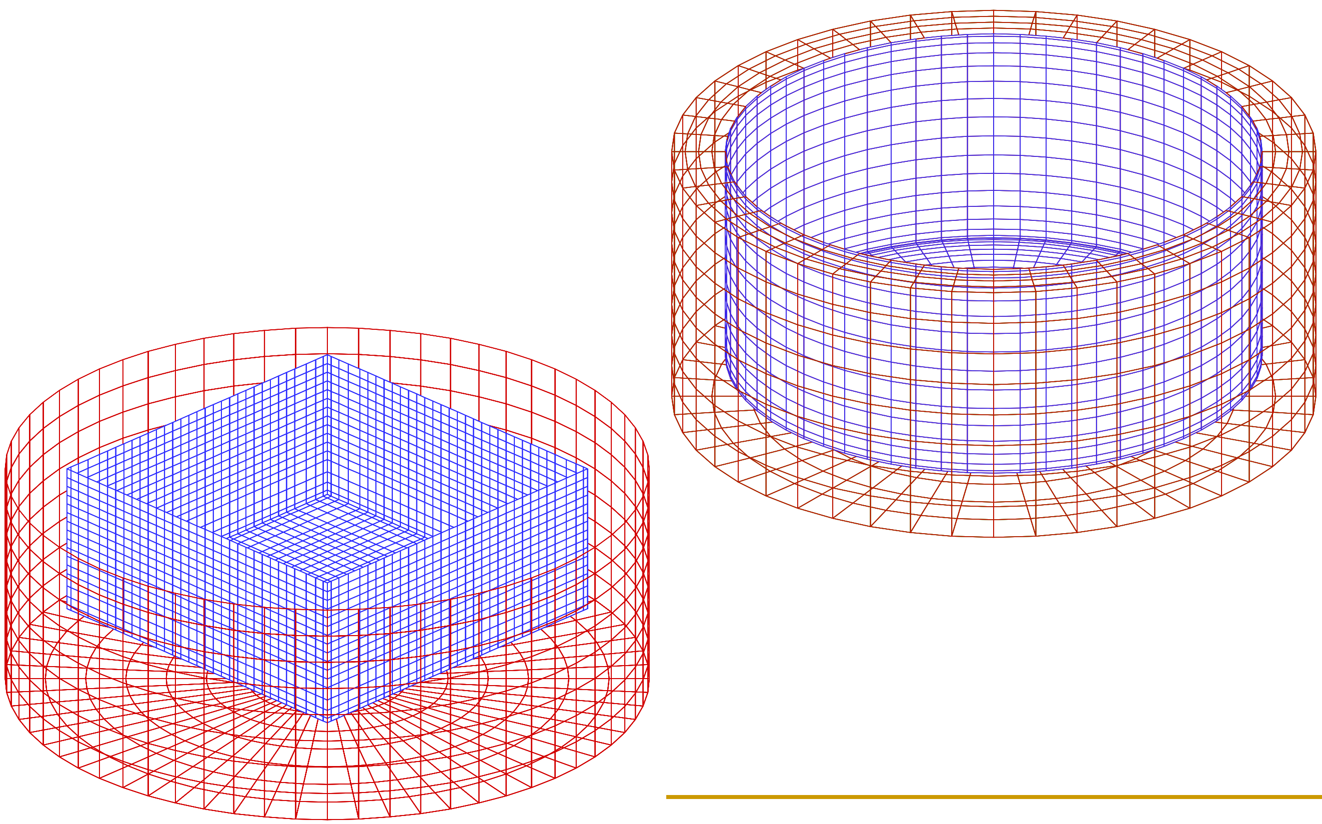

- It is simple to create CSF as all available GDF input option can be used for CSF.

Low-order method: Flat panels

Higher-order method: Flat panels

B-splines

MultiSurf patches

Exact geometry

*If vertical component is not of interest and WAMIT may generate CSF internally for most arrangements.

- The pressure (or momentum flux) on CS are integrated in piecewise manner for low-order method or based on Gauss-quadrature in higher-order method
- The accuracy of the integration over control surface is determined by the number of panels in the low-order
- In higher-order method, it is determined by a parameter specifying panel size in each CSF
- Additional input in configuration file (CFG)

  ICTRSURF=0 Pressure Integration

  ICTRSURF=1 Control Surface

- Contribution from the tanks can be evaluated as current pressure integration and added to the exterior forces

- Fluid pressure and velocity are evaluated at large number of field points on the control surface and the run time of Force module increases.

  In practice, this would be compensated by reduced run time of Poten module because the method is less sensitive to the discretization of the body surface than the pressure integration.

All quadrants/halves of body geometry can be input when body has symmetric planes

In V6.2, when ISX=1 or ISY=1, only x>0 or y>0 of body geometry should be specified in GDF

In V6.3, any one of the quadrant or half can be specified in GDF

Thin flat elements can be specified at x=0 or y=0 plane without loosing symmetry

- In V6.2, when thin flat elements are on the planes of symmetry both sides of the symmetric plane must be specified GDF.

  For example, for a ship with bilge keel along the centerline, the entire hull should be in GDF.

- In V6.3, a half of the ship + thin element can be specified in GDF and the symmetry of hull itself is exploited.

Works on the 2^{nd}-order module

- Investigation has been made to find an improvement in efficiency of proposed approach to storing Rankine part of subdivision

- Following numbers are required on the free surface
  around bottom mounted cylinder due to the subdivision
  4x 4   panels 120k free surface points
  2 x 2 panels 55k
  1 x 1 panels 15k
  (Free surface forcing are evaluated at these points.)

- Sorting the same points within some tolerance reduces numbers.
  Within1E-5 the number reduced by an order of magnitude

- The computation for the velocity potential on the waterline reveals inaccuracy of the potential near the waterline due to current integration scheme in V6.1S, although the global quantities are more accurate than the low order output, illustrating more accurate approach is required in the higher-order method.

  The result in the attached paper by Molin et al. is made using low order option.

Geometry considered in Molin et al.

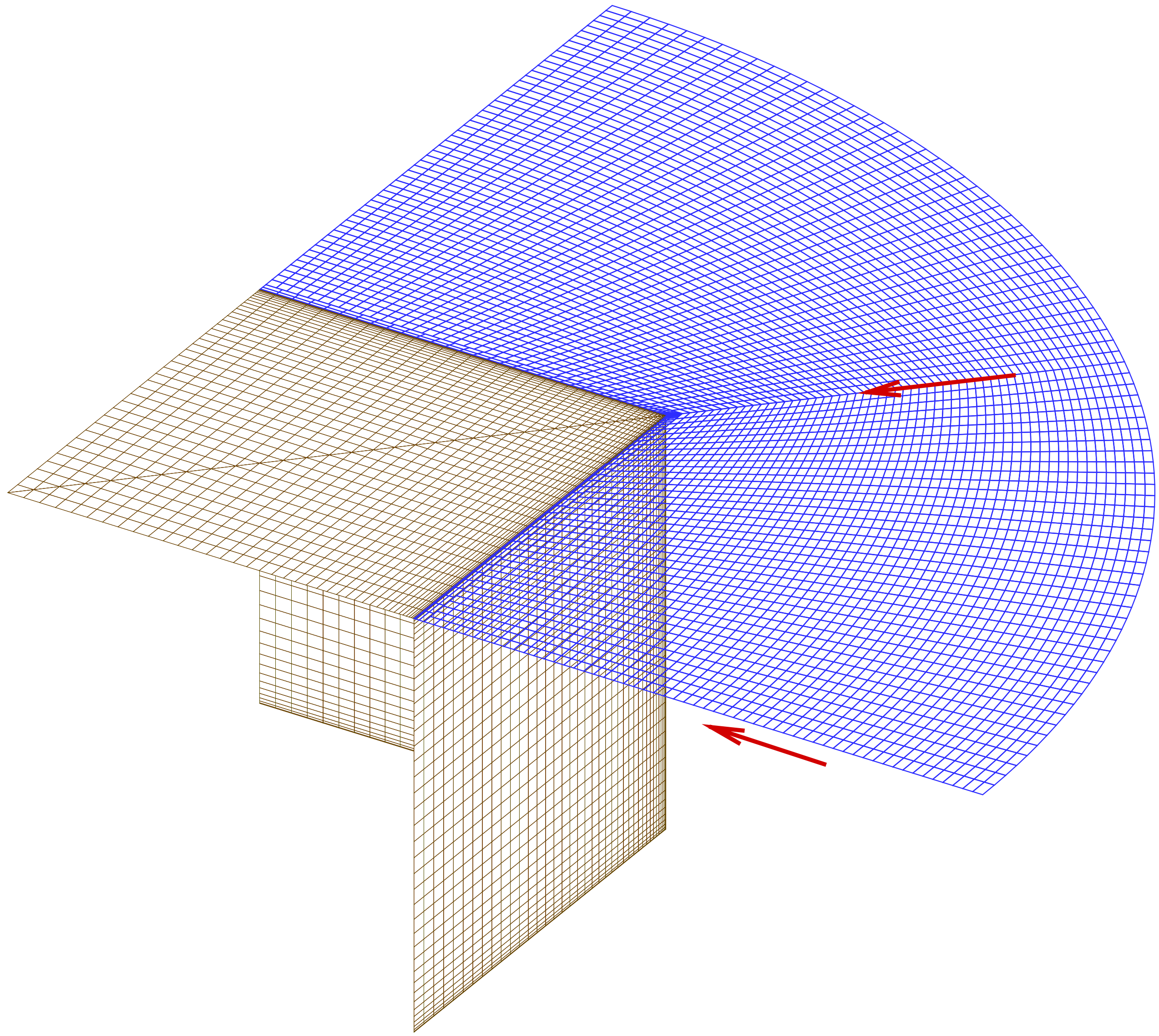

Proposed delivery sequence

V6.3

V6.3 + Quadratic forces including Tank and Lid for Multi-Body interaction

V6.3S

Evaluation of quadratic force using control surface

Mean drift force by momentum conservation

- Newman (1967) – far field
- Ferreira and Lee (1994)-near field-numerical but accurate

Quadratic force by pressure integration

- Lee and Newman(1991) – numerical, not always robust due to body velocity.

  Nonuniform discretization and mapping are used normally.

  Fine discretization may be necessary and can be expansive especially in multi-body interaction. Sometimes convergence can't be confirmed.

Quadratic force by use of control surface + body surface, proposed by Chen(2005), appears useful. The rederivation of the expressions for this approach is in the appendix and the method is implemented in WAMIT

Quadratic forces

$$
\begin{aligned}
\vec{F}^{(2)} &= -\frac{1}{2}\frac{\rho}{g}\int_{CL}\vec{n}'\phi_t^2 dl - \rho g\int_{WL}[\zeta(\vec{\Xi}\cdot\vec{n}')]\hat{k}dl \\
&- \rho\int\int_{S_c}[\nabla\phi\frac{\partial\phi}{\partial n} - \frac{1}{2}\vec{n}(\nabla\phi\cdot\nabla\phi)]ds \\
&- \rho\int\int_{S_f}[\nabla\phi\frac{\partial\phi}{\partial n} - \frac{1}{2}\vec{n}(\nabla\phi\cdot\nabla\phi)]ds + \frac{\rho}{g}\int\int_{S_f}\phi_t\nabla'\phi_t ds \\
&+ \vec{F}_S^{(2)} \\
&- \rho\int\int_{S_b}[\nabla\phi(\frac{d\vec{\Xi}}{dt}\cdot\vec{n}) + (\Xi\cdot\vec{n})\nabla\phi_t]ds
\end{aligned}
$$

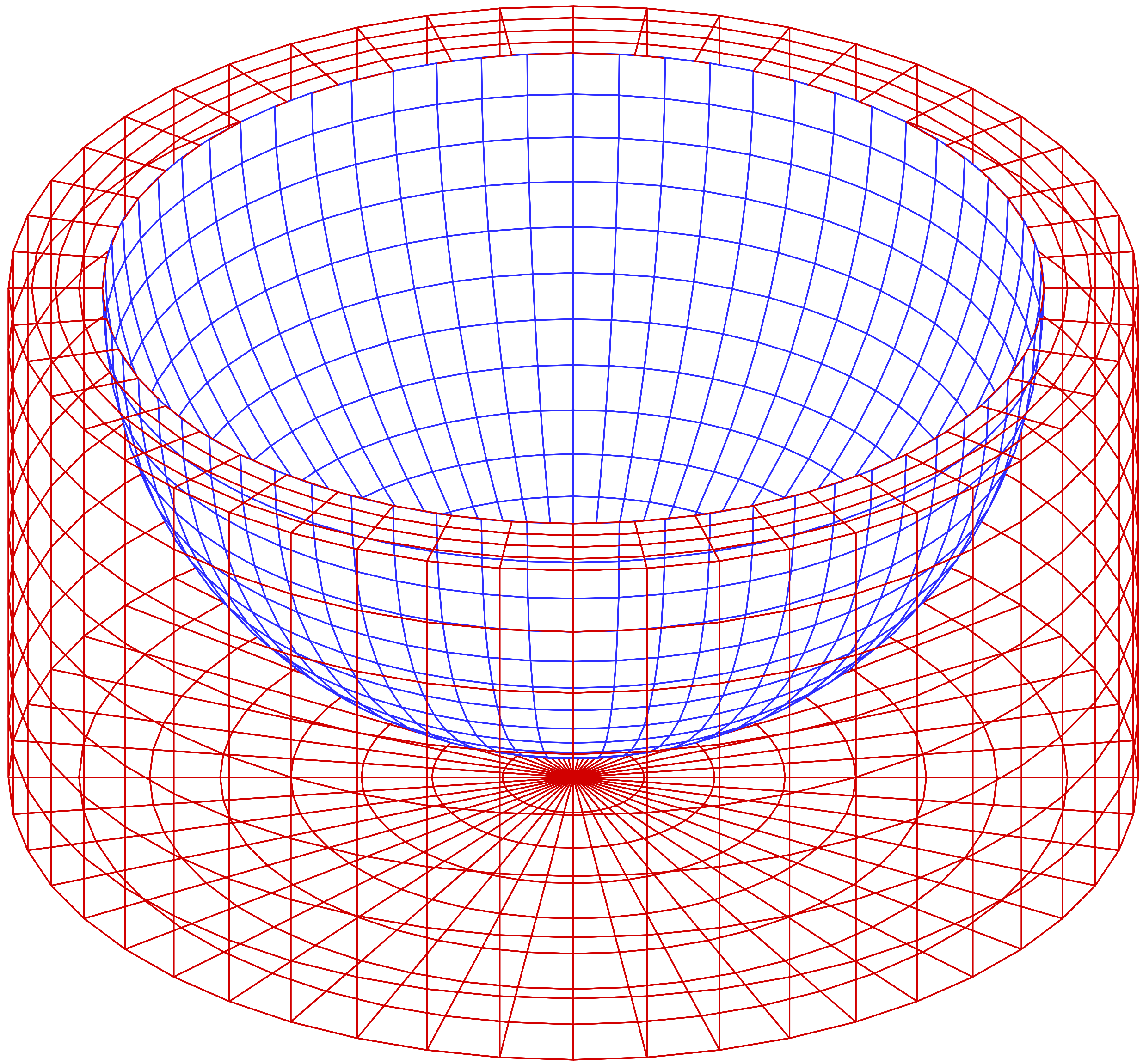

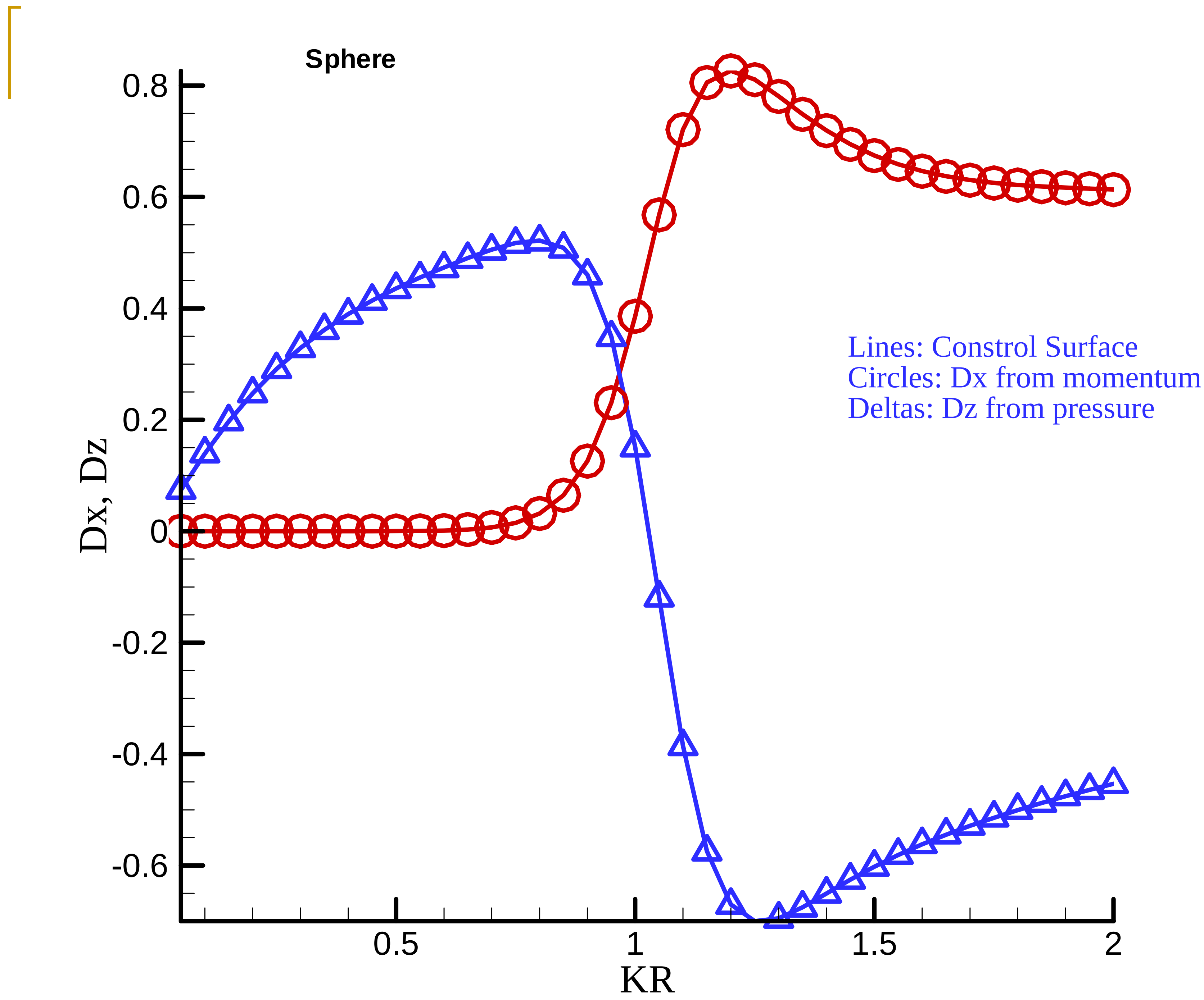

Sphere
0.8
0.6
0.4
0.2
0
-0.2
-0.4
-0.6
Dx, Dz
0.5
1
1.5
2
KR
Lines: Constrol Surface
Circles: Dx from momentum
Deltas: Dz from pressure

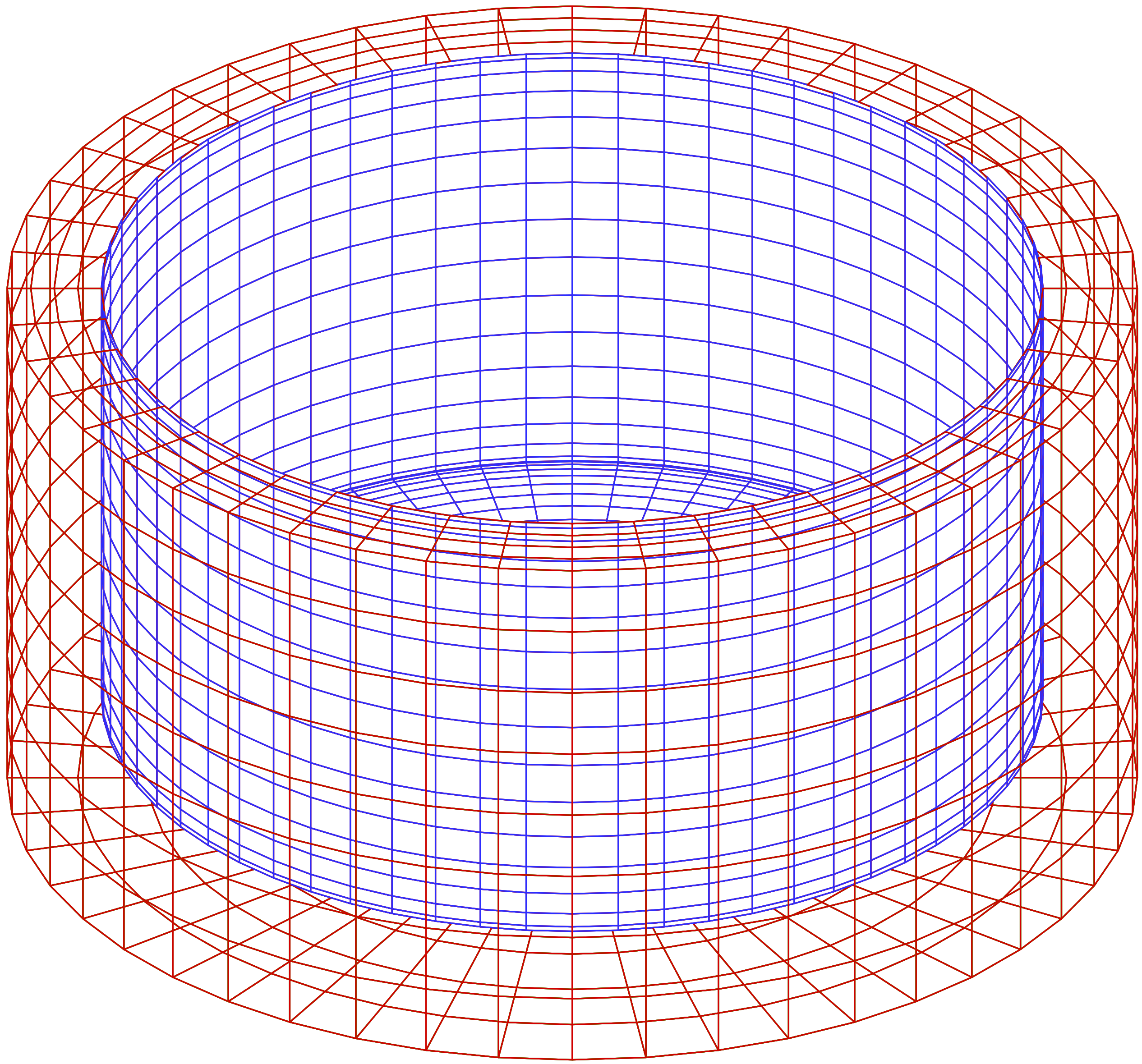

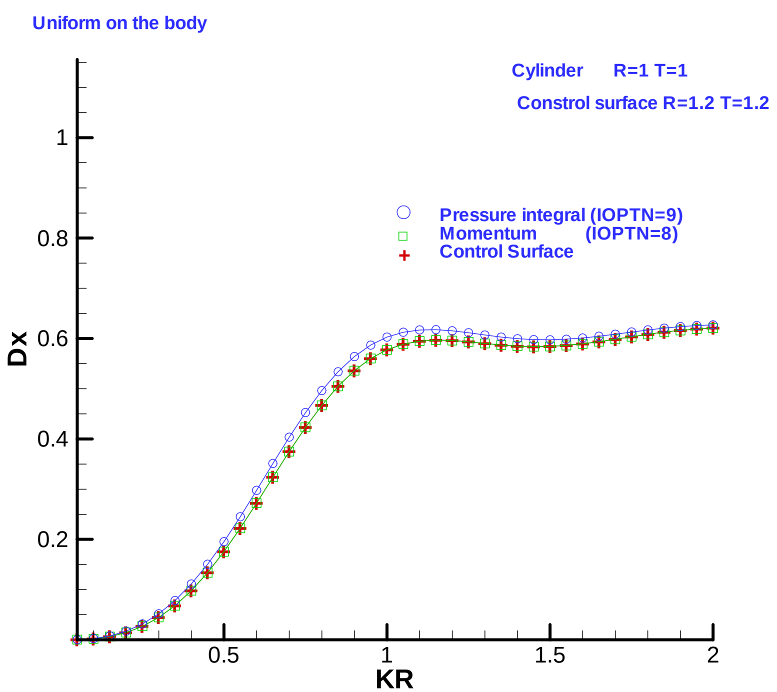
Uniform on the body
Cylinder R=1 T=1
Constrol surface R=1.2 T=1.2
Pressure integral (IOPTN=9)
Momentum (IOPTN=8)
Control Surface
Dx
KR
1
0.8
0.6
0.4
0.2
0.5
1
1.5
2

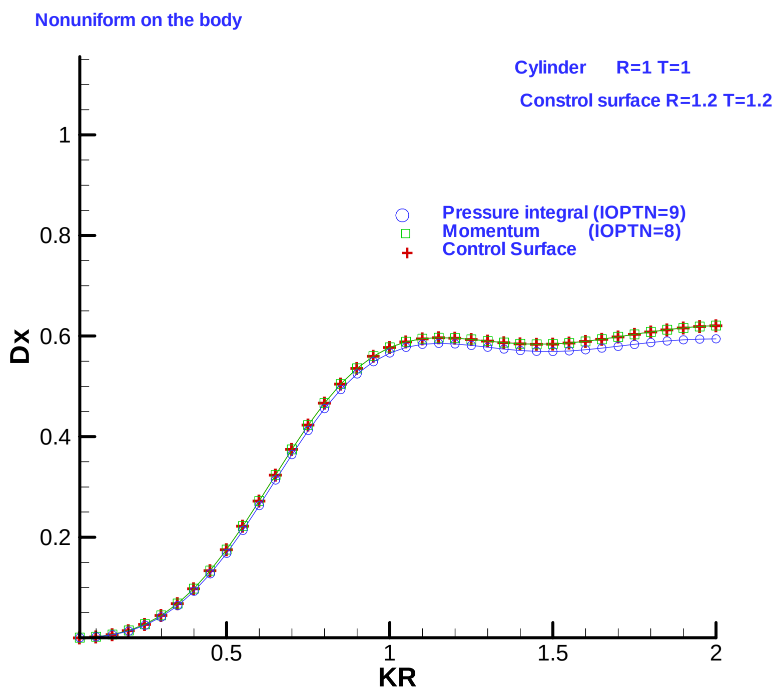
Nonuniform on the body
Cylinder R=1 T=1
Constrol surface R=1.2 T=1.2
Pressure integral (IOPTN=9)
Momentum (IOPTN=8)
Control Surface
Dx
KR
1
0.8
0.6
0.4
0.2
0.5
1
1.5
2

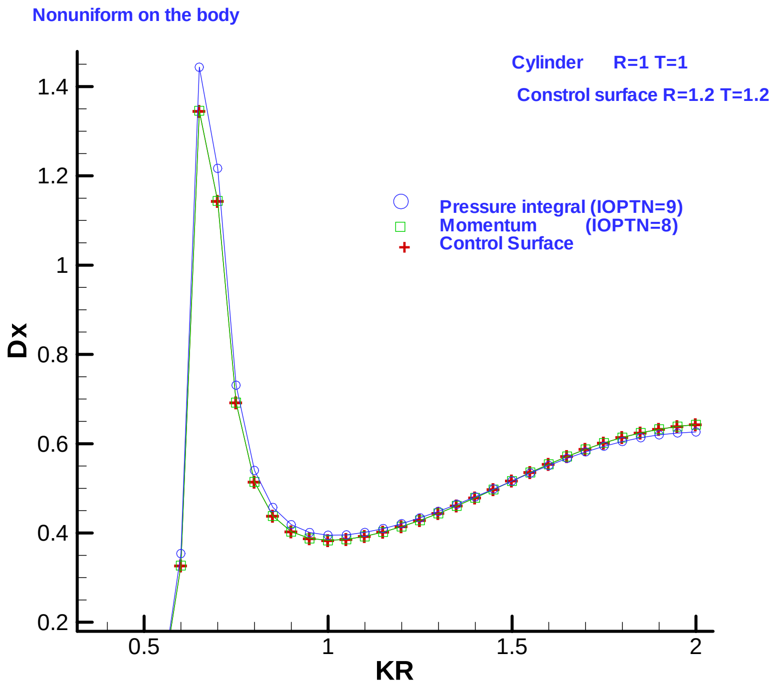
Nonuniform on the body
Cylinder R=1 T=1
Constrol surface R=1.2 T=1.2
Pressure integral (IOPTN=9)
Momentum (IOPTN=8)
Control Surface
Dx
KR
0.2
0.4
0.6
0.8
1
1.2
1.4
0.5
1
1.5
2

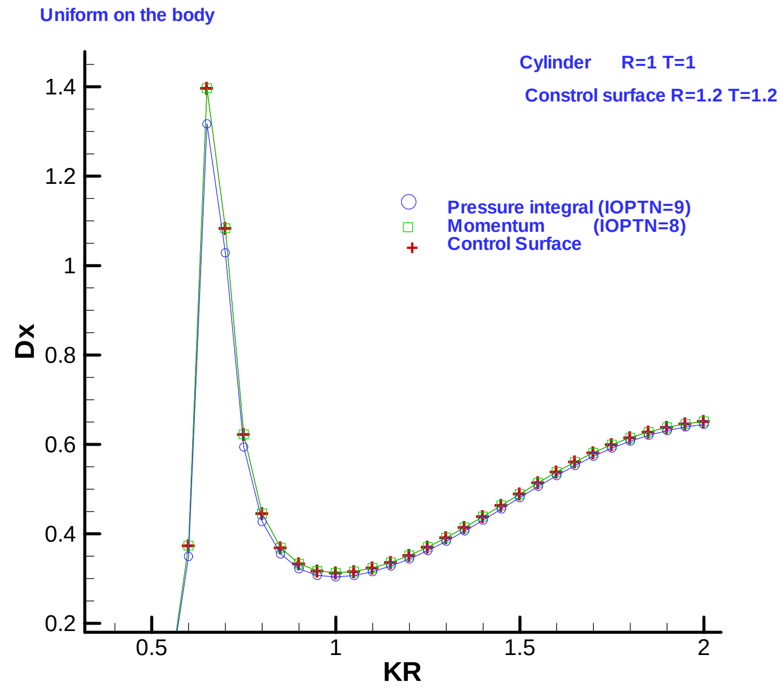
Uniform on the body
Cylinder R=1 T=1
Constrol surface R=1.2 T=1.2
Pressure integral (IOPTN=9)
Momentum (IOPTN=8)
Control Surface
Dx
KR
0.2
0.4
0.6
0.8
1
1.2
1.4
0.5
1
1.5
2

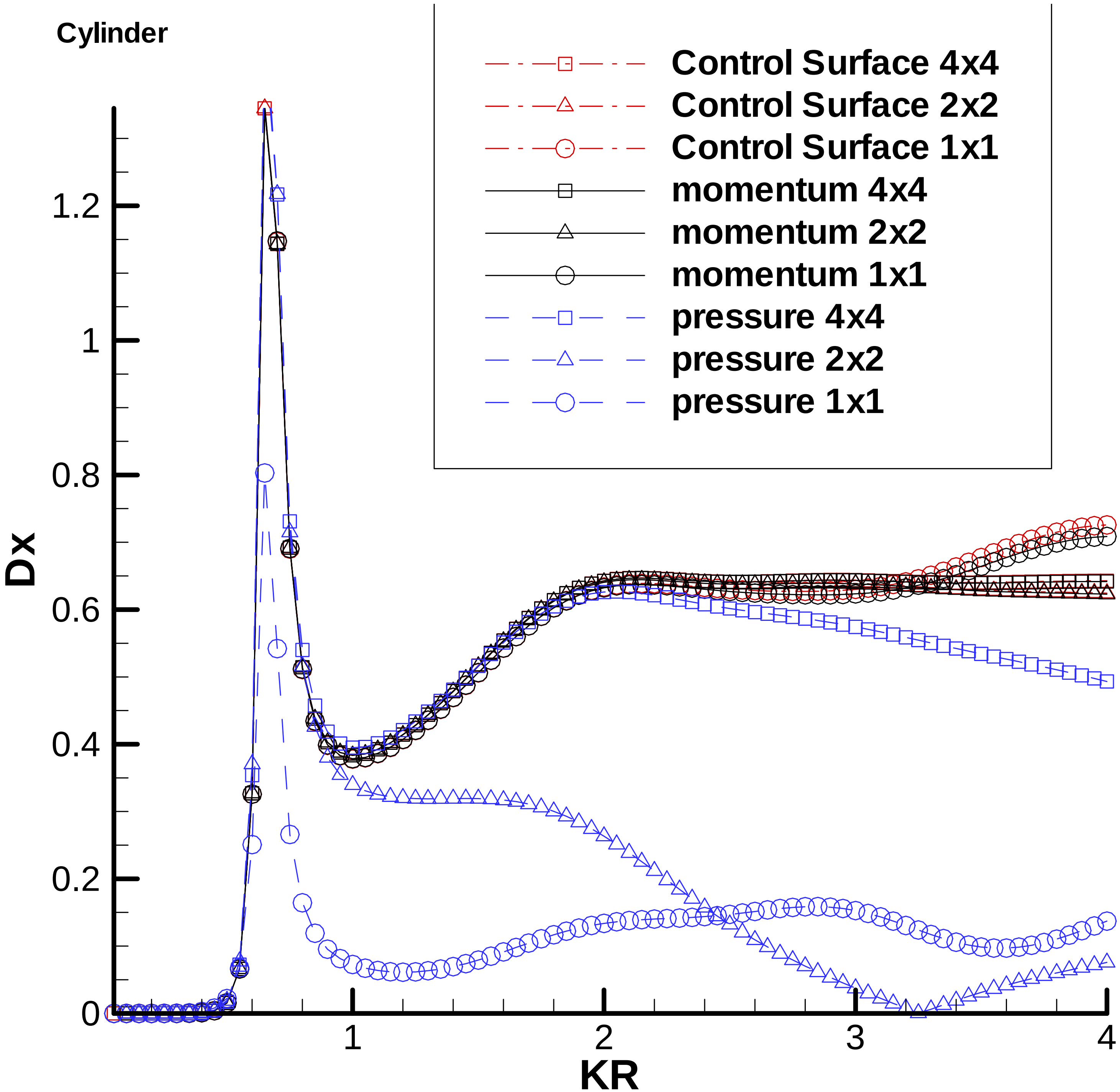

Cylinder
Control Surface 4x4
Control Surface 2x2
Control Surface 1x1
momentum 4x4
momentum 2x2
momentum 1x1
pressure 4x4
pressure 2x2
pressure 1x1
Dx
0
0.2
0.4
0.6
0.8
1
1.2
1
2
3
4
KR

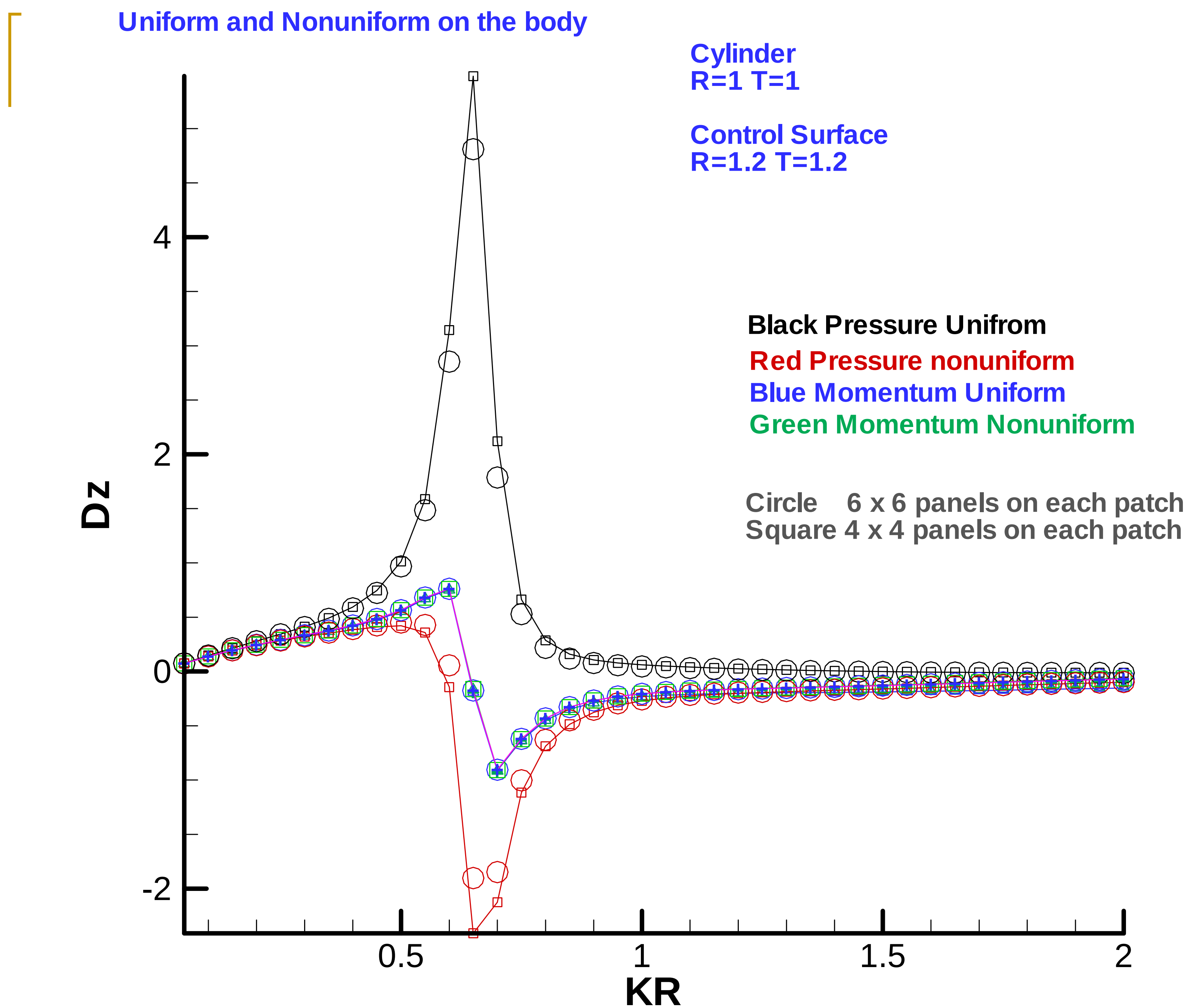

Uniform and Nonuniform on the body
Cylinder
R=1 T=1
Control Surface
R=1.2 T=1.2
Black Pressure Unifrom
Red Pressure nonuniform
Blue Momentum Uniform
Green Momentum Nonuniform
Circle 6 x 6 panels on each patch
Square 4 x 4 panels on each patch
Dz
KR
4
2
0
-2
0.5
1
1.5
2

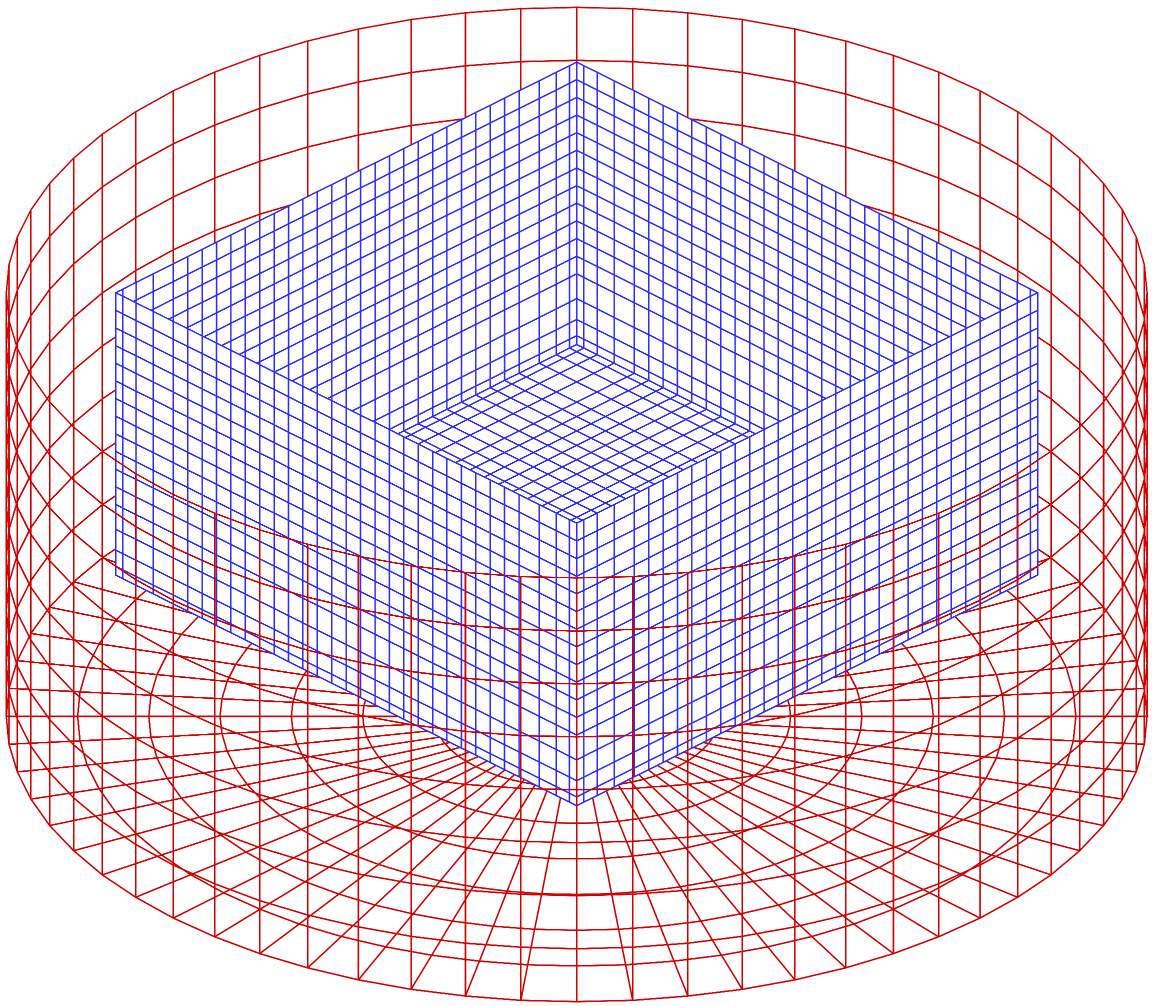

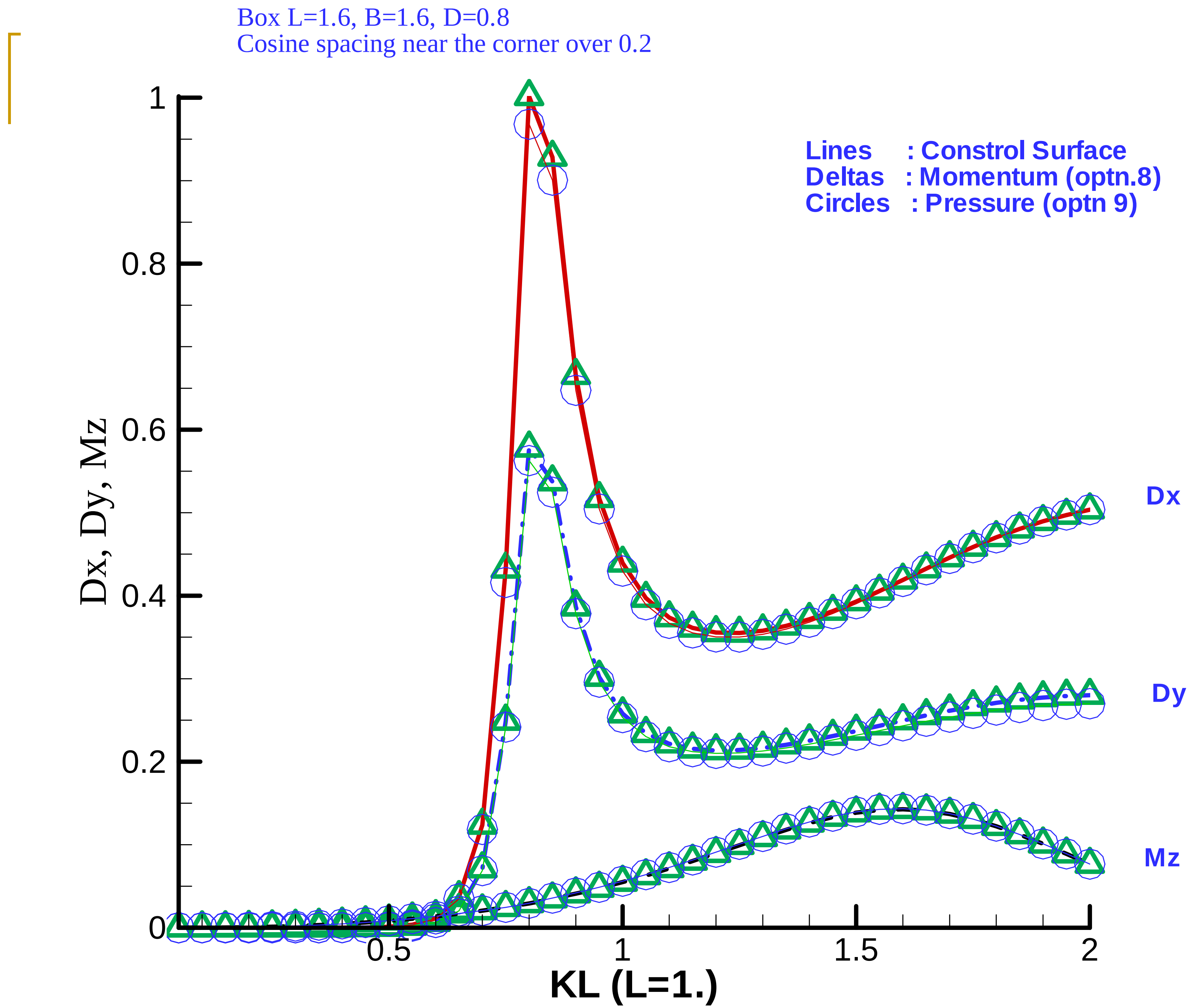
Box L=1.6, B=1.6, D=0.8
Cosine spacing near the corner over 0.2
Lines : Constrol Surface
Deltas : Momentum (optn.8)
Circles : Pressure (optn 9)
Dx
Dy
Mz
Dx, Dy, Mz
KL (L=1.)
0
0.2
0.4
0.6
0.8
1
0.5
1
1.5
2

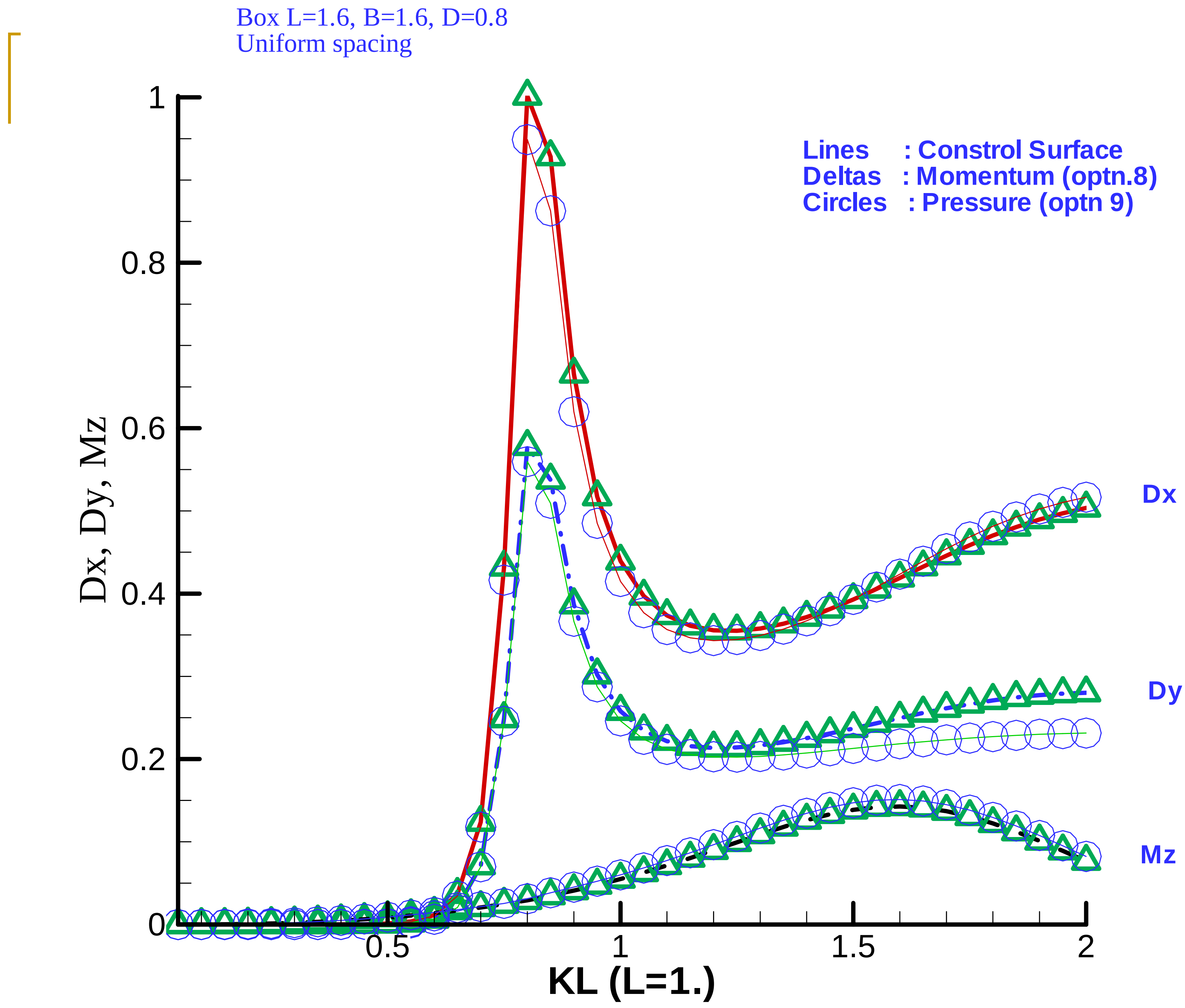
Box L=1.6, B=1.6, D=0.8
Uniform spacing
Lines : Constrol Surface
Deltas : Momentum (optn.8)
Circles : Pressure (optn 9)
Dx
Dy
Mz
Dx, Dy, Mz
KL (L=1.)
0
0.2
0.4
0.6
0.8
1
0.5
1
1.5
2

Advantages

Mean force:
The fluid velocity on the body is not necessary. Thus the results are very accurate and not as much sensitive to the discretization.

All components of mean drift force can be evaluated for the bodies with thin elements in principle.

Quadratic force:
For fixed body, integration of the pressure is not required at all for the quadratic forces

No quadratic terms of the velocity.

Disadvantages

The control surfaces is required. It can be simple when free surface is not included, however, such as the submerged bodies or when surge, sway and yaw are only of interest for the surface piercing bodies.

Additional computational time in Force module for large number of field points.

- Thus far Dx, Dy, Dz and Mz are correctly evaluated
- Bottom mounted structures are not considered which needs a control line on the bottom

Effect of tanks or springs on mean drift forces

by J. N. Newman

October 2005

OUTLINE

- Last year results were shown for the effect of tanks on drift forces, with substantial reduction of the drift forces in some cases
- These results were surprising to us and others
- This effect is apparently due to the (negative) added mass of the fluid in the tanks
- Similar results can be found for a vessel with linear-stiffness (`spring’) mooring constraints

Spheroid with four tanks

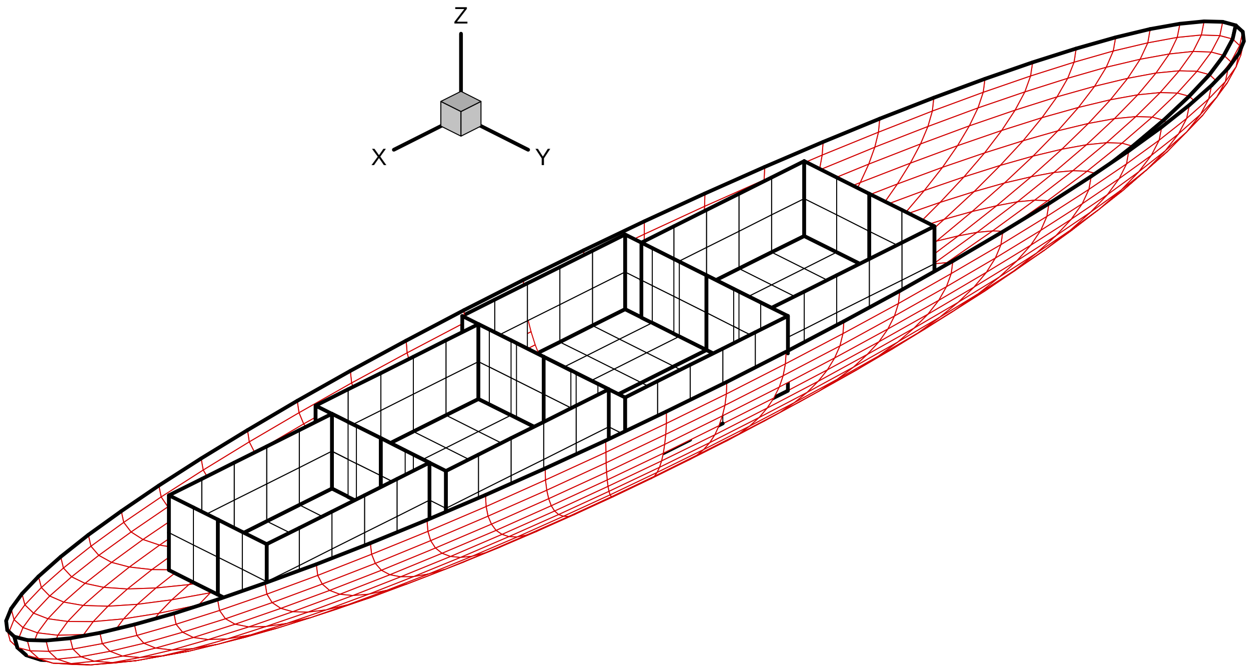

Mean drift forces
(solid=momentum, dashed=pressure)

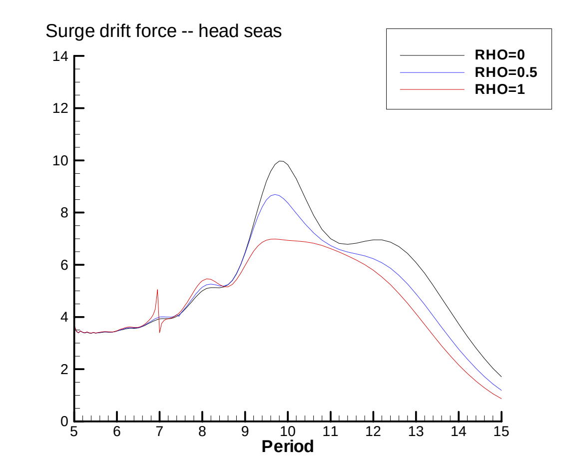

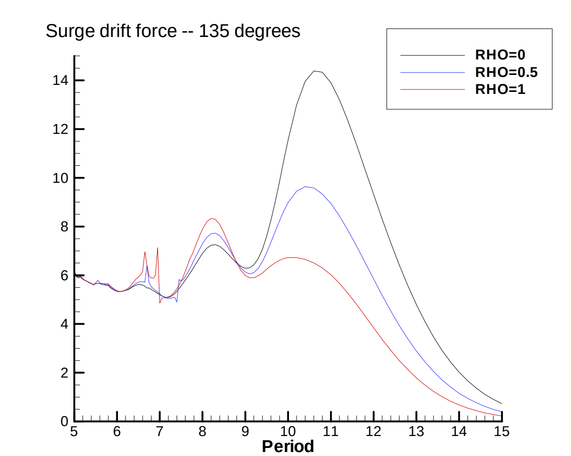

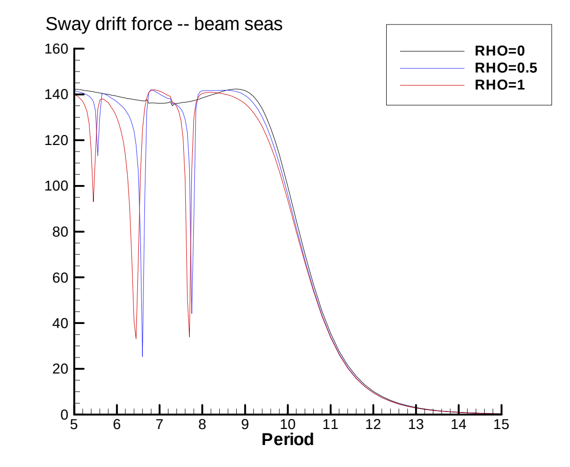

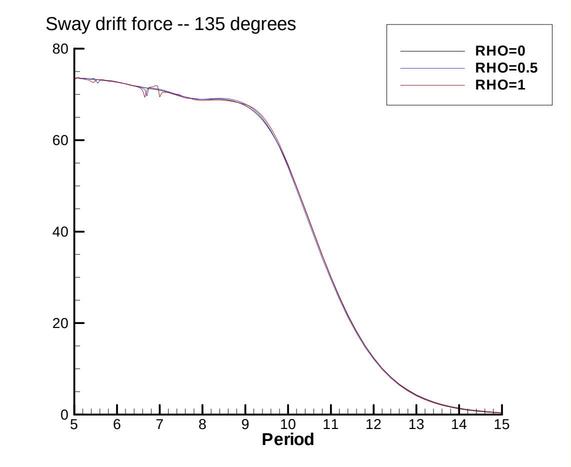

Generic FPSO (GEOMXACT) 300x50x15m
Tanks 40x40x15m, 3m above hull

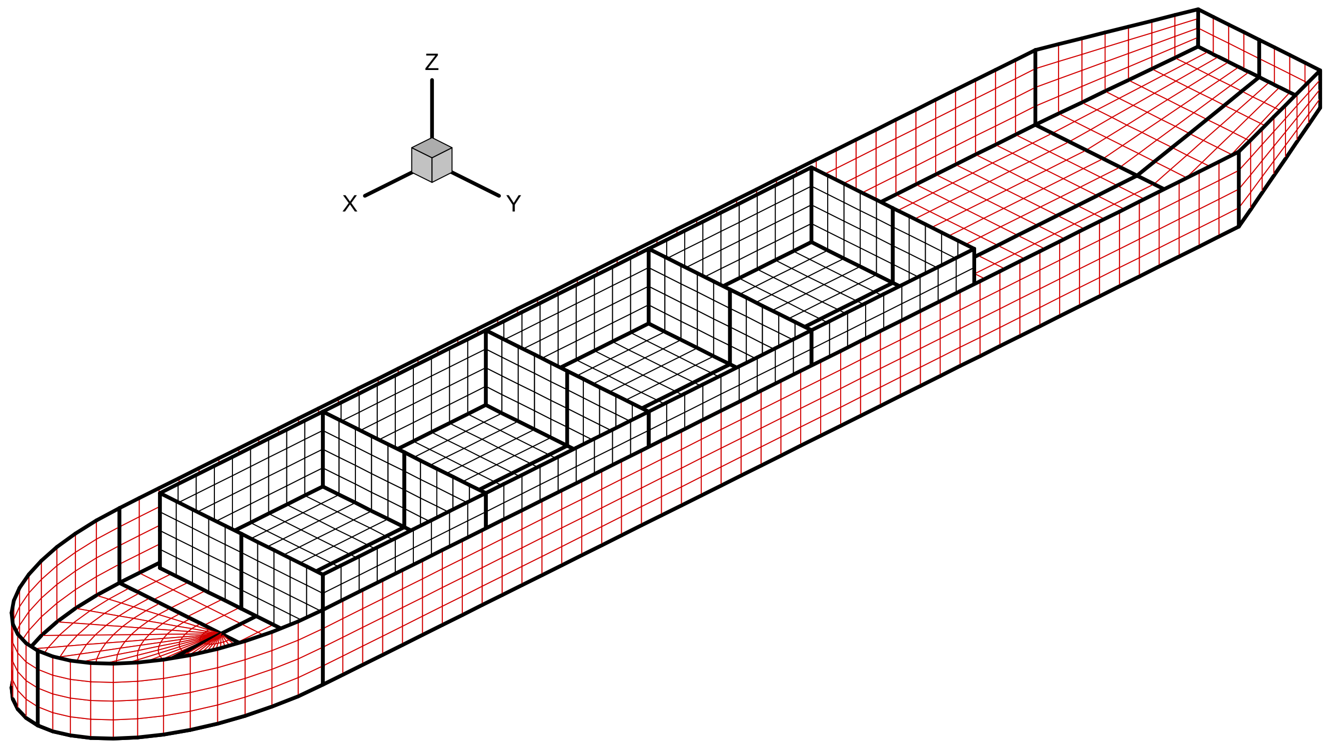

RAO’s and drift forces in head/beam waves

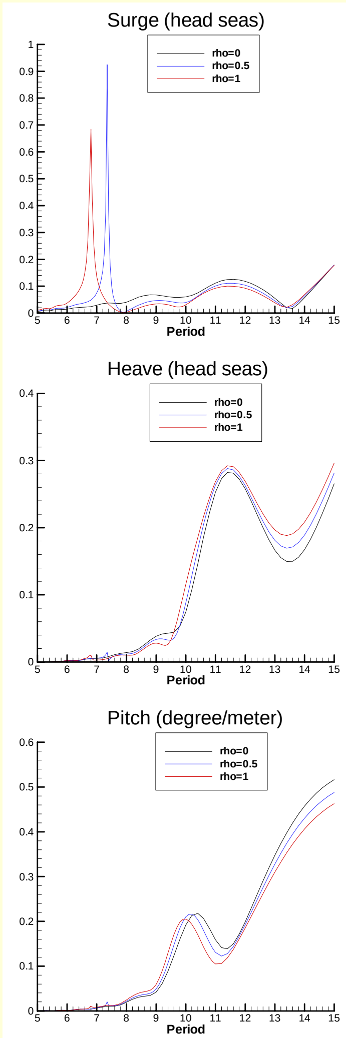

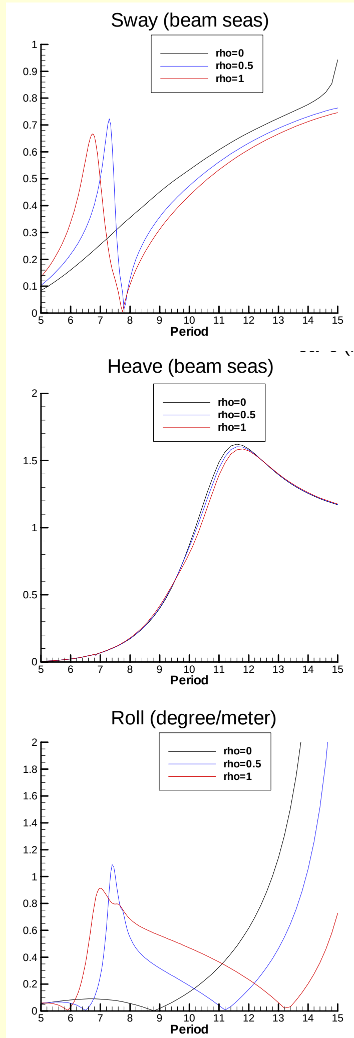

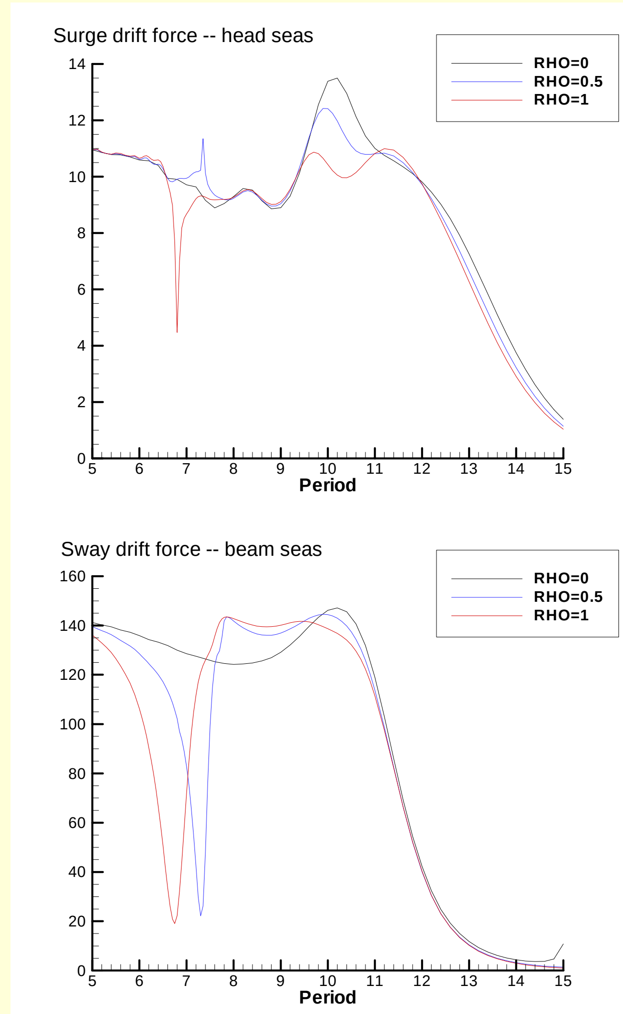

Inviscid linear theory

- From momentum conservation, there is no mean horizontal force on the tanks
- The only effect of the tanks on the vessel's drift force is via the 1^{st} order motions
- The only effect of the tanks on the 1^{st} order motions of the vessel is from the added mass (and hydrostatic restoring forces) of the tanks

Spheroid with 3 tanks

(See Appendix for more details)

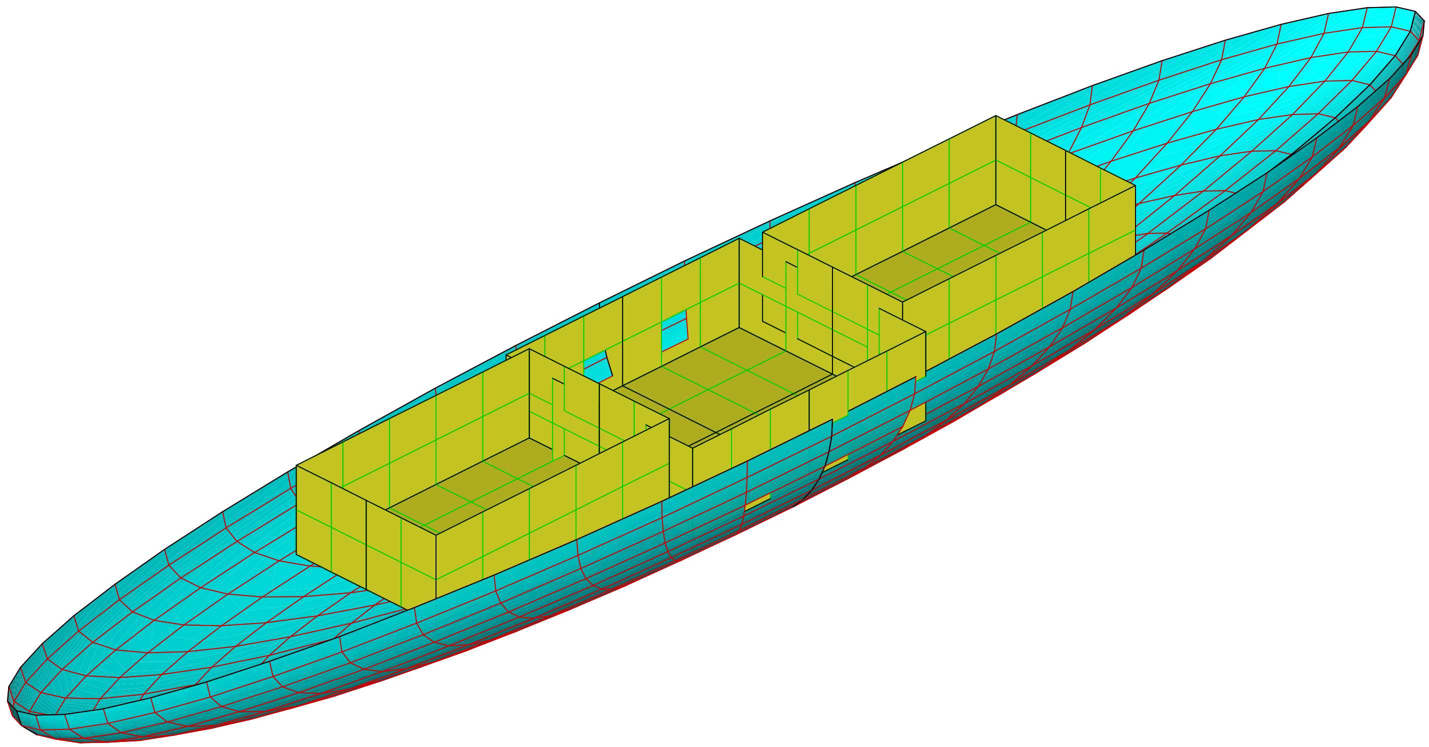

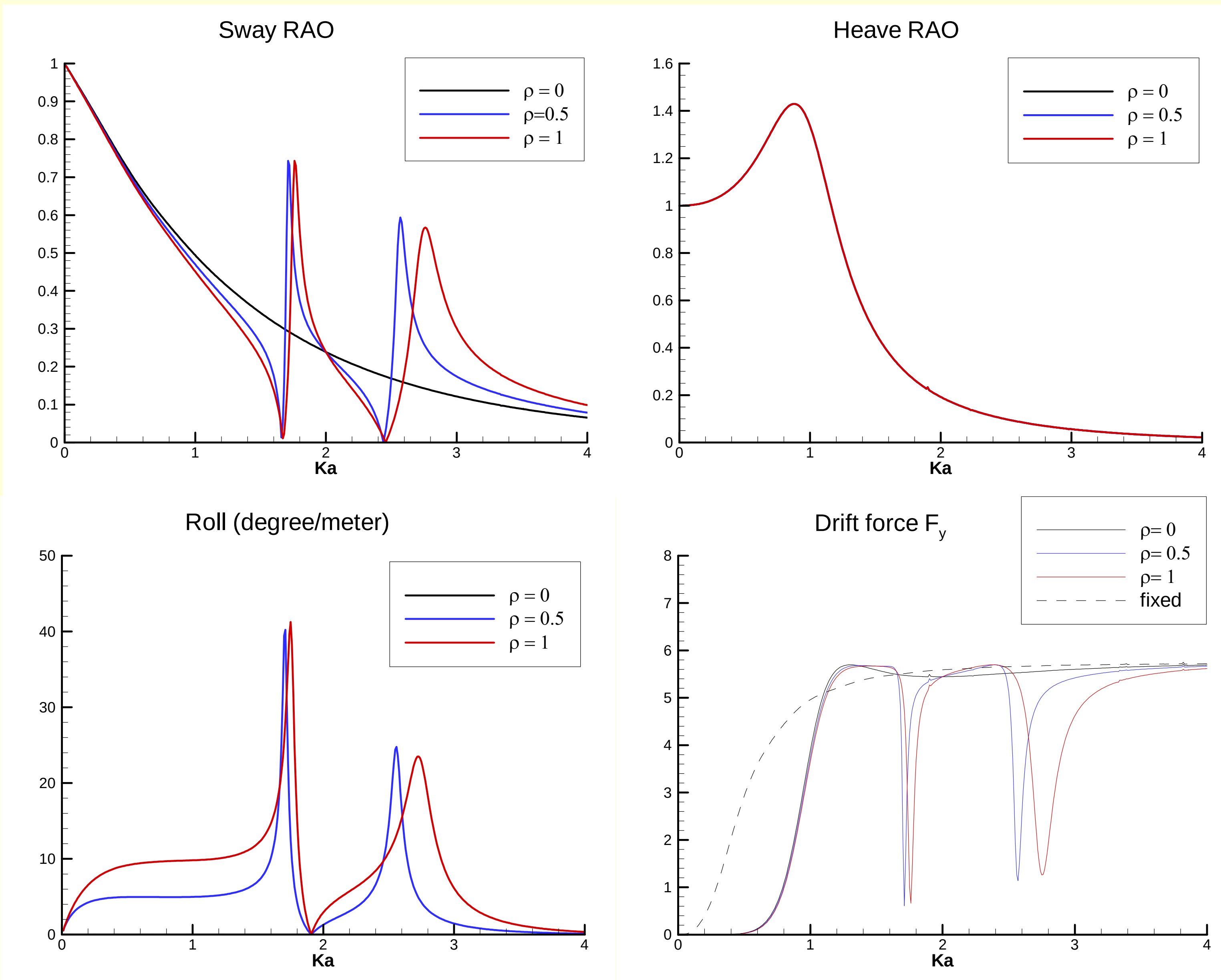

Sway RAO
ρ = 0
ρ=0.5
ρ = 1
Ka
Heave RAO
ρ = 0
ρ = 0.5
ρ = 1
Ka
Roll (degree/meter)
ρ = 0
ρ = 0.5
ρ = 1
Ka
Drift force F y
ρ= 0
ρ= 0.5
ρ= 1
fixed
Ka

Spheroid – Added Mass Coefficients

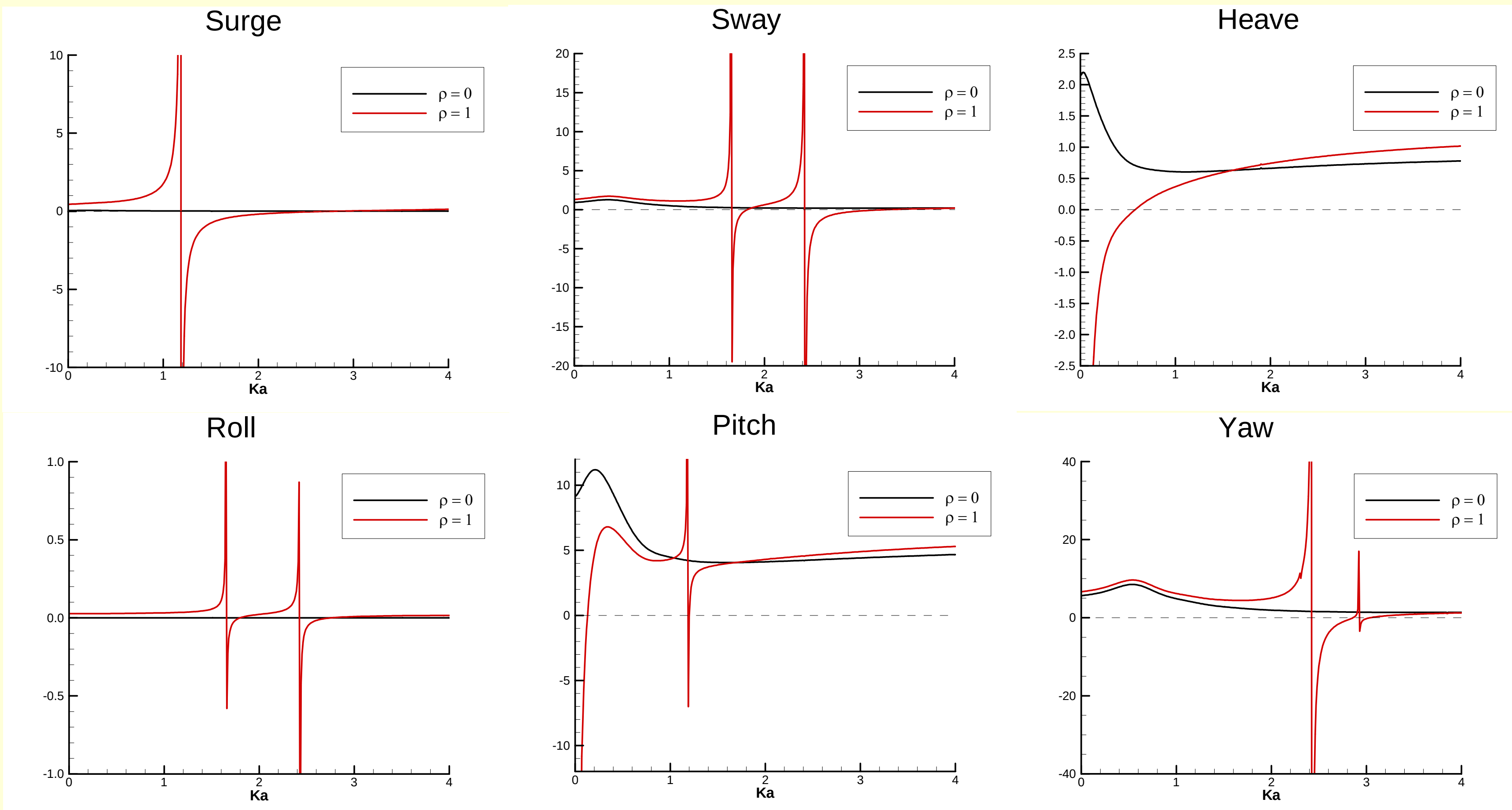

Spheroid with spring restraint in sway mode (no tanks)

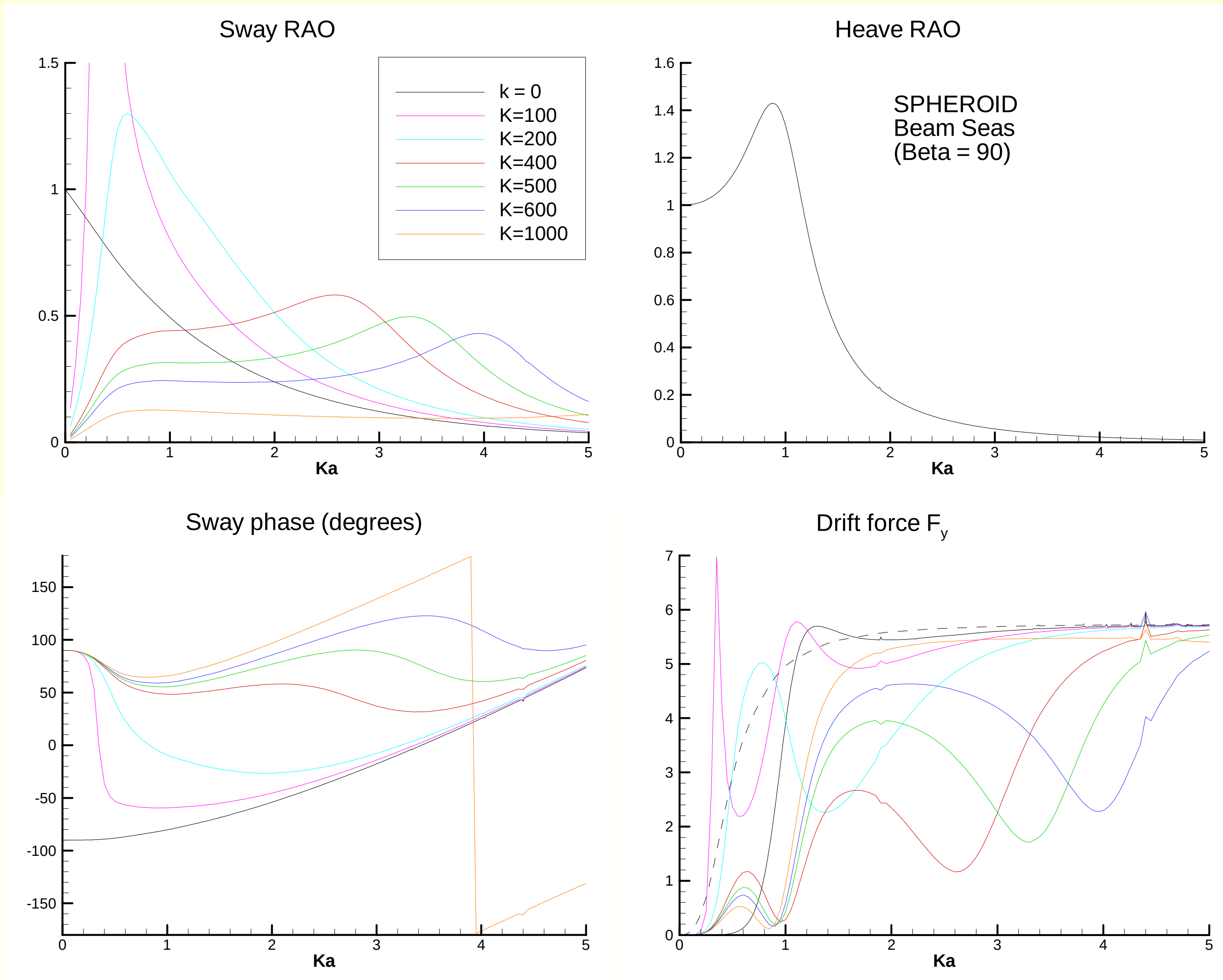

FPSO with springs in beam seas

(See Appendix for more details)

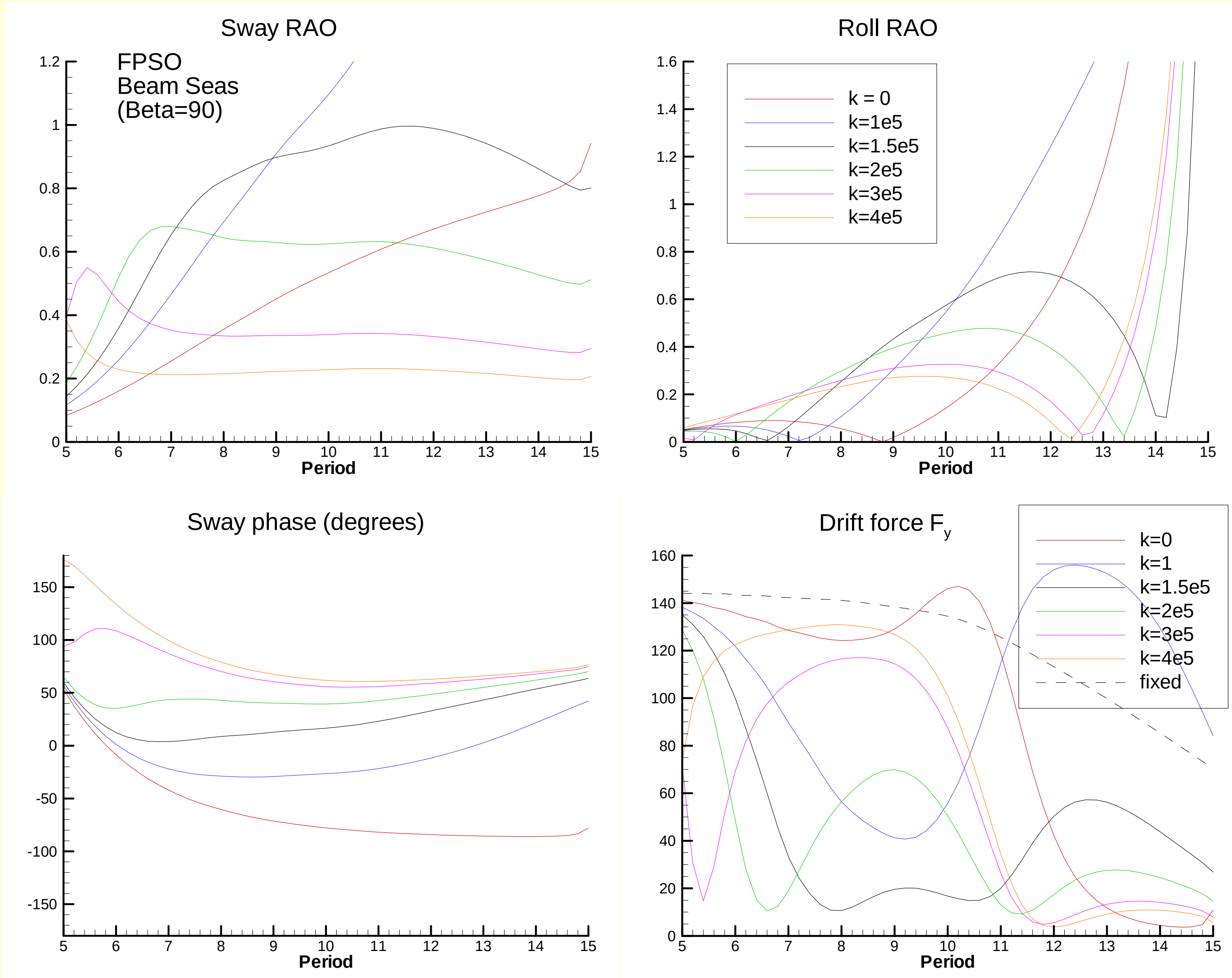

Conclusions

- Only effect on vessel’s motions is from added mass of tanks (and hydrostatics)
- Drift force reduced by tanks, in regions where the tank added mass is negative
- This is equivalent to a positive stiffness mooring restraint, which is more effective over a broad band of wave periods
- For elongated vessels this effect is only substantial for the sway drift force in beam seas

Notes on the computation with an artificial lid for the analysis of two-bodies interaction

- Newman devised a method to absorb resonant energy by placing a flexible lid on the free surface inside the gap (2003 WAMIT meeting and OMAE 2004)

Rigid body modes of ships
+
Flexible lid in-between

Applied damping force to
Flexible modes of the lid
using external damping
matrix in FRC

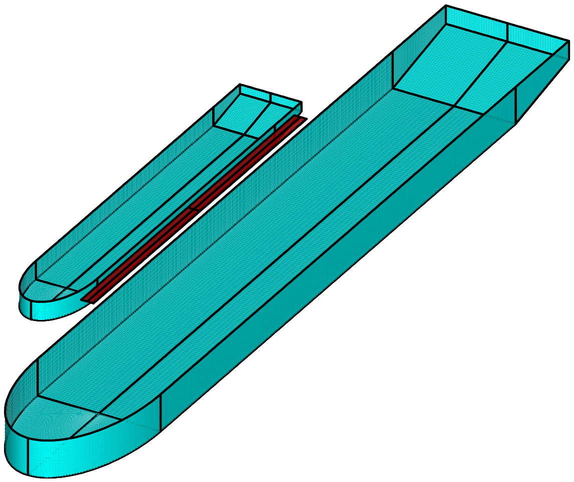

- The same procedure is followed with a difference geometry.

- Input files are included in the report which may be used for other geometry with minor modifications.

- With the lid, the wave exciting forces should be evaluated using fixed mode option and added mass and damping coefficient by an additional post-processing.

Complete radiation/diffraction solution is the sum of
a) radiation/diffraction solution with fixed lid and
b) all radiation solutions for generalized modes of the lid

RAO, fluid pressure and velocity on the body and at the field points and mean drift forces Include a) and b)

Added mass, damping coefficient and wave exciting force, in .2 or .3, includes a) only

- Wave exciting forces can be evaluated using fixed body option in optn.4

  IRAD=1 in POT

  IOPTN(4) < 0 in FRC

  Set MODE=0 for all modes of structures

  Set MODE=1 for all generalized modes of lid

Evaluate lid amplitude due to the body motion j from

$$[-\omega^2 A_{l,k} + i\omega(B_{l,k} + B^E_{l,k}) + C_{l,k}]\zeta_k = \omega^2 A_{l,j} - i\omega B_{l,j} \tag{1}$$

or from the normalized equation

$$[-K\bar{A}_{l,k} + iK(\bar{B}_{l,k} + \bar{B}^E_{l,k}) + \bar{C}_{l,k}]\zeta_k = K\bar{A}_{l,j} - iK\bar{B}_{l,j} \tag{2}$$

Here $K = \omega^2/g$. $\bar{A}$s and $\bar{B}$s are added masses and damping coefficients output in optn.1. $\bar{B}^E_{l,k}$ is the damping forces in FRC normalized by $\rho\omega$.

$$\bar{C}_{l,k} = \iint_{lid} L_l L_k dxdy \tag{3}$$

The complete added mass and damping coefficient in i mode due to j mode are then evaluated from

$$\bar{A}^c_{i,j} - i\bar{B}^c_{i,j} = \bar{A}_{i,j} - i\bar{B}_{i,j} + \sum_k \zeta_k(\bar{A}_{i,k} - i\bar{B}_{i,k}) \tag{4}$$

Barge L=160 B=60 D=15

Lid L=160 B=8

Gap=8

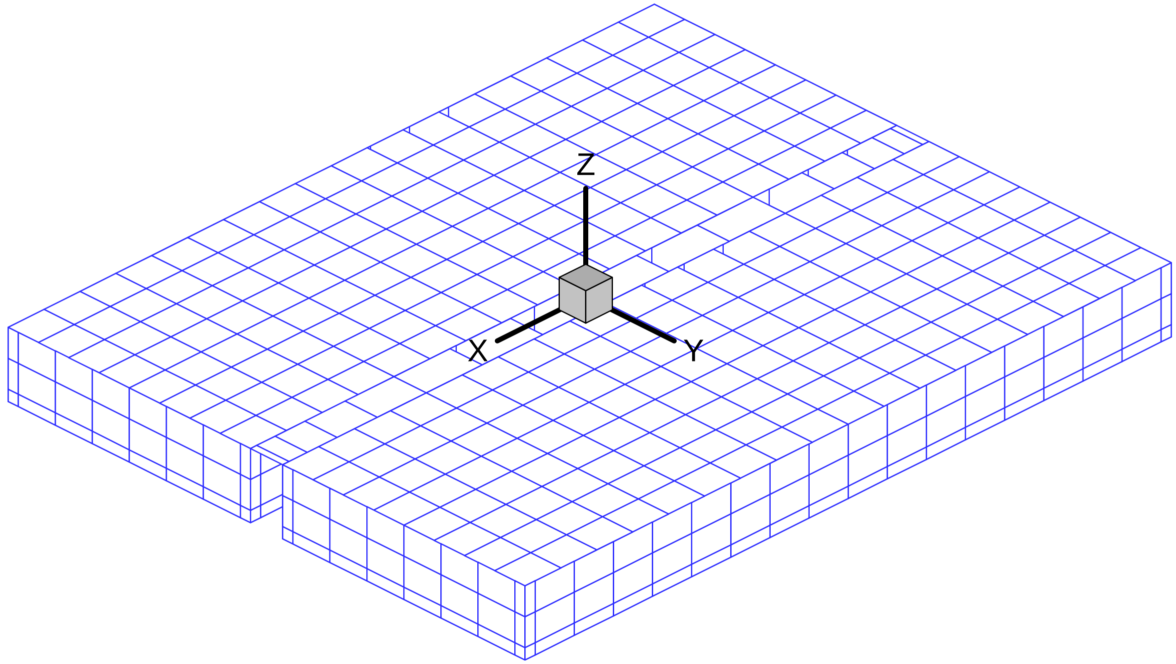

Three existing subroutines of WAMIT are used

- GAPLID is used for lid geometry. Non-uniform spacing in the longitudinal direction as Chebyshev polynomials used as generalized modes of the lid motion.

- GAP_FS describes the product of Chebyshev polynomial and Fourier Series.

- BARGENUC is used for barge. Non-uniform spacing only near the corner.

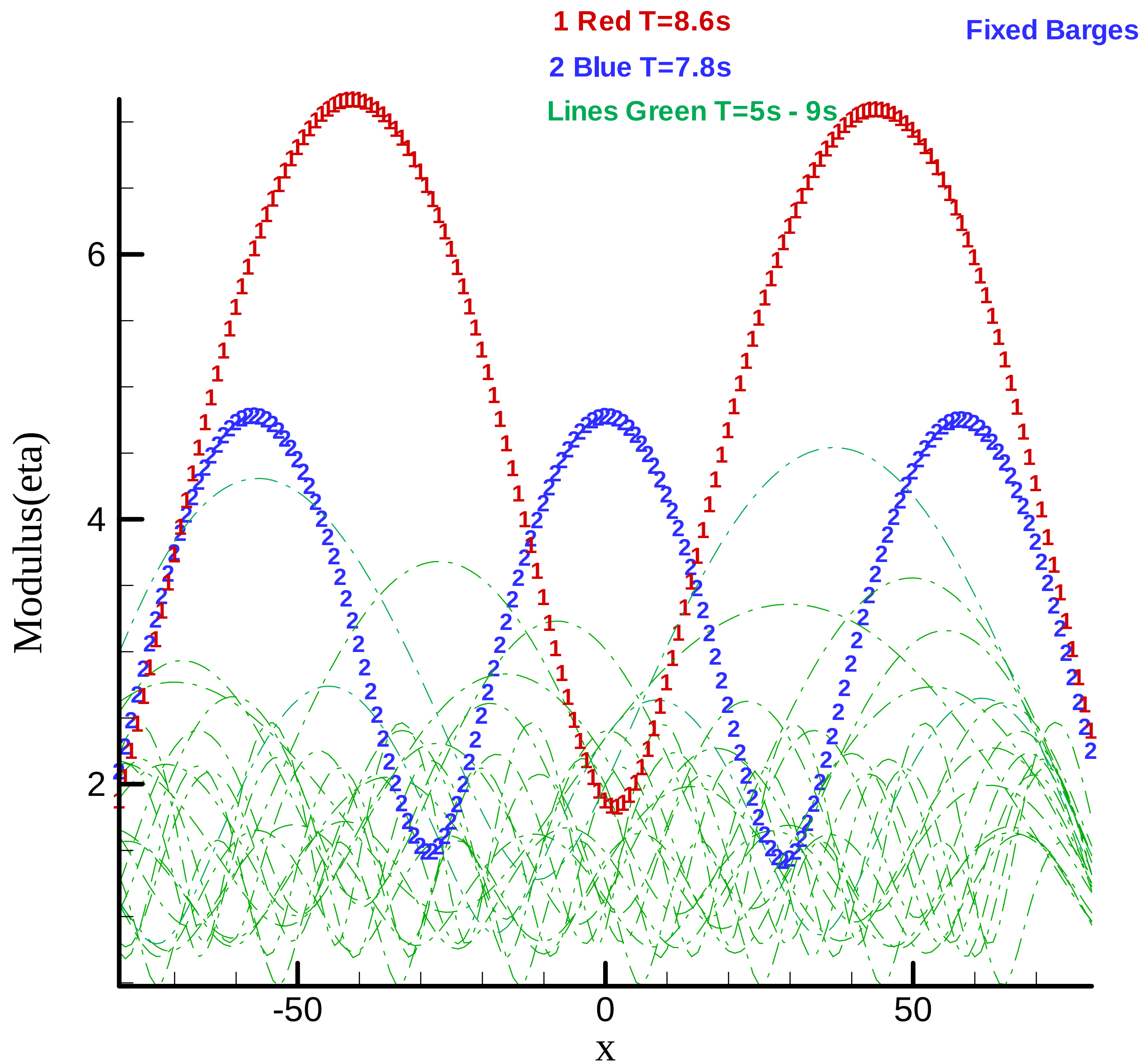
1 Red T=8.6s
2 Blue T=7.8s
Lines Green T=5s - 9s
Fixed Barges
Modulus(eta)
6
4
2
-50
0
50
x

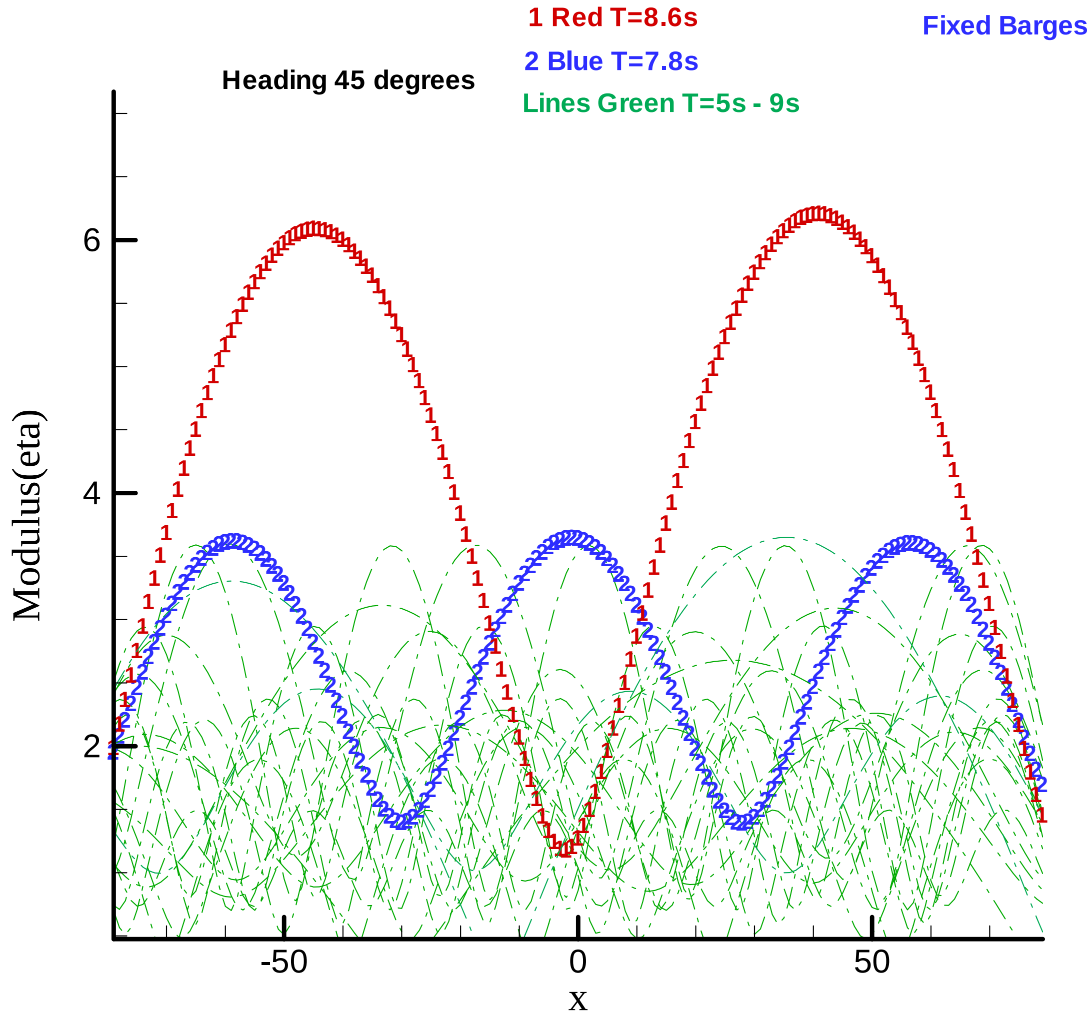

1 Red T=8.6s
2 Blue T=7.8s
Lines Green T=5s - 9s
Fixed Barges
Heading 45 degrees
Modulus(eta)
6
4
2
-50
0
50
x

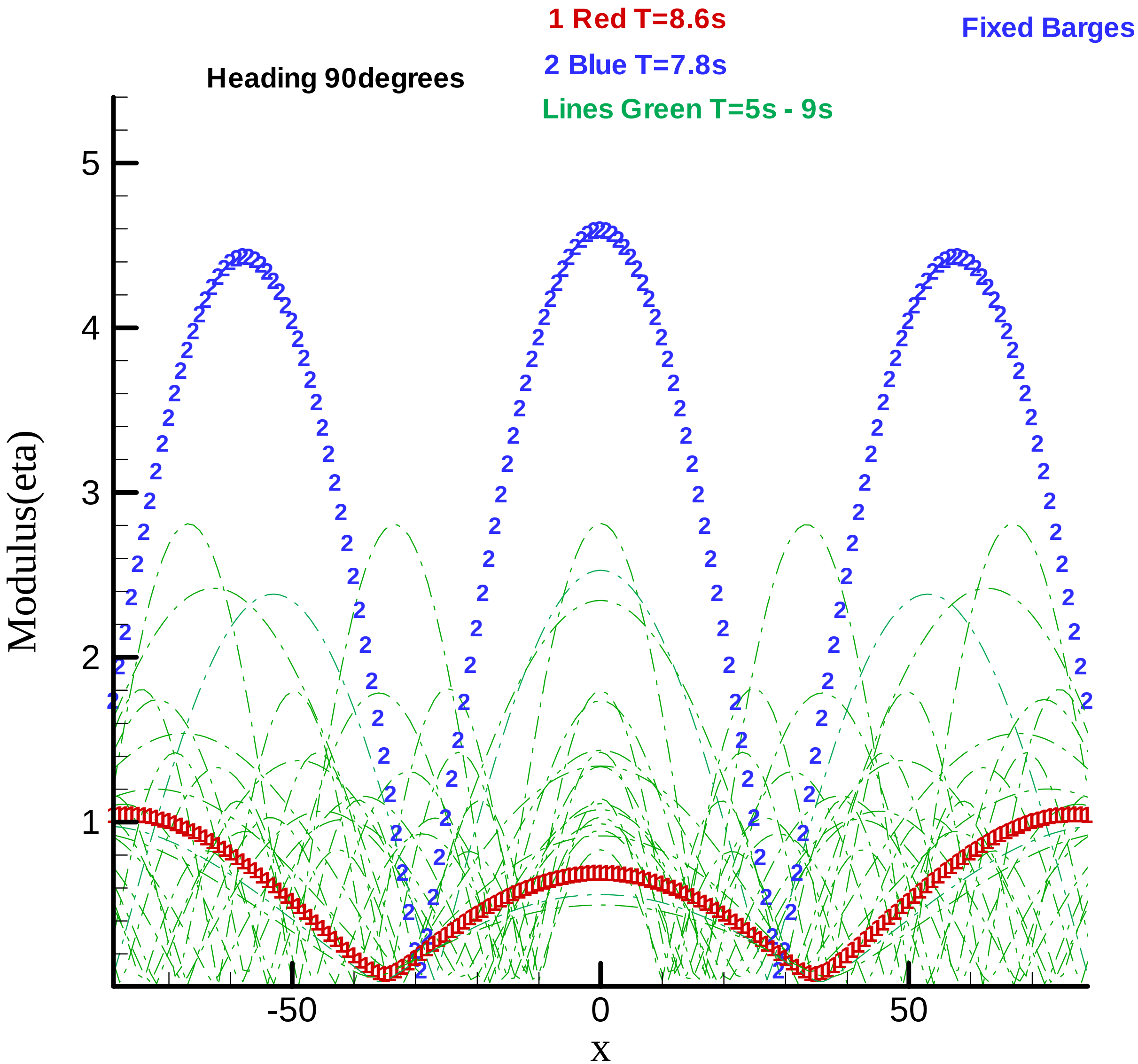
1 Red T=8.6s
2 Blue T=7.8s
Lines Green T=5s - 9s
Fixed Barges
Heading 90degrees
Modulus(eta)
x
5
4
3
2
1
-50
0
50

Free Barges

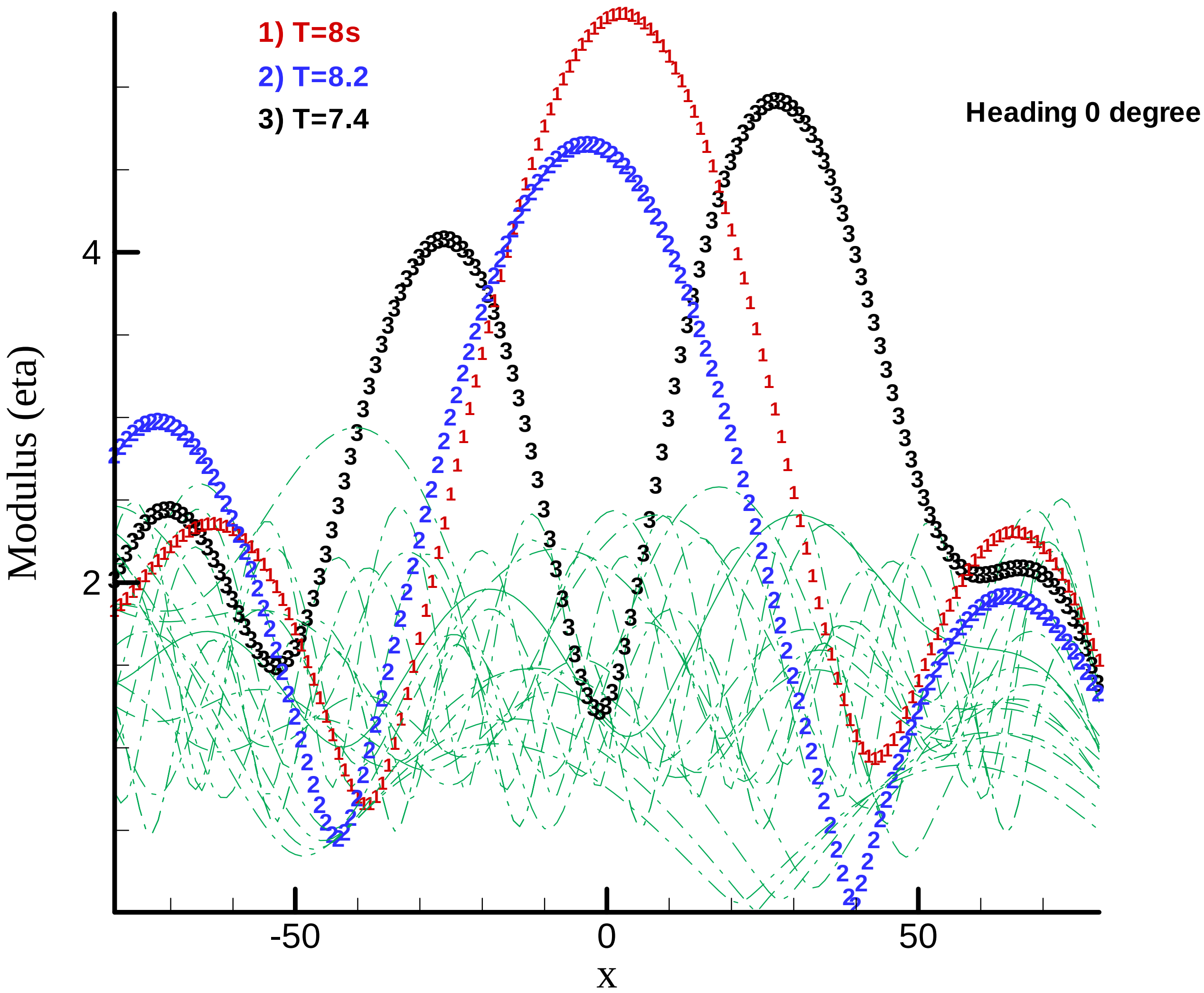

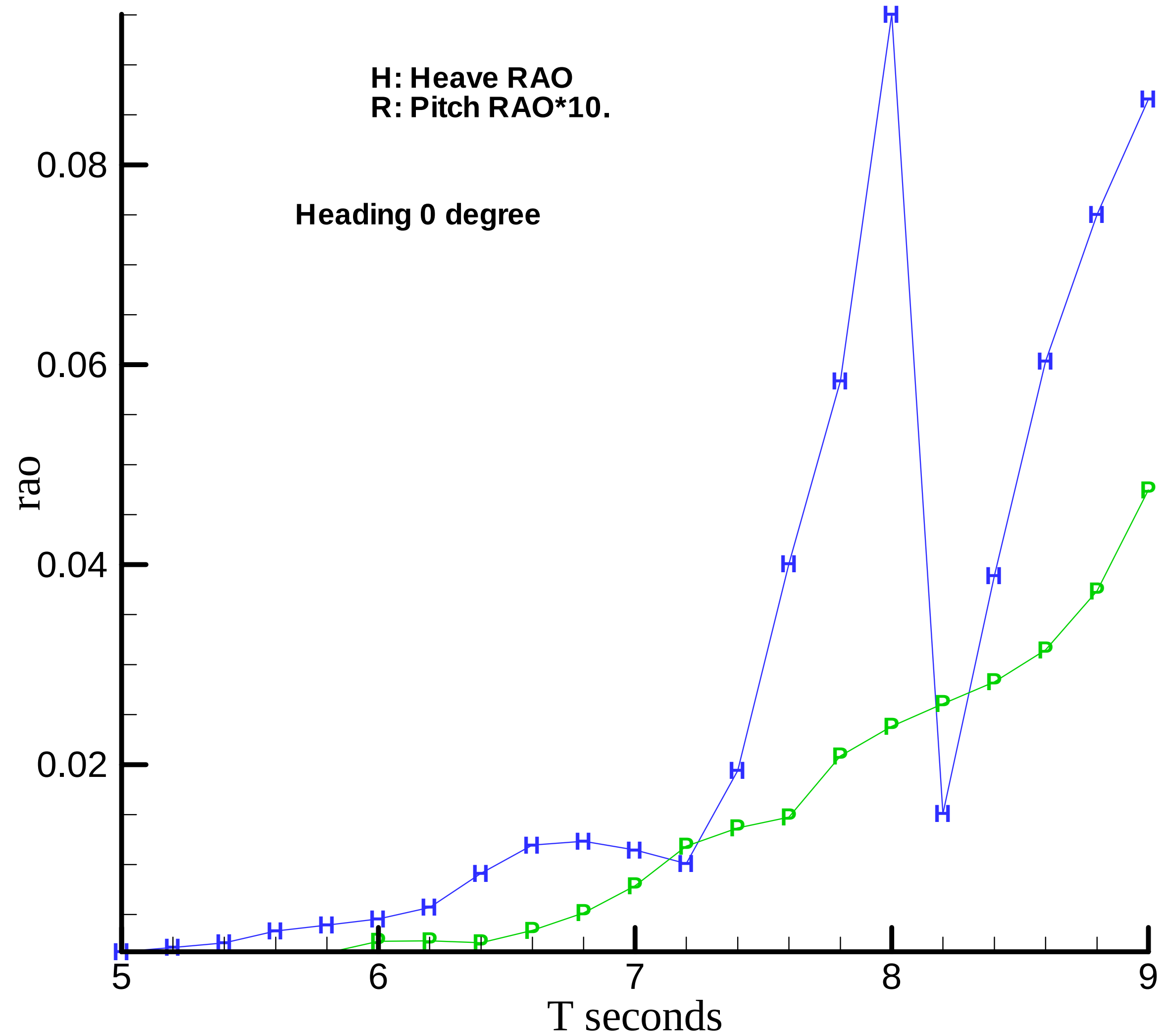
H: Heave RAO
R: Pitch RAO*10.
Heading 0 degree
0.08
0.06
0.04
0.02
rao
5
6
7
8
9
T seconds

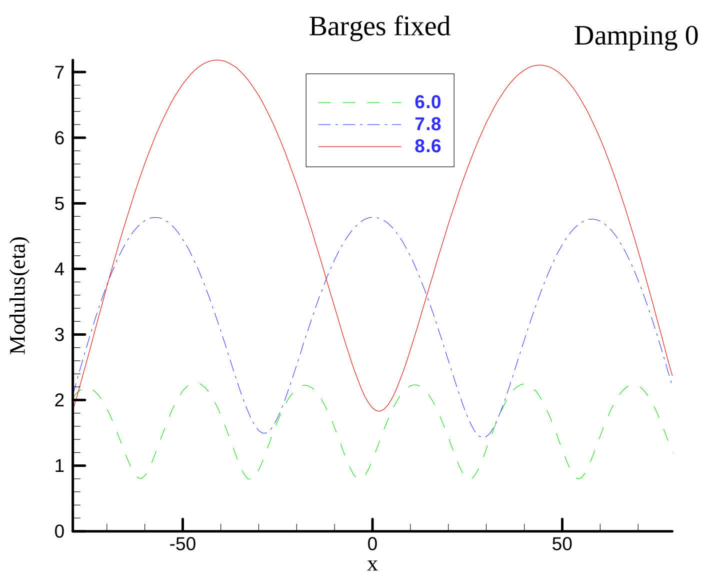
Barges fixed
Damping 0
6.0
7.8
8.6
Modulus(eta)
x

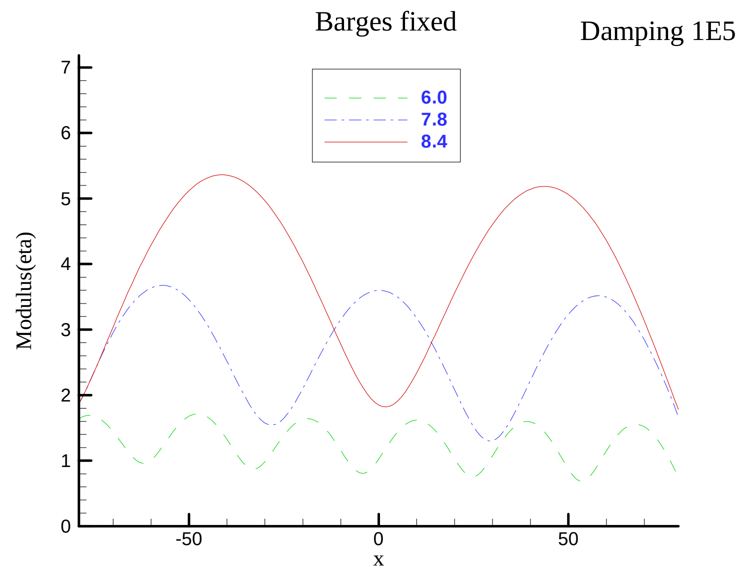
Barges fixed
Damping 1E5
6.0
7.8
8.4
Modulus(eta)
x

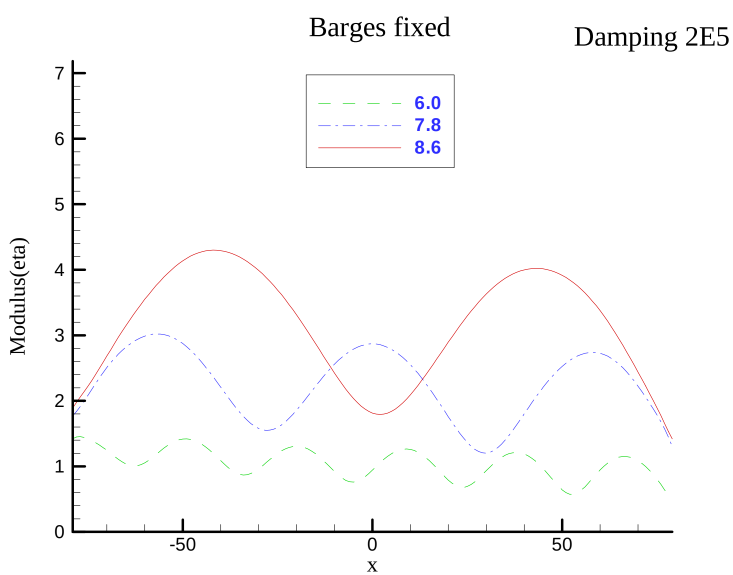
Barges fixed
Damping 2E5
6.0
7.8
8.6
Modulus(eta)
x

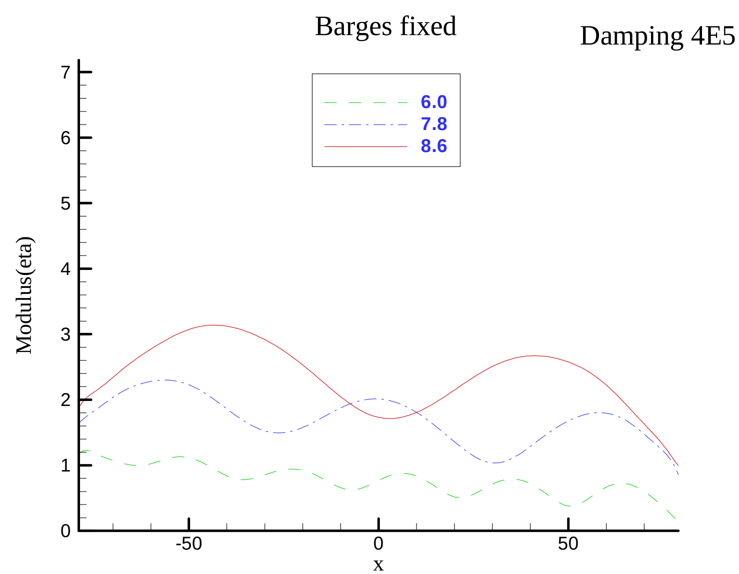
Barges fixed
Damping 4E5
6.0
7.8
8.6
Modulus(eta)
x

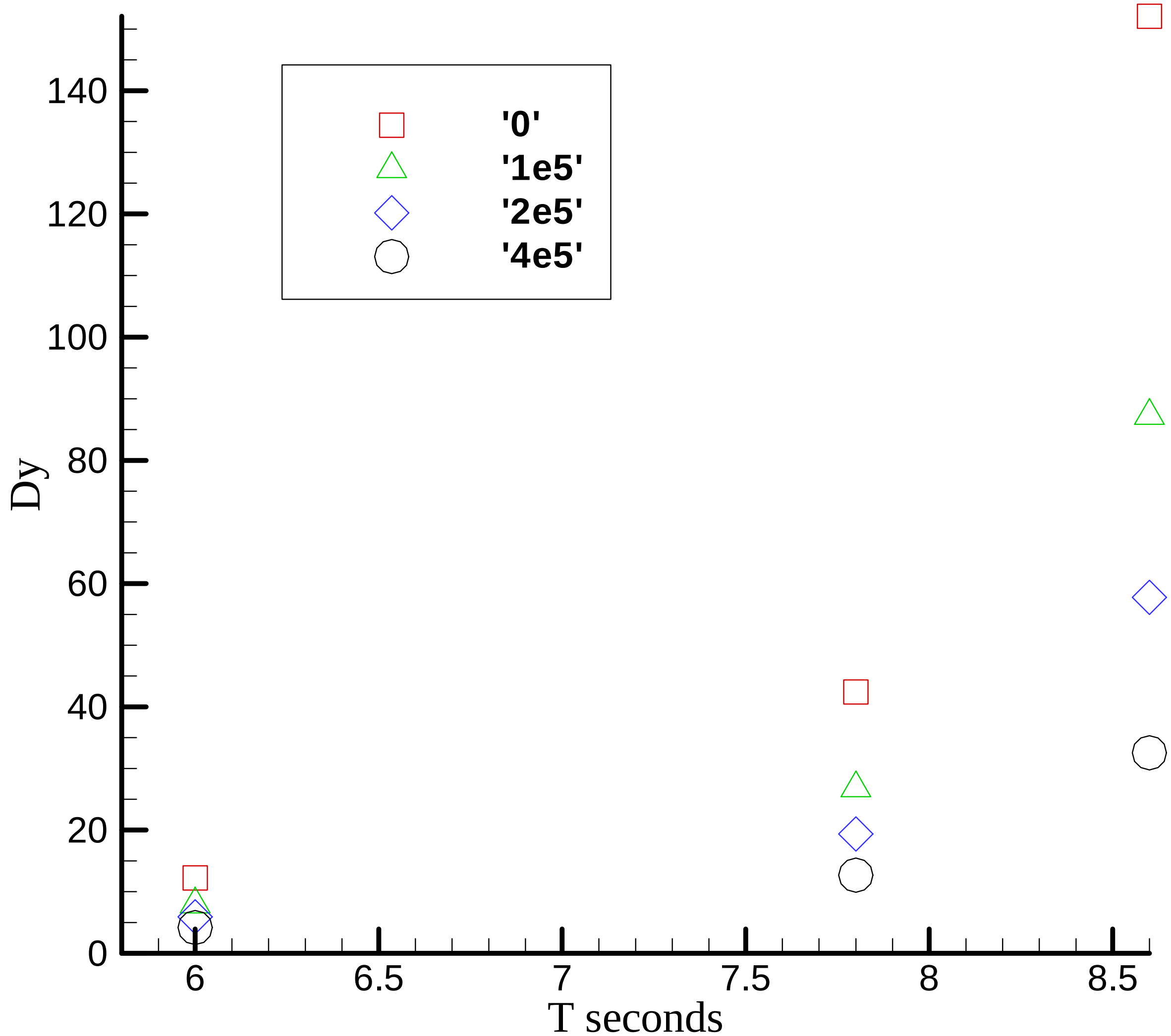
'0'
'1e5'
'2e5'
'4e5'
Dy
0
20
40
60
80
100
120
140
6
6.5
7
7.5
8
8.5
T seconds

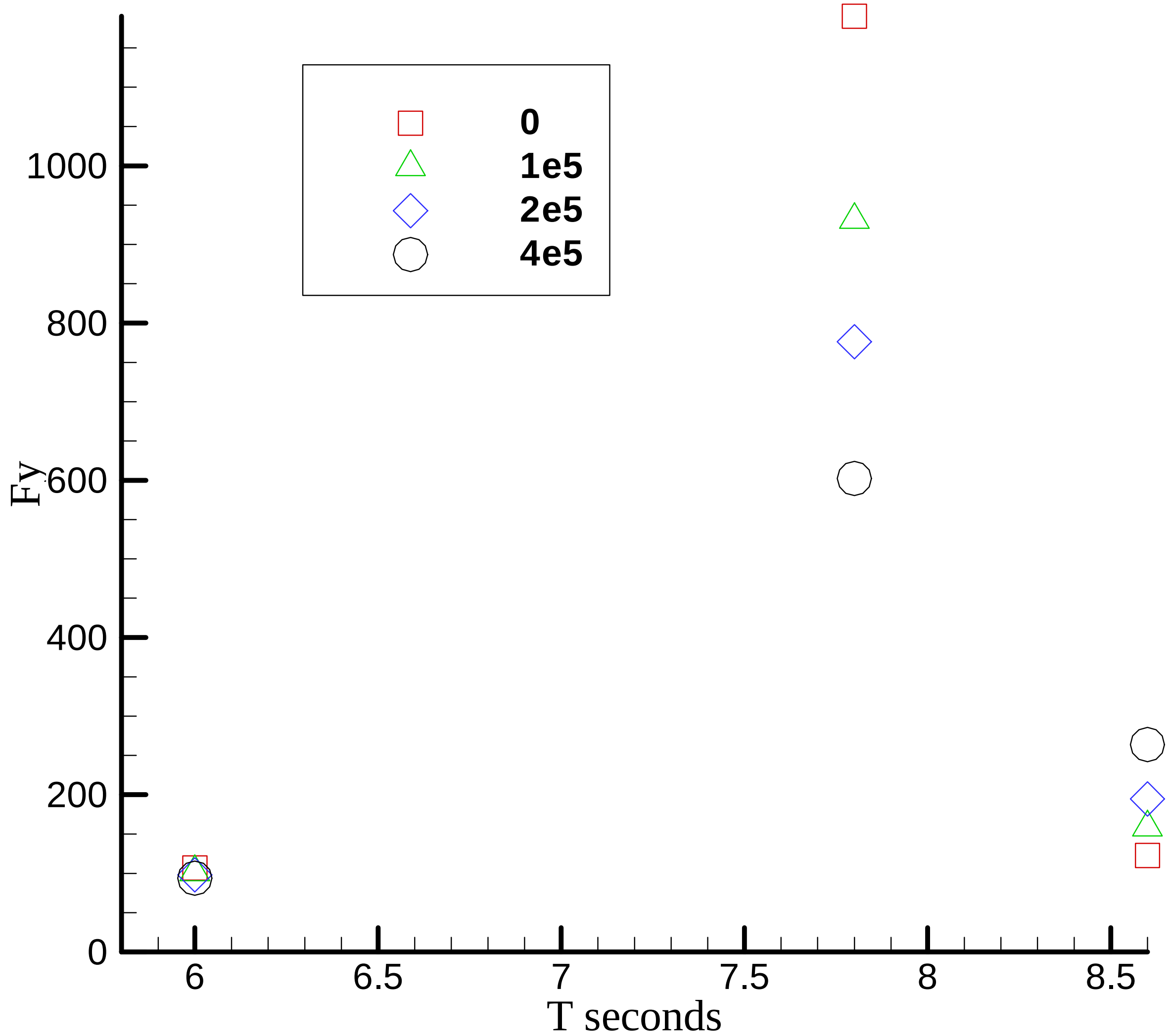

0
1e5
2e5
4e5
Fy
0
200
400
600
800
1000
6
6.5
7
7.5
8
8.5
T seconds

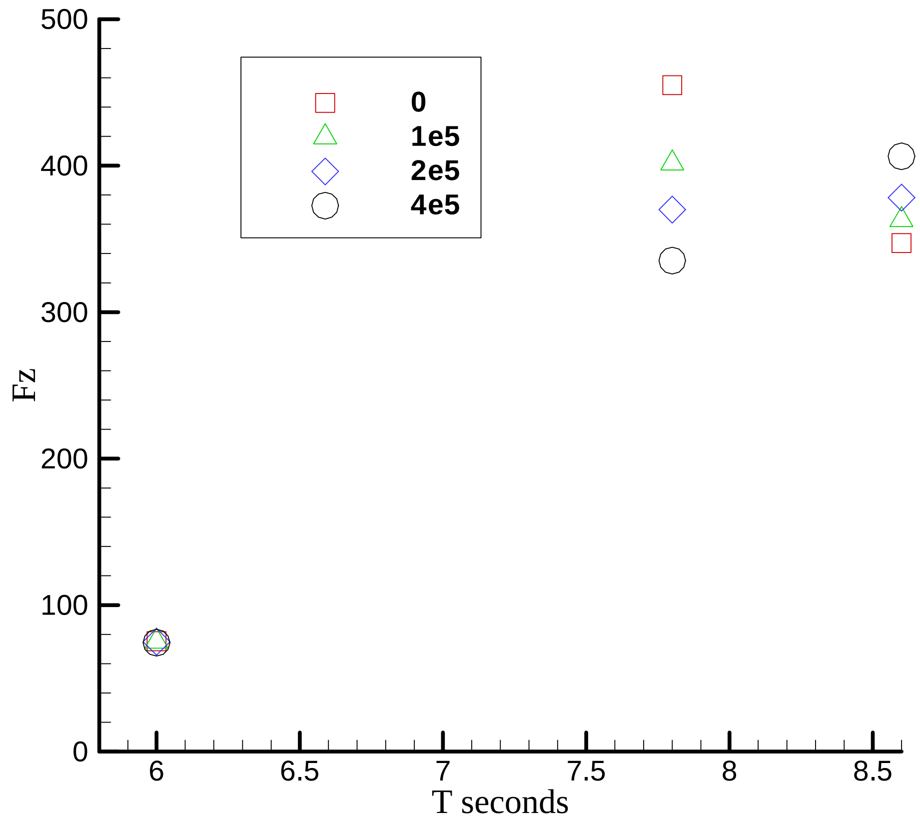

500
400
300
200
100
0
Fz
6
6.5
7
7.5
8
8.5
T seconds
0
1e5
2e5
4e5

B=0

	A22	B22	A33	B33	A55	B55	A35	B35
6.0	-1.1e4	1.7e4	2.3e5	1.6e3	3.3e8	1.8e6	9.3e0	7.7e0
7.8	-4.5e4	9.3e4	2.0e5	1.2e4	3.0e8	1.3e7	3.4e0	-9.8e0
8.6	-1.4e5	4.3e4	1.7e5	1.3e4	1.9e8	2.1e8	6.8e0	2.0e1

B=4E5

6.0	-1.1E4	2.0E4	2.3E5	2.1E3	3.3E8	2.6E6	1.2E1	5.0E0
7.8	-5.3E4	6.4E4	2.0E5	1.2E4	3.0E8	1.9E7	2.9E0	-6.2E0
8.6	-1.4E5	6.6E4	1.7E5	1.9E4	2.8E8	1.1E8	-2.6E-01	3.8E1

Table 1: Added mass and damping coefficient calculated with and without lid damping

It is showed that all conventional outputs of WAMIT can be evaluated with the lid presence

Both diffraction solution and hydrodynamic coefficients are affected by the damping on the lid.

Summing linear and 2^{nd}-order wave elevations

Using utility program FS_ELV

The linear incident wave is determined by specifying the complex wave amplitudes for all frequencies and headings under consideration.

By definition (in WAMIT), the crest of unit amplitude incident wave is above x=0 (the origin of the global coordinates system) at t=0. The phase of the complex amplitude is relative to this reference point and time.

NP=number of frequencies
NB=number of wave headings

$$\begin{aligned}
\boldsymbol{\zeta}_I^1(\mathbf{x},t) &= Real[\sum_i^{N_P}\sum_k^{N_B}\zeta_I^1(\omega_i,\beta_k)] \\
&= Real[\sum_i^{N_P}\sum_k^{N_B}A(\omega_i,\beta_k)\bar{\zeta}_I^1(\omega_i,\beta_k)] \\
&= Real[\sum_i^{N_P}\sum_k^{N_B}A(\omega_i,\beta_k)e^{i(\omega_i t-\mathbf{K}_k\cdot\mathbf{x})}]
\end{aligned}$$

Total wave elevation up to the 2nd-order is obtained by the sum of linear and sum-frequency and difference frequency components.

Linear : .6
Sum frequency : .15s
Difference frequency : .15d

$$
\begin{aligned}
\boldsymbol{\zeta}(\mathbf{x},t) &= \boldsymbol{\zeta}^1(\mathbf{x},t) + \boldsymbol{\zeta}^+(\mathbf{x},t) + \boldsymbol{\zeta}^-(\mathbf{x},t) \\
&= Real[\sum_{i=1}^{N_P}\sum_{k=1}^{N_B} \zeta^1(\mathbf{x},\omega_i,\beta_k)e^{i\omega_i t} \\
&+ \sum_{i=1}^{N_P}\sum_{j=1}^{N_P}\sum_{k=1}^{N_B}\sum_{l=1}^{N_B} \zeta^+(\mathbf{x},\omega_i,\omega_j,\beta_k,\beta_l)e^{i(\omega_i+\omega_j)t} \\
&+ \sum_{i=1}^{N_P}\sum_{j=1}^{N_P}\sum_{k=1}^{N_B}\sum_{l=1}^{N_B} \zeta^-(\mathbf{x},\omega_i,\omega_j,\beta_k,\beta_l)e^{i(\omega_i-\omega_j)t}]
\end{aligned}
$$

.6 contains normal linear pressure for all field points (including the submerged points). For field points on z=0, the output also represents the normalized linear wave elevation.

.15s and .15d contains the normalized wave elevation only for the points on the free surface. (The values of the normalized 2nd-order pressures differ from the wave elevations and they are output in .14s and .14d)

$$
\begin{aligned}
\zeta^1(\mathbf{x},\omega_i,\beta_k) &= A(\omega_i,\beta_k)\bar{\zeta}^1(\mathbf{x},\omega_i,\beta_k) \\
\zeta^+(\mathbf{x},\omega_i,\omega_j,\beta_k,\beta_l) &= (A(\omega_i,\beta_k)A(\omega_j,\beta_l)/L)\bar{\zeta}^+(\mathbf{x},\omega_i,\omega_j,\beta_k,\beta_l) \\
\zeta^-(\mathbf{x},\omega_i,\omega_j,\beta_k,\beta_l) &= (A(\omega_i,\beta_k)A^*(\omega_j,\beta_l)/L)\bar{\zeta}^-(\mathbf{x},\omega_i,\omega_j,\beta_k,\beta_l)
\end{aligned}
$$

$$
\begin{aligned}
\bar{\zeta}^+(\mathbf{x},\omega_i,\omega_j,\beta_k,\beta_l) &= \bar{\zeta}^+(\mathbf{x},\omega_j,\omega_i,\beta_k,\beta_l) \\
&\text{and} \\
\bar{\zeta}^-(\mathbf{x},\omega_i,\omega_j,\beta_k,\beta_l) &= \bar{\zeta}^{-*}(\mathbf{x},\omega_j,\omega_i,\beta_k,\beta_l)
\end{aligned}
$$

WAMIT outputs a half of the full QTF if IXSUM=2 or IXDIF=2. These are sufficient because of the symmetry relation. However complete combinations of i and j may be input to WAMIT (IXSUM=1 or IXDIF=1) but **the frequencies i is always assumed greater or equal to j for the difference frequency output**.

$$
\begin{aligned}
\boldsymbol{\zeta}(\mathbf{x},t) \quad = \quad & Real[\sum_{i=1}^{N_P}\sum_{k=1}^{N_B} A(\omega_i,\beta_k)\bar{\zeta}^1(\mathbf{x},\omega_i,\beta_k)e^{i\omega_i t} \\
+ \quad & \sum_{i=1}^{N_P}\sum_{k=1}^{N_B}\sum_{l=1}^{N_B}(A^2(\omega_i,\beta_k)/L)\bar{\zeta}^+(\mathbf{x},\omega_i,\omega_i,\beta_k,\beta_l)e^{i(\omega_i+\omega_j)t} \\
+ \quad & 2\sum_{i=1}^{N_P}\sum_{j=1}^{i-1}\sum_{k=1}^{N_B}\sum_{l=1}^{N_B}(A(\omega_i,\beta_k)A(\omega_j,\beta_l)/L)\bar{\zeta}^+(\mathbf{x},\omega_i,\omega_j,\beta_k,\beta_l)e^{i(\omega_i+\omega_j)t} \\
+ \quad & \sum_{i=1}^{N_P}\sum_{k=1}^{N_B}\sum_{l=1}^{N_B}(|A(\omega_i,\beta_k)|^2/L)\bar{\zeta}^-(\mathbf{x},\omega_i,\omega_i,\beta_k,\beta_l) \\
+ \quad & 2\sum_{i=1}^{N_P}\sum_{j=1}^{i-1}\sum_{k=1}^{N_B}\sum_{l=1}^{N_B}(A(\omega_i,\beta_k)A^*(\omega_j,\beta_l)/L)\bar{\zeta}^-(\mathbf{x},\omega_i,\omega_j,\beta_k,\beta_l)e^{i(\omega_i-\omega_j)t}]
\end{aligned}
$$

FS_ELV is an utility program combining the linear and 2nd-order wave elevation output from WAMIT and producing dimensional wave elevations for specified incident wave field

A) Required WAMIT output files:

a) .6, .15s and.15d

b) .fpt: to find the field points on the free surface

B) An additional input file to FS_ELV

***out*.FEI**

C) Output files from FS_ELV

***out*.FEO, *out*_FEO.DAT**

Input parameters in .FEI

- NUMHDR
- ULEN
- NT
- T1, DT
- NF
- IF(1),IF(2),...,IF(NF) (do not specify when NF < 0)
- NP
- IP(1),IP(2),...,IP(NP) (do not specify when NF < 0)
- NB
- IB(1),IB(2),...,IB(NB) (do not specify when NF < 0)
- ABSA(1,1),ABSA(2,1),...,ABSA(NB,1)
- ABSA(2,1),...
- ...
- ABSA(1,NP),ABSA(2,NP),...,ABSA(NB,NP)
- PHSA(1,1),PHSA(2,1),...,PHSA(NB,1)
- PHSA(2,1),...
- ...
- PHSA(1,NP),PHSA(2,NP),...,PHSA(NB,NP)

Output quantities in .FEO

- IF(1)
- T1 ELV(T1) ELV1(T1) ELVS(T1) ELVD(T1)
- T2 ELV(T2) ELV1(T2) ELVS(T2) ELVD(T2)
- .
- .
- Ti ELV(Ti) ELV1(Ti) ELVS(Ti) ELVD(Ti)
- .
- .
- TN ELV(TN) ELV1(TN) ELVS(TN) ELVD(TN)
- IF(2)
- .

An additional output _FEO.DAT for x-y plots

Computational note:

In principle, when .14s, 14d, 15s or 15d are computed the partition radius (and intermediate partition radius) should be move further out as much as the distance to the field point from the body surface

2^{nd}-order incident wave is computed in WAMIT and input wave amplitude should have linear component only t=0

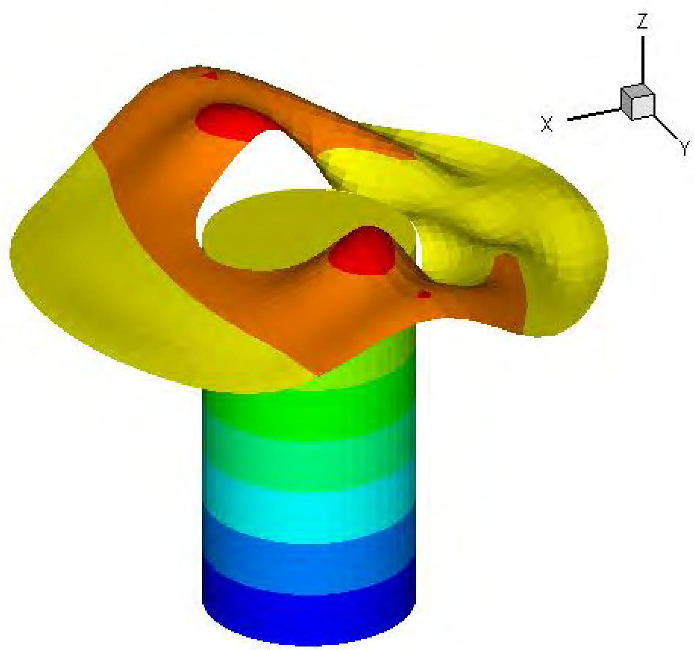

t=0.5

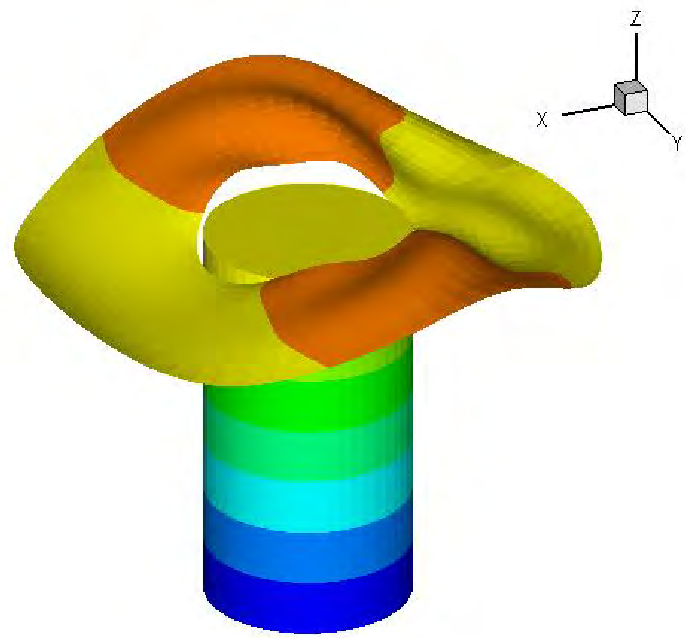

5 second wave (about 40m length) in infinite depth. Cylinder diameter is 16.8m and 35m draft. Wave amplitude is 3m
Wave direction toward negative x-axis.

t=1

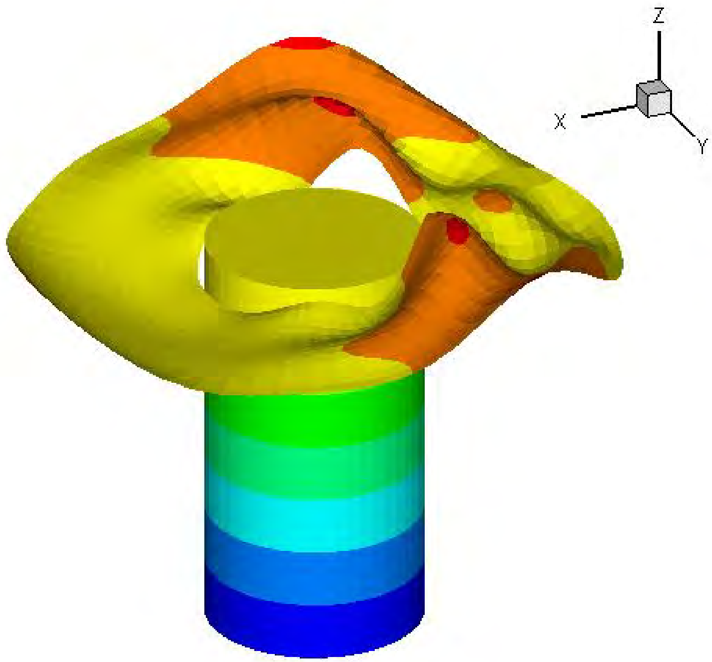

t=2

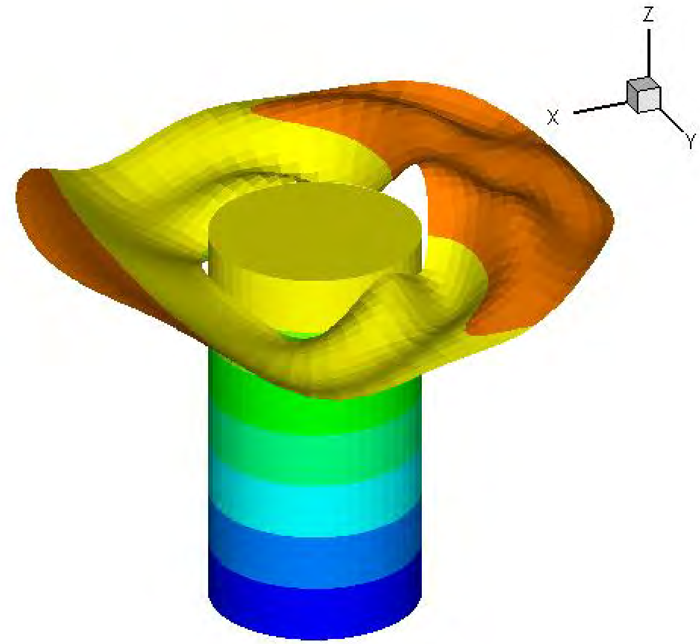

t=2

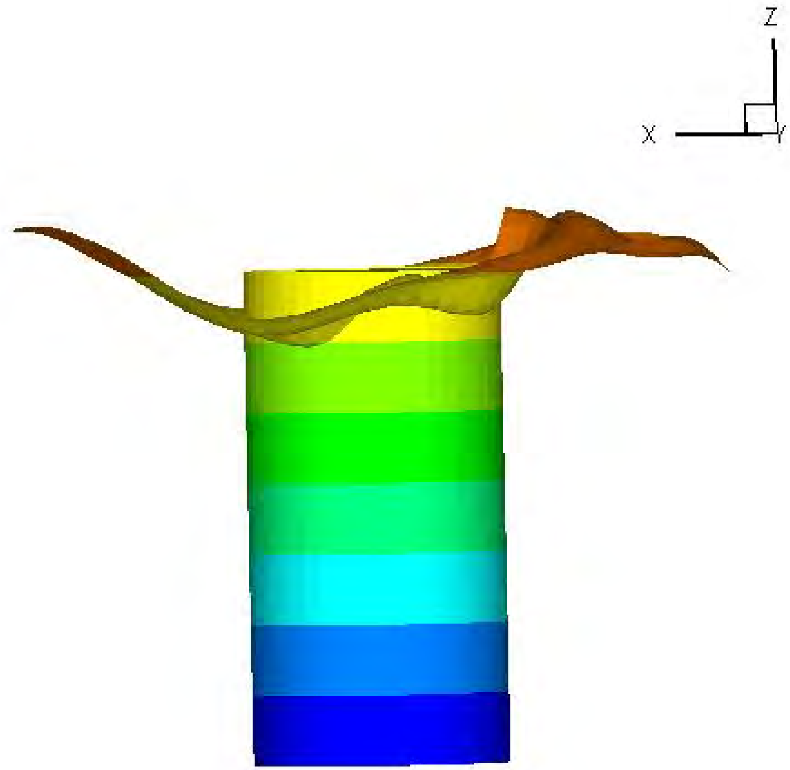

Animation using Tecplot.

- Apparently the 2nd-order effects are from locked waves

- The 2nd-order effects are conspicuous toward lee-side
  Combined with linear waves, the surface becomes steep
  i) along the side of the cylinder as the crest passes
  ii) at the lee side

Note:

- Data in FEO must be rearranged to make 3D view in Tecplot (or using other program)
  _FEO.dat can be used for 2D view (variation in time for each field point) in Tecplot

- Field points, 2048 total inside R=24m, in FRC are arranged with an order for easy conversion of the output to Tecplot format. (Points from the centroids of the free surface panels in FDF are used.)

Current Participants

Chevron

Conoco

Norsk Hydro

OTRC

Petrobras/
USP

Shell

Statoil

Marcos Ferreira
Petrobras
Cenpes-Diprex-Sedem
Cidade Universitaria Quadra 7
21949-900 Ilha do Fundao
Rio de Janeiro, Brazil
marcos.donato@petrobras.com.br

Tim Finnigan
ChevronTexaco Energy Co.
6001 Bollinger Canyon Road
Room L-4296
San Ramon, CA 94583-2324
TimFinnigan@ChevronTexaco.com

George Gu
ConocoPhillips
OF 1004, 1E & PM
600 North Dairy Ashford
Houston, TX 77079
george.z.gu@conocophillips.com

Kjell Herford
Norsk Hydro ASA
PO Box 7190
N-5020 Bergen, Norway
Kjell.Herfjord@hydro.com

Street Address
Sandsliveien 90
N-5254 Sandsli, Norway

Kazuo Nishimoto
University of Sao Paulo
Department of Naval Architecture and Ocean Engineering
2231, Av. Prof. Mello Moraes
Cidade Universitaria
Sao Paulo, SP, Brazil CEPO05508-900
knishimo@usp.br

Stergios Liapis
Shell Oil Company
Offshore Structures
3737 Bellaire Blvd.
Houston, TX 77025
stergios.liapis@Shell.Com

Rick Mercier
Offshore Technology Research Center
1200 Mariner Drive
College Station, TX 77845-3400
rmercier@civil.tamu.edu

John Niedzwecki
Offshore Technology Research Center
1200 Mariner Drive
College Station, TX 77845-3400
j-Niedzwecki@.tamu.edu

Per Teigen

STATOIL	Street Address
Postuttak	Ark, Ebbels v.10
N 7005 Trondheim	Rotvoll
Norway	Trondheim, Norway

pte@statoil.com

John Letcher
AeroHydro
54 Herrick Road/PO Box 684
Southwest Harbor, ME 04679-0684
jletcher@aerohydro.com

Michael Shook
AeroHydro
54 Herrick Road/PO Box 684
Southwest Harbor, ME 04679-0684
mshook@aerohydro.com

Michael Graham
Dept. of Aeronautics
Imperial College
London, SW7 2BY
United Kingdom
m.graham@imperial.ac.uk

Nick Newman
WAMIT
1 Bowditch Road
Woods Hole, MA 02543
jnn@mit.edu

Chang-Ho Lee
WAMIT
822 Boylston Street, Suite 202
Chestnut Hill, MA 02467
chlee@wamit.com

Appendices

NON-LINEAR WAVE INTERACTION WITH A SQUARE CYLINDER

B. Molin[1], E. Jamois[1,2], C.H. Lee[3] & J.N. Newman[4]

[1] École généraliste d'ingénieurs de Marseille, 13 451 Marseille cedex 20
[2] Saipem SA, 78 884 Saint-Quentin Yvelines cedex, France
[3] WAMIT Inc., 822 Boylston Street, Chestnut Hill, MA 02467-2504, USA
[4] 1 Bowditch Rd, Woods Hole, MA 02543, USA

1 Introduction

A companion paper offered at the workshop (Jamois *et al.*, 2005a) describes the application of a high-order Boussinesq model to oblique wave interaction with a vertical plate. This model, under development at EGIM, is further described in Jamois *et al.* (2004, 2005b). It has proved to properly reproduce the run-up effect, attributed to third-order interactions between the incoming and reflected wave-fields (Molin *et al.*, 2005).

Here we move one step backward and focus on second-order quantities, with the same aim of validating the Boussinesq model against reference results. There have been numerous studies dealing with second-order wave interaction with vertical circular cylinders (e.g. see Molin & Marion, 1986; Eatock Taylor & Hung, 1987; Newman, 1996; Ferrant, Malenica & Molin, 1999). However, in its present stage, the Boussinesq model can only handle (wall-sided) rectangular geometries, as it is based on regular cartesian discretizations in the horizontal plane. So we consider the parent case of a vertical cylinder with a square cross section, standing on the sea-floor. The first and second-order diffraction problems are solved numerically with WAMIT, convergence being assessed through successively finer discretizations. The Boussinesq model is run with incoming regular waves of such low steepnesses that no (third-order) run-up effects are observed. Fourier analysis of the time series yields fundamental and double frequency components that are compared with the results from WAMIT.

2 Test cases

In dimensional form, the waterdepth h is taken equal to 1 m, while the square cylinder side d is 2 m. WAMIT calculations have been made for two headings (0 and 45 degrees) and three wave periods (2.30, 1.45 and 1.16 s), leading to $kh = 1, 2$ and 3.

The Boussinesq model was run only at zero degree heading. Advantage was taken of the symmetry to model only one half of the square cylinder, protruding from one of the side-walls. The numerical domain has a width of 12 m and a length of 10 wavelengths, with the (half) square starting 4 wavelengths from the wave generation zone. Of these the first two are used to damp out reflected waves, meaning that they propagate freely only over two wavelengths. This short distance was chosen in order to minimize nonlinear interactions between the incoming and reflected wave systems. It might have the drawback that the second-order forcing at the free surface is confined to a small domain.

3 First-order results

We consider the case $kh = 3$ with normal incidence. The Boussinesq model was run with a wave steepness H/L equal to 0.002, leading to incoming waves of wavelengths $L = 2.094$ m. At such a low wave steepness non-linear effects do not appear. The wavemaker region is relaxed over a single wavelength in the direction of propagation. Input wave conditions are obtained using the theoretical stream function solution given by Fenton (1988). A relaxation zone and a sponge layer extending over two wavelengths allow respectively the damping of backward reflected wave fields due to the structure and of outgoing waves. The discretization used for this linear case, is $\Delta y = L/20 = 0.1047$ m, $\Delta x = 0.1043$ m (the end of the structure should lie half way between grid points) and $\Delta t = T/20 = 0.058$ s. Consequently, the half square cylinder dimensions actually are 2.09 x 1 m. The simulation was run up to a stationary state. Figure **??** show the free surface elevations around the cylinder and the vertical pressure profile at midpoint on the weather side computed by the Boussinesq model and by WAMIT. A very good agreement is obtained between the two numerical models. Some weak discrepancies appear in the vicinity of corner points. They might be linked to the local smoothing applied in the Boussinesq model.

4 Second-order results

We focus on the second-order diffraction potential at the double frequency 2ω. Figure 1 shows WAMIT results (in the case $kh = 3$) obtained through different discretizations. It shows, in non-dimensional form $(2\,\omega\,|\varphi_D^{(2)}(x, y, 0)|\,d/(g\,A^2))$, the modulus of the second-order scattered potential along the waterline, at the two headings of 0° (red) and 45° (blue). Two discretizations were used, corresponding to, respectively, 6, 9, 12 and 15 higher-order panels over one half-side of the cylinder. Similar densities have been used vertically. It can be observed that the two finest discretizations lead to quasi identical values. At lower kh values convergence is obtained more quickly.

The Boussinesq model was run at the same kh value of 3, for incoming wave steepnesses H/L of 1, 2 and 3 %. The second-order potential at $z = 0$ was derived from the potential at the free surface $\widetilde{\Phi}(x, y, \eta, t)$ by dividing it with $1 + \omega^2\,\eta/g$ and extracting the double frequency component through Fourier analysis. (At $kh = 3$ the second order incident potential is completely negligible.)

Figure **??** shows the obtained modulus of $\Phi_D^{(2)}$ on the weather side of the cylinder, compared with the results from WAMIT. The Boussinesq model provides quite similar results when the steepness varies, suggesting that the differences are actually of higher (fourth?) order. The agreement between WAMIT and the Boussinesq model can only be qualified of "fair".

These results are very preliminary. Further investigations will be presented at the workshop.

References

Eatock Taylor R. & Hung S.M. 1987 Second-order diffraction forces on a vertical cylinder in regular waves, *Applied Ocean Research*, **9**, 19-30.

Fenton J.D. 1988 The numerical solution of steady water waves problems, *Computers and Geosciences*, **14**, 357-368.

Ferrant P., Malenica Š. & Molin B. 1999 Nonlinear wave loads and runup on a vertical cylinder. In *Advances in Fluid Mechanics, Nonlinear Water Wave Interaction, WIT Press*.

Jamois E., Fuhrman D.R., Bingham H.B., Molin B. & Remy F. 2005a Oblique wave interaction with reflective structures by a high-order velocity potential Boussinesq-type model,

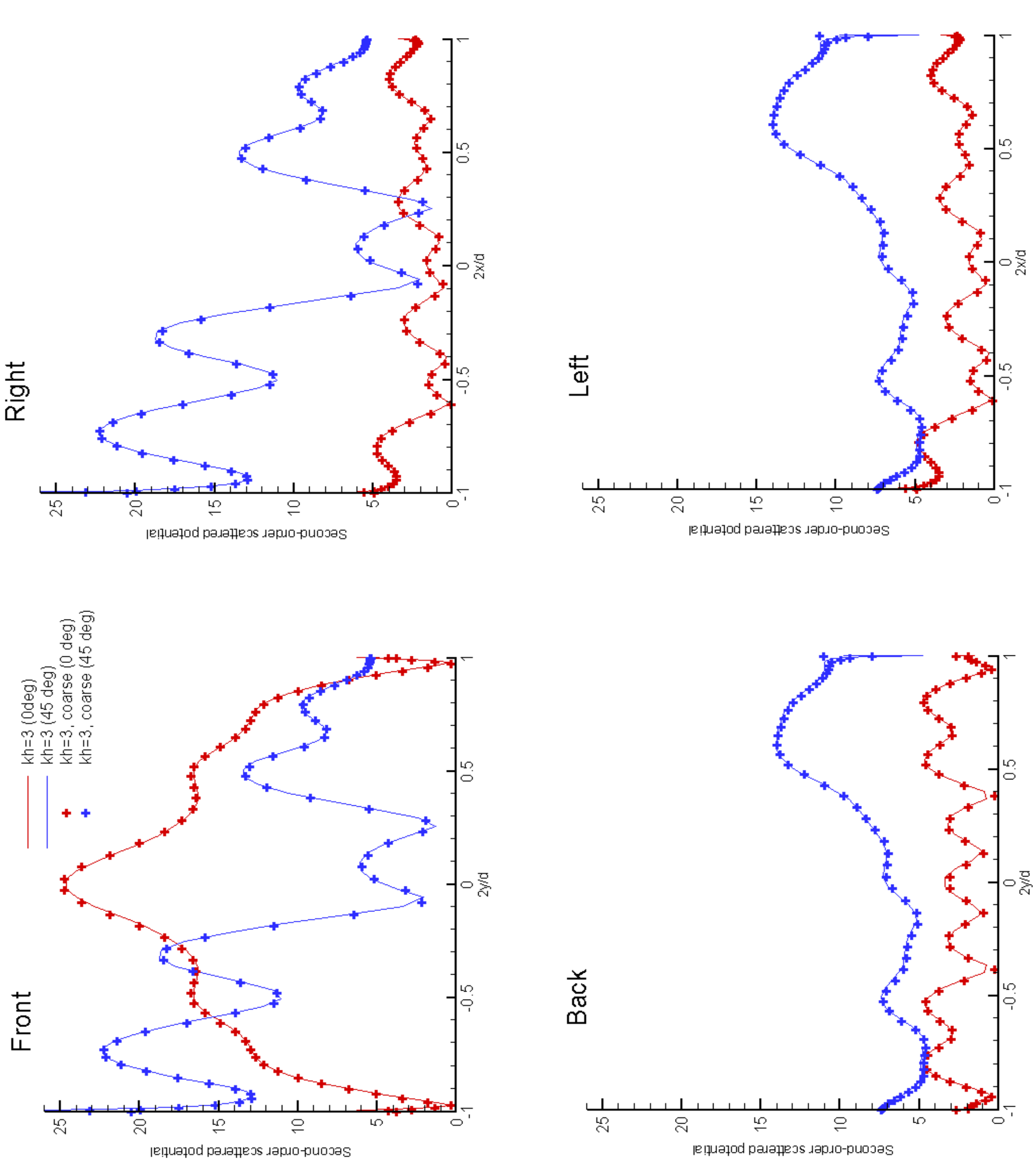

Figure 1: Second-order scattered potential along the waterline, as obtained by WAMIT. Red: heading 0°. Blue: heading 45°. Lines: 4840 and 4720 panels, respectively, on a quadrant of the body and 4720 the free surface inside of a circle of radius 2.4m. Dotted lines: 2730panels on the body and 2700 on the free surface. Gauss quadrature is applied with single precision accuracy for the interatation of forcing on the annulus of inner and outer radii of 2.4m and 5.4m. Beyond outer circle, the far field approximation is used.

abstract proposed to the 20th IWWWFB.
Jamois E., Fuhrman D.R. & Bingham H.B. 2005b Wave-structure interactions and nonlinear wave processes on the weather side of reflective structures, in preparation.
Jamois E., Kimmoun O., Molin B. & Stassen Y. 2004 Nonlinear interactions and wave run-up near a gravity base structure, *Proc. ICCE Conf.*, Lisboa.
Molin B. & Marion A. 1986 Second-order loads and motions for floating bodies in regular waves, *Proc. OMAE Conf.*, Tokyo.
Molin B., Remy F., Kimmoun O. & Jamois E. 2005 The role of tertiary wave interactions in wave-body problems, *J. Fluid Mech.*, in press.
Newman J.N. 1996 The second-order wave force on a vertical cylinder, *J. Fluid Mech.*, **320**, 417-443.

Wave effects on vessels with internal tanks

by J. N. Newman
<jnn@mit.edu>

(20th Workshop on Water Waves and Floating Bodies – Spitsbergen – 29 May - 1 June 2005)

The motions of fluid in internal tanks have important effects on the dynamic response of vessels in waves, particularly during loading and unloading operations when the tanks are partially filled. This topic is of special interest for LNG tankers and FPSO vessels. Coupled tank/ship motions have been studied by Kim (2001) and Rognebakke & Faltinsen (2001, 2003), with nonlinear analyses of the interior flow in the tanks, and by Molin *et al* (2002) and Malenica *et al* (2003) with linear analyses. In these works the tank dynamics are analysed separately from the exterior radiation and diffraction problems. The solution of the coupled equations of motion follows by combining the hydrodynamic forces for the tanks with the vessel's added-mass, damping, and exciting forces. When the tank motions are linearized, their only effect on the vessel's motions is to modify the added mass.

Recently we have extended the panel code WAMIT to analyse coupled tank/ship motions, following a unified approach where the interior wetted surfaces of the tanks are included as an extension of the conventional computational domain defined by the exterior wetted surface of the body. All of the tank and hull wetted surfaces form one large global boundary surface. The principal modification is to impose the condition that the separate fluid domains are independent. This is achieved trivially, by setting equal to zero all coefficients of the linear system for the potential where the source and field points are in different fluid domains. This is equivalent to forming separate linear equations for each domain, and concatenating these into one global system in a block-diagonal manner. The exterior free-surface Green function is used for each domain, with vertical shifts of the coordinates corresponding to the free-surface elevation in each tank.

The principal advantage of this approach is that the exterior panel code can be extended to include internal tanks with relatively few modifications. All of the usual hydrodynamic parameters can be evaluated in a similar manner as for vessels without tanks, including the added-mass and damping coefficients, exciting forces, RAO's, and the mean second-order drift forces and moments. Local values of the free-surface elevation, pressure and velocity can be evaluated both inside and outside the tanks. The geometry of the tanks can be described in the same manner as the exterior hull surface. Disadvantages include the larger size of the linear system, which implies some loss of computational efficiency, and the need to re-run the complete interior/exterior analysis in situations where only one or the other is changed, e.g. when the tank depths are modified. Since the entire analysis is linearized, nonlinear sloshing effects are not included.

It is not obvious that a conventional exterior panel code can be applied to an internal problem. We have found the higher-order method to be robust in this respect, with B-spline representation of the solution and accurate definitions of the geometry. The low-order panel method also appears to work for tanks, although with somewhat slower convergence. Computations have been made for various vessels, including the barge model studied by Molin *et al* (2002) where experimental and computational data are available for comparison. Some of these results are shown by Newman (2004).

Results are presented here for the hemispheroid shown in Figure 1. This vessel has three internal tanks, with the same depth of fluid in each tank. The tank lengths are the same, but the widths and elevations are different. Figure 2 shows the first-order motions and drift force in beam waves, for three relative densities of the tank fluid (ρ=0, 0.5, 1.0). The total displacement and waterline plane are fixed as the tank density is varied. The results with zero density are equivalent to the conventional case without internal tanks. All results are normalized by the exterior fluid density, gravity, wave amplitude, and a characteristic length scale of 1m, and plotted vs. the nondimensional wavenumber $Ka = \omega^2 a/g$, where ω is the radian frequency and a=1m is the maximum radius of the spheroid. The vertical center of gravity is in the waterplane, and the radii of gyration are k_x=50cm, and $k_y = k_z$=3m.

Figure 3 shows the six principal added-mass coefficients, normalized by the mass of fluid displaced by the hull. Since the added mass is the sum of the separate pressure forces on the hull and tanks, the coefficients in Figure 3 are linear functions of the tank density.

Most of the added-mass coefficients are singular at the resonant periods of antisymmetric sloshing modes. The surge resonance at Ka=1.184 is the same for all three tanks. In sway there are two resonant frequencies (Ka=1.653, 2.427) due to the different widths. The first singularity in yaw corresponds to the sway mode of the outer tanks (Ka=2.427); the second smaller singularity is associated with the diagonal sloshing mode of the center tank (Ka=2.922).

At resonance the added-mass coefficients tend to $\pm\infty$. This explains the rapid fluctuations of the RAO's shown in Figure 2. The sway RAO approaches zero at the resonant frequencies, where the added mass is infinite. At slightly higher frequencies, where the negative added mass cancels the body mass, the RAO is large. Since the hull is axisymmetric there is no moment from the external pressure, but the tanks induce roll motions when the density is nonzero.

For heave the tank fluid translates uniformly and the RAO is not affected. The frequency-dependence of the tank component of the heave added mass is an interesting feature in Figure 3. The velocity potential in each tank is $\phi = (z_t - 1/K)$, per unit heave velocity, where z_t is the local vertical coordinate above the tank free surface and the constant $1/K$ is required by the free-surface condition. Thus, for a tank with volume V_t and waterplane area S_t, the added mass is $\rho_t(V_t - S_t/K)$. In the equations of motion the contribution from the term S_t/K is canceled by the hydrostatic restoring force.

The most surprising results are the sharp reductions in the sway drift force, which coincide with the peak sway response. From momentum conservation the tanks only affect the horizontal drift force indirectly, by modifying the motions of the hull. Since roll has no effect, the reduced drift force is associated primarily with the sway RAO.

References

Kim, Y., 2001, 'Coupled analysis of ship motions and sloshing flows,' 16th IWWWFB, Hiroshima.

Malenica, Ŝ., Zalar, M. & Chen, X. B. 2003, 'Dynamic coupling of seakeeping and sloshing,' Paper No. 2003-JSC-267, ISOPE.

Molin, B., Remy, F., Rigaud, S., & de Jouette, Ch., 2002, 'LNG-FPSO's: frequency domain, coupled analysis of support and liquid cargo motions,' IMAM Conf., Rethymnon, Greece.

Newman, J.N., 2004, 'Progress in wave load computations on offshore structures', Invited Lecture, 23th OMAE Conference, Vancouver, Canada, http://www.wamit.com/publications.

Rognebakke, O. F. & Faltinsen, O. M., 2001, 'Effect of sloshing on ship motions,' 16th IWWWFB, Hiroshima.

Rognebakke, O. F. & Faltinsen, O. M., 2003, 'Coupling of sloshing and ship motions,' *J. Ship Research,* **47**, 3, 208-221.

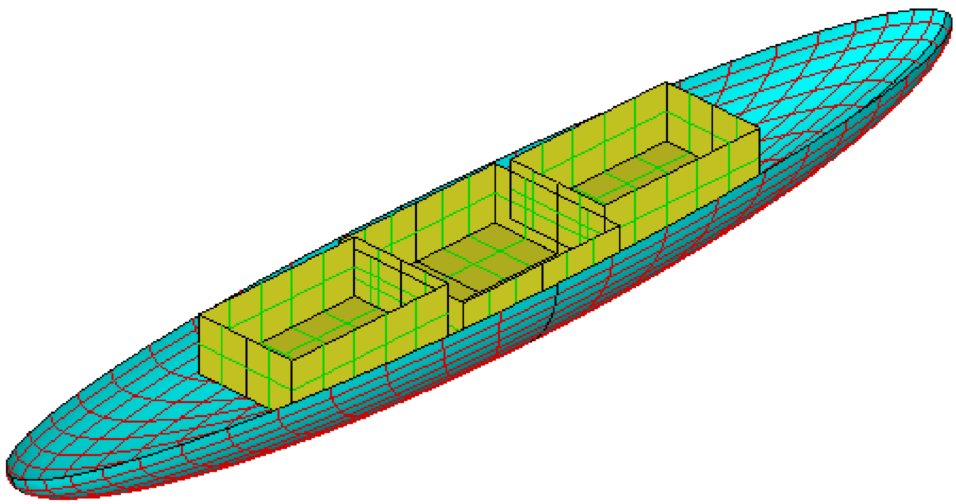

Figure 1: Perspective view of the spheroidal hull. The length is 12m and the midship section is a semi-circle of radius 1m. Each tank is 2m long, and 62.5cm deep. The tank widths are 120cm, 160cm, and 120cm. The free surfaces are at $z=$ 25cm, 12.5cm, and 25cm above the exterior waterplane.

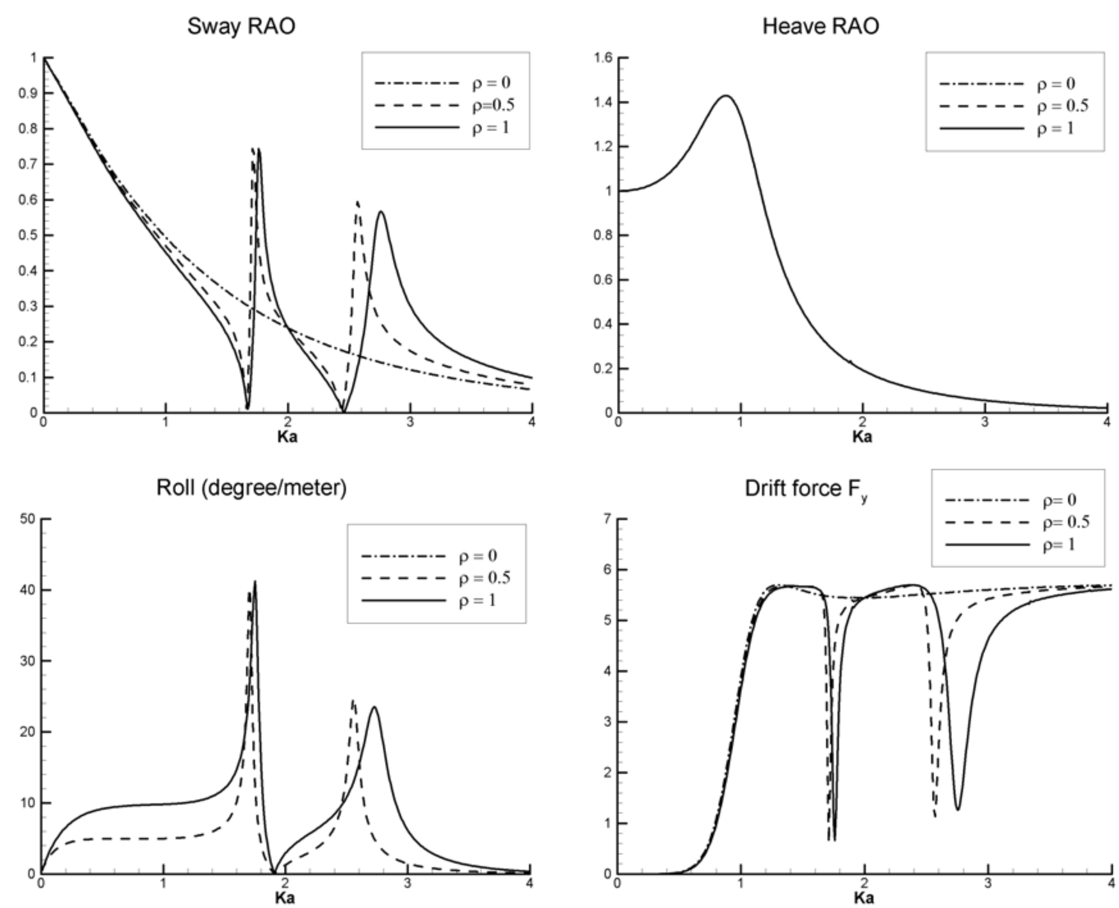

Figure 2: RAO's and drift force for the spheroidal hull in beam waves.

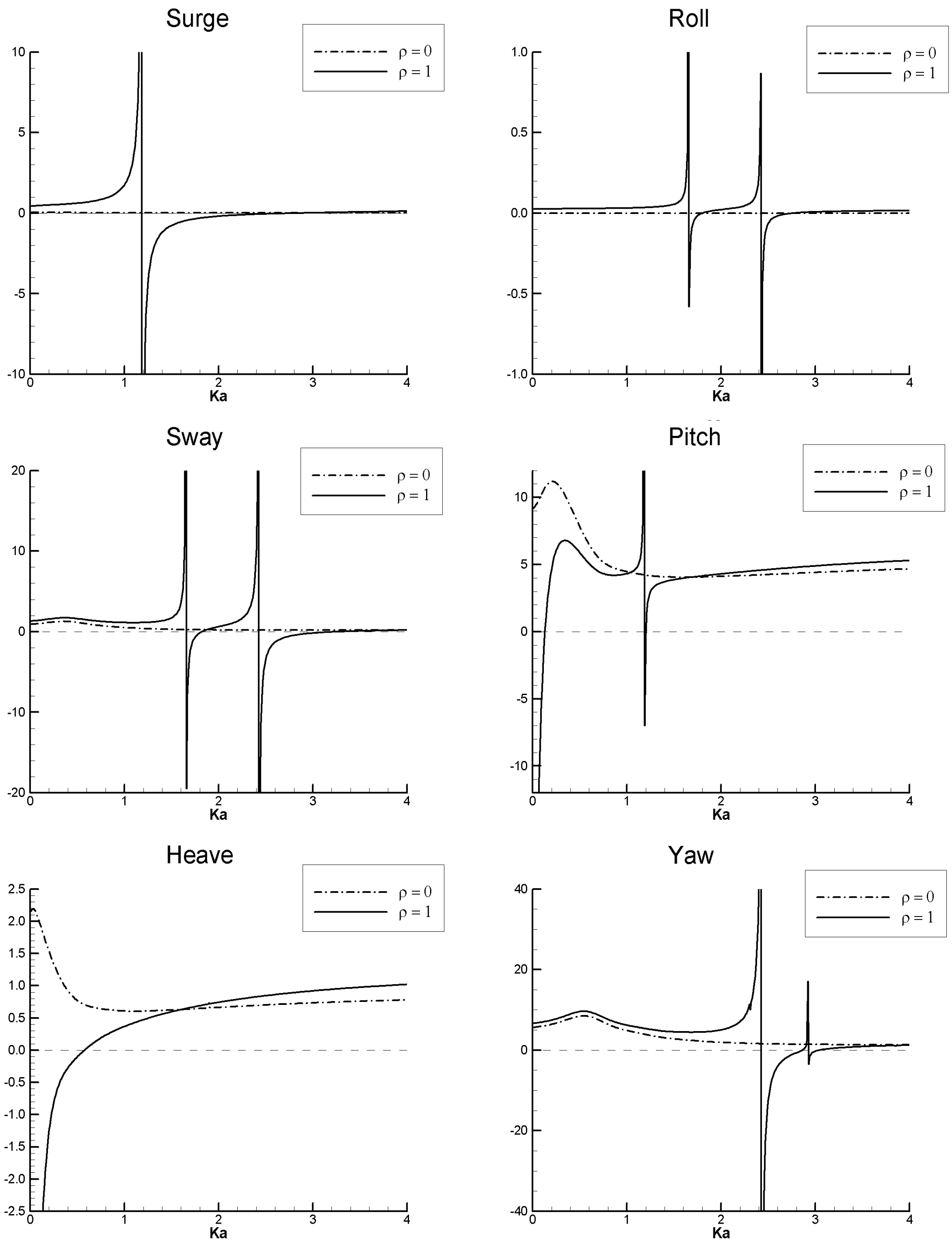

Figure 3: Added-mass coefficients of the spheroidal hull. All coefficients are normalized by the displaced mass and a length of 1m.

Note on the effect of sway spring restoring

by J. N. Newman
<jnn@mit.edu>

January 2, 2005

The following figures show the effects of an external spring restoring force applied to the sway mode only, for the spheroid in beam seas and for the FPSO in beam seas and bow seas. The drift force plots include the fixed case, where all motions are zero, shown by the dashed lines.

The spheroid has maximum radius $a = 1$m and a length of 12m. The FPSO has a length of 300m, beam 50m, draft 15m. The characteristic length scale and density are equal to one. Roll is in degrees per meter. VCG=0.0.

In beam seas an optimum spring constant k reduces the drift force, except for long waves. It appears that this is primarily due to the phase shift of the sway motion. For example, comparing the spheroid results at Ka=1.6, for k=0 and k=500, the sway RAO's have the same magnitude but substantially different drift forces, and the phases differ by about 100 degrees. Surprisingly, it seems that the reduced drift force occurs when the sway drift is out of phase with the orbital motion of the incident wave.

In bow seas, where the sway amplitude is relatively small, the effect of the springs is negligible.

There is a small irregularity in the spheroid drift force near Ka=4.5, probably due to irregular frequency effects. IRR=0 is used for all of the present results.

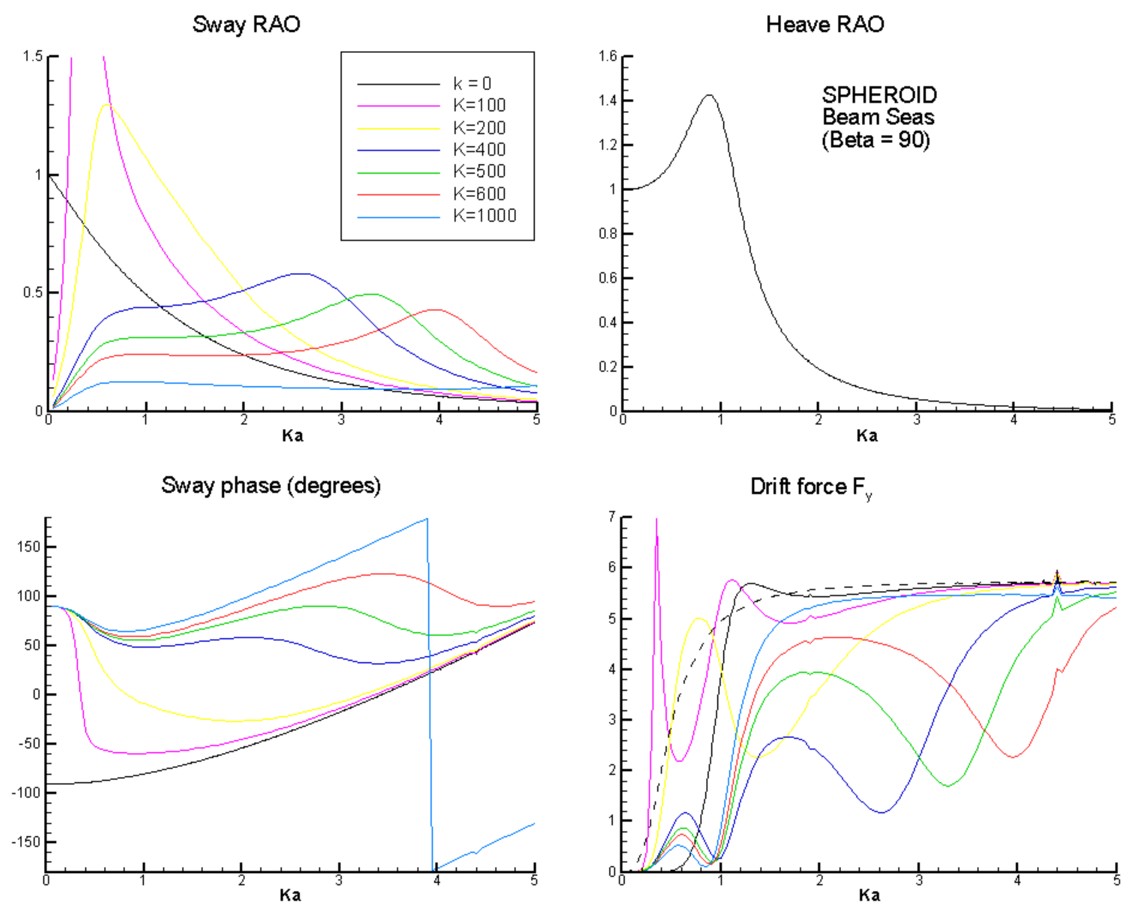

Figure 1: RAO's and drift force for the spheroidal hull in beam waves.

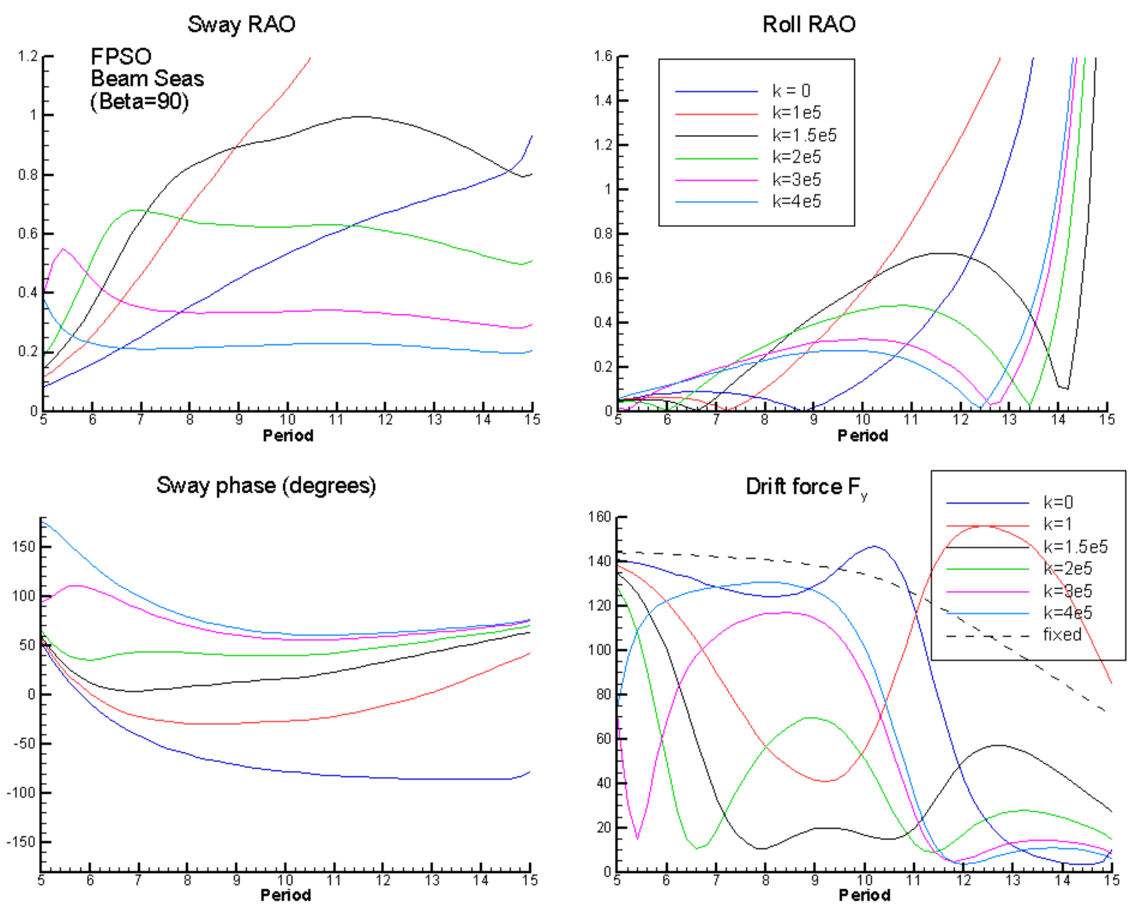

Figure 2: RAO's and drift force for the FPSO hull in beam waves.

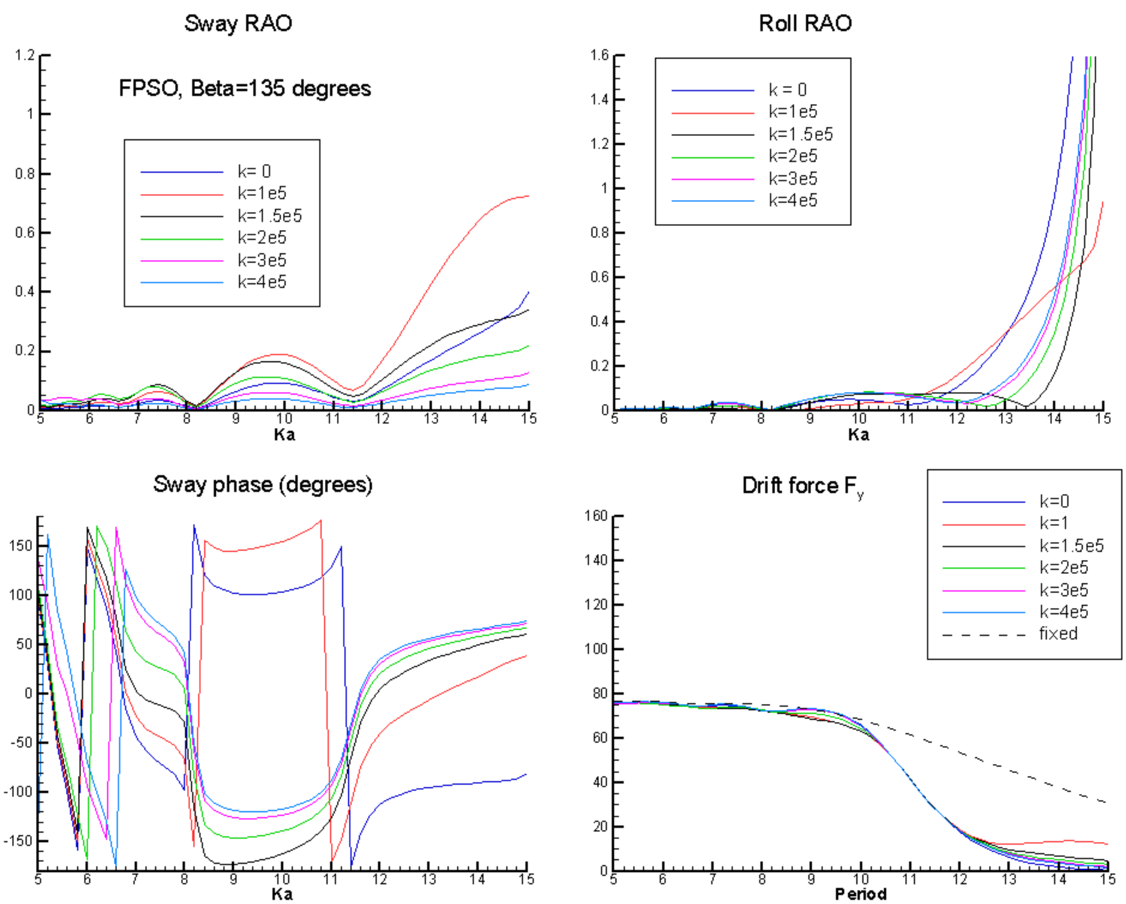

Figure 3: RAO's and drift force for the FPSO hull in bow waves ($\beta = 135°$).

Evaluation of quadratic forces using control surfaces

Chang-Ho Lee

October 10, 2005

1 Summary

The quadratic forces contribute to the excitation at low or high frequencies than those of incident waves which may be important for the analysis of structures with certain resonance features. The forces can be evaluated in principle by the integration of the quadratic pressure over the instantaneous wetted surface. As a special case, the mean drift force can also be evaluted using momentum conservation principle. The momentum conservation over entire fluid volume is advantageous in terms of accuracy and computational efficiency. But only the horizontal forces and vertical moment on a single body can be obtained from this approach and thus not applicable, for example, for multiple body interactions or bodies near the infinite walls (WAMIT low order option has this capability). The pressure integrations have been applied for these cases as well as for full quadratic force transfer functions.

The computational accuracy of the quadratic pressure forces is generally worse than that of the first order forces and it requires significanly more refined descritization entailing increased computing time. This is because of the evaluation of first order fluid velocity is, in general, less accurate than the pressure on the body surface or in its proximity. When the body has sharp corners, the quadratic pressure near the corner is singular, though integrable, and it renders the computational result significantly inaccurate. Nonuniform discretization near the corner (Lee and Newman (1992)[1] in the low order method or nonuniform mapping in the higher order method (Lee, Farina, and Newman,(1998)) [2] do produce more accurate results than otherwise. However the convergence of the results is still very poor.

Ferreira and Lee (1994)[3] applied momentum conservation over finite volume surrounting the structures. The force on the body is then evaluated by the momentum flux through the control surface enclosing the body. The computational result is significantly more accurate by avoiding evaluation of the fluid velocity on the body surface. Recently Chen (2005)[4] transformed the pressure integration over the body surface into those both on the body and control surfaces in the evaluation of the quadratic forces. For monochromatic waves, the difference frequency forces should be the same as Ferreira and Lee(1994). One obvious advantage of this new expression is the fluid velocity is not required on the body surface for fixed body for the bichromatic waves. It is also suggested, even for the moving body, that accuracy would improve for low frequency forces.

In this note, we rederived these expressions for quadratice forces.

[1]Lee, C.-H. and Newman, J. N. "Sensitivity of wave loads to the discretization of bodies" BOSS '92, London.

[2]Lee C.-H., Farina L., and Newman J. N., "A Geometry-Independent Higher-Order Panel Method and its Application to WaveBody Interactions", Engineering Mathematics and Applications Conference, Adelaide, 1998.

[3]Ferreira, M. D., and Lee, C.-H. "Computation of second-order mean wave forces and moments in multibody interaction," BOSS '94, MIT

[4]Chen X.-B. "Computation of low-frequency loads by the middle-field formulation' 20th workshop for water waves and floating bodies", 2005

2 Quadratic forces

In WAMIT V6.2 User Manual (2005), the quadratic forces and moments take forms,

$$
\begin{aligned}
\vec{F}^{(2)} &= \frac{1}{2}\rho g \int_{WL} \vec{n}[\zeta - \Xi_3]^2 (1-n_z^2)^{-\frac{1}{2}} dl \\
&\quad -\rho \iint_{S_b} \vec{n}(\frac{1}{2}\nabla\phi \cdot \nabla\phi + \vec{\Xi}\cdot\nabla\phi_t) ds + \vec{\alpha}\times(\vec{F}_D^{(1)} + \vec{F}_S^{(1)}) \\
&\quad -\rho g A_{wp}[\alpha_1\alpha_3 x_f + \alpha_2\alpha_3 y_f + \frac{1}{2}(\alpha_1^2+\alpha_2^2)Z_o]\vec{k}
\end{aligned} \tag{1}
$$

$$
\begin{aligned}
\vec{M}^{(2)} &= \frac{1}{2}\rho g \int_{WL} (\vec{x}\times\vec{n})[\zeta - (\Xi_3)]^2 (1-n_z^2)^{-\frac{1}{2}} dl \\
&\quad -\rho \iint_{S_b} (\vec{x}\times\vec{n})(\frac{1}{2}\nabla\phi\cdot\nabla\phi + \vec{\Xi}\cdot\nabla\phi_t) ds \\
&\quad +\vec{\alpha}\times\vec{M}_D^{(1)} + \vec{\xi}\times(\vec{F}_D^{(1)} + \vec{F}_S^{(1)}) \\
&\quad +\rho g[-A_{wp}(\xi_3\alpha_3 x_f + \frac{1}{2}(\alpha_1^2+\alpha_2^2)Z_o y_f) - 2\alpha_1\alpha_3 L_{12} + \alpha_2\alpha_3(L_{11}-L_{22}) \\
&\quad +\forall(\alpha_1\alpha_2 x_b - \frac{1}{2}(\alpha_1^2+\alpha_3^2)y_b)]\vec{i} \\
&\quad +\rho g[-A_{wp}(\xi_3\alpha_3 y_f - \frac{1}{2}(\alpha_1^2+\alpha_2^2)Z_o x_f) + 2\alpha_2\alpha_3 L_{12} + \alpha_1\alpha_3(L_{11}-L_{22}) \\
&\quad +\forall\frac{1}{2}(\alpha_2^2+\alpha_3^2)x_b)]\vec{j} \\
&\quad +\rho g[A_{wp}\xi_3(\alpha_1 x_f + \alpha_2 y_f) + (\alpha_1^2-\alpha_2^2)L_{12} + \alpha_1\alpha_2(L_{22}-L_{11})]\vec{k}
\end{aligned} \tag{2}
$$

where

$$
\begin{aligned}
\vec{F}_D^{(1)} &= -\rho \iint_{S_b} \vec{n}\phi_t ds \\
\vec{F}_S^{(1)} &= -\rho g A_{wp}(\xi_3 + \alpha_1 y_f - \alpha_2 x_f)\vec{k}
\end{aligned} \tag{3}
$$

$$
\vec{M}_D^{(1)} = -\rho \iint_{S_b} (\vec{x}\times\vec{n})\phi_t ds \tag{4}
$$

$$
\vec{\Xi} = \vec{\xi} + \vec{\alpha}\times x \qquad (\Xi_3 = \xi_3 + \alpha_1 y - \alpha_2 x) \tag{5}
$$

ζ is the first order runup, A_{wp} is the waterplane area and $\forall$ is the volume of the body. In addition (x_f, y_f) are the coordinates of the center of flotation, (x_b, y_b, z_b) are the coordinates of the center of buoyancy, $(\vec{i}, \vec{j}, \vec{k})$ are positive unit vectors relative to the x, y, z coordinates, and $L_{ij} = \int_{wp} x_i x_j ds$ denotes the moments of the waterplane area.

In equations (1) and (2), the contributions from the quadratic of Ξ_3 in the waterline integral are purely hydrostatic[5] and they are added, along with the contributions from F_S, with other hydrostatic forces and moments (See Appendix A) to have

$$\begin{aligned}\vec{F}^{(2)} &= \frac{1}{2}\rho g \int_{WL} \vec{n}'(\zeta^2 - 2\zeta\Xi_3)dl \\ &-\rho \iint_{S_b} \vec{n}(\frac{1}{2}\nabla\phi\cdot\nabla\phi + \vec{\Xi}\cdot\nabla\phi_t)ds + \vec{\alpha}\times\vec{F}_D^{(1)} \\ &+F_S^{(2)}\end{aligned} \tag{6}$$

$$\begin{aligned}\vec{M}^{(2)} &= \frac{1}{2}\rho g \int_{WL} (\vec{x}\times\vec{n}')(\zeta^2 - 2\zeta\Xi_3)dl \\ &-\rho \iint_{S_b} (\vec{x}\times\vec{n})(\frac{1}{2}\nabla\phi\cdot\nabla\phi + \vec{\Xi}\cdot\nabla\phi_t)ds \\ &+\vec{\alpha}\times\vec{M}_D^{(1)} + \vec{\xi}\times\vec{F}_D^{(1)} \\ &+M_S^{(2)}\end{aligned} \tag{7}$$

$F_S^{(2)}$ and $M_S^{(2)}$ are given in Appendix A.

In the above equations, we focus on two terms containing fluid velocity

$$I = -\rho \iint_{S_b} \vec{n}(\frac{1}{2}\nabla\phi\cdot\nabla\phi + \vec{\Xi}\cdot\nabla\phi_t)ds \tag{8}$$

and

$$J = -\rho \iint_{S_b} (\vec{x}\times\vec{n})(\frac{1}{2}\nabla\phi\cdot\nabla\phi + \vec{\Xi}\cdot\nabla\phi_t)ds \tag{9}$$

and as shown in Appendix B, these terms are tranformed into integrals including the control surfaces to have the results

$$\begin{aligned}\vec{F}^{(2)} &= \frac{1}{2}\rho g \int_{WL} \vec{n}'\zeta^2 dl - \rho g \int_{WL} [\zeta(\vec{\Xi}\cdot\vec{n}')]\hat{k}dl \\ &- \rho \iint_{S_{c+f}} [\nabla\phi\frac{\partial\phi}{\partial n} - \frac{1}{2}\vec{n}(\nabla\phi\cdot\nabla\phi)]ds \\ &+ F_S^{(2)} \\ &- \rho \iint_{S_b} [\nabla\phi(\frac{d\vec{\Xi}}{dt}\cdot\vec{n}) + (\Xi\cdot\vec{n})\nabla\phi_t]ds\end{aligned} \tag{10}$$

$$\vec{M}^{(2)} = \frac{1}{2}\rho g \int_{WL} (\vec{x}\times\vec{n}')\zeta^2 dl - \rho g \int_{WL} \zeta(\vec{\Xi}\cdot\vec{n}')(\vec{x}\times\hat{k})dl$$

[5]In the subsequent derivation, we ignore the vertical components of the waterline integral assuming that the body is wallsided

$$
\begin{aligned}
&- \quad \rho \iint_{S_{c+f}} [(\vec{x} \times \nabla\phi)\frac{\partial\phi}{\partial n} - \frac{1}{2}(\vec{x} \times \vec{n})(\nabla\phi \cdot \nabla\phi)]ds \\
&+ \quad \vec{M}_S^{(2)} \\
&- \quad \rho \iint_{S_b} [(\vec{x} \times \nabla\phi)(\frac{d\vec{\Xi}}{dt} \cdot \vec{n}) + (\Xi \cdot \vec{n})(\vec{x} \times \nabla\phi_t)]ds
\end{aligned} \tag{11}
$$

The first waterline integral can be transferred to the integrals over the free surface and boundary of control surface on the free surface as shown in Appendix C

$$
\begin{aligned}
\vec{F}^{(2)} \quad &= \quad -\frac{1}{2}\frac{\rho}{g}\int_{CL} \vec{n}'\phi_t^2 dl - \rho g \int_{WL} [\zeta(\vec{\Xi} \cdot \vec{n}')]\hat{k}dl \\
&- \quad \rho \iint_{S_c} [\nabla\phi\frac{\partial\phi}{\partial n} - \frac{1}{2}\vec{n}(\nabla\phi \cdot \nabla\phi)]ds \\
&- \quad \rho \iint_{S_f} [\nabla\phi\frac{\partial\phi}{\partial n} - \frac{1}{2}\vec{n}(\nabla\phi \cdot \nabla\phi)]ds + \frac{\rho}{g}\iint_{S_f} \phi_t\nabla'\phi_t ds \\
&+ \quad \vec{F}_S^{(2)} \\
&- \quad \rho \iint_{S_b} [\nabla\phi(\frac{d\vec{\Xi}}{dt} \cdot \vec{n}) + (\Xi \cdot \vec{n})\nabla\phi_t]ds
\end{aligned} \tag{12}
$$

$$
\begin{aligned}
\vec{M}^{(2)} \quad &= \quad -\frac{1}{2}\frac{\rho}{g}\int_{CL} (\vec{x} \times \vec{n}')\phi_t^2 dl - \rho g \int_{WL} \zeta(\vec{\Xi} \cdot \vec{n}')(\vec{x} \times \hat{k})dl \\
&- \quad \rho \iint_{S_c} [(\vec{x} \times \nabla\phi)\frac{\partial\phi}{\partial n} - \frac{1}{2}(\vec{x} \times \vec{n})(\nabla\phi \cdot \nabla\phi)]ds \\
&- \quad \rho \iint_{S_f} [(\vec{x} \times \nabla\phi)\frac{\partial\phi}{\partial n} - \frac{1}{2}(\vec{x} \times \vec{n})(\nabla\phi \cdot \nabla\phi)]ds + \frac{\rho}{g}\iint_{S_f} \phi_t(\vec{x} \times \nabla'\phi_t)ds \\
&+ \quad \vec{M}_S^{(2)} \\
&- \quad \rho \iint_{S_b} [(\vec{x} \times \nabla\phi)(\frac{d\vec{\Xi}}{dt} \cdot \vec{n}) + (\Xi \cdot \vec{n})(\vec{x} \times \nabla\phi_t)]ds
\end{aligned} \tag{13}
$$

In the presence of bichromatic waves, one of 4 force components is considered. Denoting the frequency components as subscripts i and j and sum and difference frequencies as superscripts $+$ and $-$, we have

$$
\begin{aligned}
4\vec{F}_{ij}^{\pm} \quad &= \quad \pm\frac{\rho}{g}\omega_i\omega_j \int_{CL} \vec{n}'\phi_i\phi_j^{\pm}dl + \rho\int_{WL} [(i\omega_i\phi_i)(\Xi_j^{\pm} \cdot \vec{n}) + (\pm i\omega_j\phi_j^{\pm})(\Xi_i \cdot \vec{n})]\hat{k}dl \\
&- \quad \rho \iint_{S_c} [\nabla\phi_i\frac{\partial\phi_j^{\pm}}{\partial n} + \nabla\phi_j^{\pm}\frac{\partial\phi_i}{\partial n} - \vec{n}(\nabla\phi_i \cdot \nabla\phi_j^{\pm})]ds \\
&- \quad \rho \iint_{S_f} (\nabla'\phi_i\phi_{zj}^{\pm} + \nabla'\phi_j^{\pm}\phi_{zi}) - \vec{n}(\nabla'\phi_i \cdot \nabla'\phi_j^{\pm} - \phi_{zi}\phi_{zj}^{\pm})ds \\
&\mp \quad \frac{\rho\omega_i\omega_j}{g}\iint_{S_f} \phi_i\nabla'\phi_j^{\pm} + \phi_j^{\pm}\nabla'\phi_i ds \\
&+ \quad \vec{F}_S^{\pm}
\end{aligned}
$$

$$
\begin{aligned}
&- \quad i\rho(\omega_i \pm \omega_j)\iint_{S_b} \nabla\phi_i(\Xi_j^{\pm}\cdot\vec{n}) + \nabla\phi_j^{\pm}(\Xi_i\cdot\vec{n})ds
\end{aligned} \tag{14}
$$

$$
\begin{aligned}
4\vec{M}_{ij}^{\pm} &= \pm\frac{\rho}{g}\omega_i\omega_j\int_{CL}(\vec{x}\times\vec{n}')\phi_i\phi_j^{\pm}dl + \rho\int_{WL}[(i\omega_i\phi_i)(\Xi_j^{\pm}\cdot\vec{n}) + (\pm i\omega_j\phi_j^{\pm})(\Xi_i\cdot\vec{n})](y\hat{i}-x\hat{j})dl \\
&- \rho\iint_{S_c}\vec{x}\times[\nabla\phi_i\frac{\partial\phi_j^{\pm}}{\partial n} + \nabla\phi_j^{\pm}\frac{\partial\phi_i}{\partial n} - \vec{n}(\nabla\phi_i\cdot\nabla\phi_j^{\pm})]ds \\
&- \rho\iint_{S_f}\vec{x}\times[(\nabla'\phi_i\phi_{z_j}^{\pm} + \nabla'\phi_j^{\pm}\phi_{z_i}) - \vec{n}(\nabla'\phi_i\cdot\nabla'\phi_j^{\pm} - \phi_{z_i}\phi_{z_j}^{\pm})]ds \\
&\mp \frac{\rho\omega_i\omega_j}{g}\iint_{S_f}\vec{x}\times(\phi_i\nabla'\phi_j^{\pm} + \phi_j^{\pm}\nabla'\phi_i)ds \\
&+ \vec{M}_S^{\pm} \\
&- i\rho(\omega_i\pm\omega_j)\iint_{S_b}\vec{x}\times[\nabla\phi_i(\Xi_j^{\pm}\cdot\vec{n}) + \nabla\phi_j^{\pm}(\Xi_i\cdot\vec{n})]ds
\end{aligned} \tag{15}
$$

The normalized forms of (14 -15) to be implemented in WAMIT are

$$
\begin{aligned}
4\vec{F}_{ij}^{\pm} &= -\int_{CL}\vec{n}'\phi_i\phi_j^{\pm}dl - \int_{WL}[\phi_i(\Xi_j^{\pm}\cdot\vec{n}) + \phi_j^{\pm}(\Xi_i\cdot\vec{n})]\hat{k}dl \\
&\pm \sqrt{\frac{1}{k_ik_j}}\iint_{S_c}[\nabla\phi_i\frac{\partial\phi_j^{\pm}}{\partial n} + \nabla\phi_j^{\pm}\frac{\partial\phi_i}{\partial n} - \vec{n}(\nabla\phi_i\cdot\nabla\phi_j^{\pm})]ds \\
&\pm \sqrt{\frac{1}{k_ik_j}}\iint_{S_f}(\nabla'\phi_i\phi_{z_j}^{\pm} + \nabla'\phi_j^{\pm}\phi_{z_i}) - \vec{n}(\nabla'\phi_i\cdot\nabla'\phi_j^{\pm} - \phi_{z_i}\phi_{z_j}^{\pm})ds \\
&+ \iint_{S_f}\phi_i\nabla'\phi_j^{\pm} + \phi_j^{\pm}\nabla'\phi_i ds \\
&+ \vec{F}_S^{\pm} \\
&+ \iint_{S_b}\frac{\Omega^{\pm}}{\omega_i}\nabla\phi_i(\Xi_j^{\pm}\cdot\vec{n}) \pm \frac{\Omega^{\pm}}{\omega_j}\nabla\phi_j^{\pm}(\Xi_i\cdot\vec{n})ds
\end{aligned} \tag{16}
$$

$$
\begin{aligned}
4\vec{M}^{\pm} &= -\int_{CL}(\vec{x}\times\vec{n}')\phi_i\phi_j^{\pm}dl - \int_{WL}[\phi_i(\Xi_j^{\pm}\cdot\vec{n}) + \phi_j^{\pm}(\Xi_i\cdot\vec{n})](y\hat{i}-x\hat{j})dl \\
&\pm \sqrt{\frac{1}{k_ik_j}}\iint_{S_c}\vec{x}\times[\nabla\phi_i\frac{\partial\phi_j^{\pm}}{\partial n} + \nabla\phi_j^{\pm}\frac{\partial\phi_i}{\partial n} - \vec{n}(\nabla\phi_i\cdot\nabla\phi_j^{\pm})]ds \\
&\pm \sqrt{\frac{1}{k_ik_j}}\iint_{S_f}\vec{x}\times[(\nabla'\phi_i\phi_{z_j}^{\pm} + \nabla'\phi_j^{\pm}\phi_{z_i}) - \vec{n}(\nabla'\phi_i\cdot\nabla'\phi_j^{\pm} - \phi_{z_i}\phi_{z_j}^{\pm})]ds \\
&+ \iint_{S_f}\vec{x}\times(\phi_i\nabla'\phi_j^{\pm} + \phi_j^{\pm}\nabla'\phi_i)ds \\
&+ \vec{M}_S^{\pm} \\
&+ \iint_{S_b}\vec{x}\times[\frac{\Omega^{\pm}}{\omega_i}\nabla\phi_i(\Xi_j^{\pm}\cdot\vec{n}) \pm \frac{\Omega^{\pm}}{\omega_j}\nabla\phi_j^{\pm}(\Xi_i\cdot\vec{n})]ds
\end{aligned} \tag{17}
$$

where k_i and k_j are normalized infinite depth wave numbers and $\Omega^{\pm} = (\omega_i \pm \omega_j)$.

3 Appendix A

Using $n' = n(1-n_z^2)^{-\frac{1}{2}}$ as two dimensional unit normal vector on Z=0, the hydrostatic terms of the waterline integral are

$$\begin{aligned} F_{WS} &= \frac{1}{2}\rho g \int_{WL} \vec{n}' \Xi_3^2 dl \\ M_{WS} &= \frac{1}{2}\rho g \int_{WL} (\vec{x} \times \vec{n}') \Xi_3^2 dl \end{aligned} \tag{18}$$

Define a vector $V = (0, 0, \Xi_3^2)$. Since $V \cdot \vec{n}' = 0$, we have

$$\begin{aligned} F_{WS} &= \frac{1}{2}\rho g \int_{WL} \vec{n}' V_3 - (V \cdot \vec{n}')\hat{k} dl = -\frac{1}{2}\rho g \int_{WL} \vec{t} \times V dl \\ M_{WS} &= \frac{1}{2}\rho g \int_{WL} \vec{x} \times [V_3 \vec{n}' - (V \cdot n)\hat{k}] dl = -\frac{1}{2}\rho g \int_{WL} \vec{x} \times (\vec{t} \times V) dl \end{aligned} \tag{19}$$

The application of Stokes theorem as shown in equations (31) and (40) over waterplane area leads to

$$F_{WS} = -\vec{\alpha} \times F_S \tag{20}$$

$$\begin{aligned} M_{WS} &= \rho g z_{wp} A_{wp} \alpha_1 (\xi_3 + \alpha_1 y_f - \alpha_2 x_f)\hat{i} \\ &+ \rho g z_{wp} A_{wp} \alpha_2 (\xi_3 + \alpha_1 y_f - \alpha_2 x_f)\hat{j} \\ &- \rho g [A_{wp} \xi_3 (\alpha_1 x_f + \alpha_2 y_f) + (\alpha_1^2 - \alpha_2^2) L_{12} + \alpha_1 \alpha_2 (L_{22} - L_{11})]\hat{k} \end{aligned} \tag{21}$$

where z_{wp} the body coordinate of the free surface and is equat to $-Z_o$. Z_o is the global vertical coordinate of the origin of the body coordinates system and is equal to XBODY(3) in WAMIT.

Adding $\vec{\xi} \times \vec{F}_S^{(1)}$, we have the quadratic hydrostatic force and moments as follows.

$$F_S^{(2)} = -\rho g A_{wp} [\alpha_1 \alpha_3 x_f + \alpha_2 \alpha_3 y_f + \frac{1}{2}(\alpha_1^2 + \alpha_2^2) Z_o]\vec{k} \tag{22}$$

$$\begin{aligned} M_S^{(2)} &= \rho g \{[-A_{wp}(\xi_3 \alpha_3 x_f + \frac{1}{2}(\alpha_1^2 + \alpha_2^2) Z_o y_f) - 2\alpha_1 \alpha_3 L_{12} + \alpha_2 \alpha_3 (L_{11} - L_{22}) \\ &+ \forall(\alpha_1 \alpha_2 x_b - \frac{1}{2}(\alpha_1^2 + \alpha_3^2) y_b)] \\ &+ [-A_{wp} \alpha_1 Z_o (\xi_3 + \alpha_1 y_f - \alpha_2 x_f) - A_{wp} \xi_2 (\xi_3 + \alpha_1 y_f - \alpha_2 x_f)]\}\vec{i} \\ &+ \rho g \{[-A_{wp}(\xi_3 \alpha_3 y_f - \frac{1}{2}(\alpha_1^2 + \alpha_2^2) Z_o x_f) + 2\alpha_2 \alpha_3 L_{12} + \alpha_1 \alpha_3 (L_{11} - L_{22}) \\ &+ \forall \frac{1}{2}(\alpha_2^2 + \alpha_3^2) x_b)] \\ &+ [-A_{wp} \alpha_2 Z_o (\xi_3 + \alpha_1 y_f - \alpha_2 x_f) + A_{wp} \xi_1 (\xi_3 + \alpha_1 y_f - \alpha_2 x_f)]\}\vec{j} \end{aligned} \tag{23}$$

4 Appendix B

We want to show two vector relations

$$\frac{1}{2}\iint_{S_C} \vec{n}(\nabla\phi\cdot\nabla\phi)ds = \iint_{S_C} \nabla\phi\frac{\partial\phi}{\partial n}ds \tag{24}$$

and

$$\frac{1}{2}\iint_{S_C} (\vec{x}\times\vec{n})(\nabla\phi\cdot\nabla\phi)ds = \iint_{S_C} (\vec{x}\times\nabla\phi)\frac{\partial\phi}{\partial n}ds \tag{25}$$

where $\iint_{S_C}$ is a surface enclosing a volume of fluid, V.

To show (24), we apply Green's theorem to $\dfrac{\partial\phi}{\partial x}$ and ϕ in V to have

$$\begin{aligned}\iint_{S_C} \vec{n}\cdot\frac{\partial\phi}{\partial x}\nabla\phi ds &= \iiint_V \frac{\partial\phi}{\partial x}\nabla^2\phi + \nabla(\frac{\partial\phi}{\partial x})\cdot\nabla\phi dv \\ &= \iiint_V \nabla(\frac{\partial\phi}{\partial x})\cdot\nabla\phi dv \\ &= \frac{1}{2}\iiint_V \frac{\partial}{\partial x}(\nabla\phi\cdot\nabla\phi)dv \end{aligned}\tag{26}$$

We have two additional relations by replacing $\dfrac{\partial\phi}{\partial x}$ with $\dfrac{\partial\phi}{\partial y}$ and $\dfrac{\partial\phi}{\partial z}$ and expressing them as a vector relation,

$$\begin{aligned}\iint_{S_C} \nabla\phi(\vec{n}\cdot\nabla\phi)ds &= \frac{1}{2}\iiint_V \nabla(\nabla\phi\cdot\nabla\phi)dv \\ &= \frac{1}{2}\iint_{S_C} \vec{n}(\nabla\phi\cdot\nabla\phi)ds \end{aligned}\tag{27}$$

Here Gauss theorem (cf. Arfken eq 1.102) is invoked to convert the volume integral into the surface integral.

Similarly for (25), we apply Greens theorem to $\vec{x}\times\nabla\phi$ and ϕ. For convenience we use a compact expression where three relations, each one of them correspoding to one of three component of $\vec{x}\times\nabla\phi$ (or $(\vec{x}\times\nabla)$) into a single vector form.

$$\begin{aligned}\iint_{S_C} (\vec{x}\times\nabla\phi)(\vec{n}\cdot\nabla\phi)ds &= \iiint_V (\vec{x}\times\nabla\phi)\nabla^2\phi + \nabla(\vec{x}\times\nabla\phi)\cdot\nabla\phi dv \\ &= \iiint_V \nabla(\vec{x}\times\nabla\phi)\cdot\nabla\phi dv \\ &= \frac{1}{2}\iiint_V (\vec{x}\times\nabla)(\nabla\phi\cdot\nabla\phi)dv \\ &= \frac{1}{2}\iiint_V [(\vec{x}\times\nabla)(\nabla\phi\cdot\nabla\phi) + (\nabla\times\vec{x})(\nabla\phi\cdot\nabla\phi)]dv \\ &= -\frac{1}{2}\iiint_V \nabla\times[(\nabla\phi\cdot\nabla\phi)\vec{x}]dv \\ &= \frac{1}{2}\iint_{S_C} (\vec{x}\times\vec{n})(\nabla\phi\cdot\nabla\phi)ds \end{aligned}\tag{28}$$

where a variant of Gauss theorem is used in the last step (cf. Arfken 1.103).

We take the surface S_C as a union of a control surface S_c in the fluid domain which surrounds the body and intersects the free surface, the body surface itself S_b and the free surface between the control and body surfaces, S_f. The latter may not necessary, if the body is completely submerged. Then from the relations (24) and (25) and the fact $d\vec{\Xi}/dt \cdot \vec{n} = \partial\phi/\partial n$ on S_b, we have

$$\frac{1}{2}\iint_{S_b} \vec{n}(\nabla\phi \cdot \nabla\phi)ds = \iint_{S_b} \nabla\phi(\frac{d\vec{\Xi}}{dt} \cdot \vec{n})ds + \iint_{S_{c+f}} [\nabla\phi\frac{\partial\phi}{\partial n} - \frac{1}{2}\vec{n}(\nabla\phi \cdot \nabla\phi)]ds \tag{29}$$

and

$$\frac{1}{2}\iint_{S_b} (\vec{x}\times\vec{n})(\nabla\phi \cdot \nabla\phi)ds = \iint_{S_b} (\vec{x}\times\nabla\phi)(\frac{d\vec{\Xi}}{dt} \cdot \vec{n})ds + \iint_{S_{c+f}} [(\vec{x}\times\nabla\phi)\frac{\partial\phi}{\partial n} - \frac{1}{2}(\vec{x}\times\vec{n})(\nabla\phi \cdot \nabla\phi)]ds \tag{30}$$

Next we transform the second terms of the integrals I and J. First we consider an integral

$$\begin{aligned}
\iint_{S_b} [\vec{n}(\vec{\Xi} \cdot \nabla\phi_t) - (\Xi \cdot \vec{n})\nabla\phi_t]ds &= \iint_{S_b} \Xi \times (\vec{n} \times \nabla\phi_t)ds \\
&= -\iint_{S_b} [(\vec{n} \times \nabla) \times \phi_t\Xi]ds + \iint_{S_b} [\phi_t(\vec{n} \times \nabla) \times \Xi]ds \\
&= -\int_{WL} (\vec{t} \times \phi_t\Xi)dl - \alpha \times \iint_{S_b} \phi_t\vec{n}ds
\end{aligned} \tag{31}$$

We invoked Stoke's theorem to have the first term on the last line and used $(\vec{n} \times \nabla) \times \Xi = \vec{n} \times \vec{\alpha}$ for the second term. Here $\vec{t} = (t_x, t_y, 0)$ is tangential vector along the waterline. When the normal vector on the body points into the body as in WAMIT, the positive $\vec{t}$ points counter-clockwise direction viewed from above. Denoting the normal vector on the waterline as $\vec{n}' = (n'_x, n'_y, 0)$, we have $t_x = n'_y$ and $t_y = -n'_x$ ($n' = n$ for wall-sided bodies only. Otherwise $(n'_x, n'_y) = (n_x, n_y)/\sqrt{n_x^2 + n_y^2}$).

$$-\int_{WL} (\vec{t} \times \phi_t\Xi)dl = \int_{WL} \phi_t[(\Xi_3\vec{n}' - (\vec{\Xi} \cdot \vec{n}')\hat{k}]dl = -g\int_{WL} \zeta[(\Xi_3\vec{n}' - (\vec{\Xi} \cdot \vec{n}')\hat{k}]dl \tag{32}$$

We now consider the second term of J integral.

$$\begin{aligned}
\iint_{S_b} [(\vec{x} \times \vec{n})(\vec{\Xi} \cdot \nabla\phi_t) - (\vec{x} \times \nabla\phi_t)(\Xi \cdot \vec{n})]ds &= \iint_{S_b} \vec{x} \times [\Xi \times (\vec{n} \times \nabla\phi_t)]ds \\
&= -\iint_{S_b} \vec{x} \times [(\vec{n} \times \nabla) \times \phi_t\Xi - \phi_t(\vec{n} \times \nabla) \times \Xi]ds
\end{aligned} \tag{33}$$

We apply the following relation to the first term of the right hand side integral of equation (33) (see Hildebrand Chapter 6 equations (74d) and (74e) and replace ∇, u and v with $\vec{x}$, $\vec{n} \times \nabla$ and $\phi_t\vec{\Xi}$),

$$\begin{aligned}
\vec{x} \times [((\vec{n} \times \nabla) \times \phi_t\vec{\Xi}) - \phi_t(\vec{n} \times \nabla) \times \Xi] &= (\vec{n} \times \nabla)(\vec{x} \cdot \phi_t\vec{\Xi}) - \phi_t\vec{\Xi} \times ((\vec{n} \times \nabla) \times \vec{x}) \\
&+ (\vec{n} \times \nabla) \times (\vec{x} \times \phi_t\vec{\Xi}) - 2(\phi_t\vec{\Xi} \cdot (\vec{n} \times \nabla))\vec{x} \\
&- \vec{x}((\vec{n} \times \nabla) \cdot \phi_t\vec{\Xi}) + \phi_t\vec{\Xi}((\vec{n} \times \nabla) \cdot \vec{x}) \\
&- \vec{x} \times [\phi_t(\vec{n} \times \nabla) \times \Xi]
\end{aligned} \tag{34}$$

In equation (34), we find

$$-\phi_t\vec{\Xi}\times((\vec{n}\times\nabla)\times\vec{x}) = 2\phi_t\vec{\Xi}\times\vec{n} \tag{35}$$

and

$$-2(\phi_t\vec{\Xi}\cdot(\vec{n}\times\nabla))\vec{x} = -2\phi_t\vec{\Xi}\times\vec{n} \tag{36}$$

cancel each other. Also we find

$$\phi_t\vec{\Xi}(\vec{n}\times\nabla)\cdot\vec{x}) = 0 \tag{37}$$

and

$$\begin{aligned}
-\vec{x}((\vec{n}\times\nabla)\cdot\phi_t\vec{\Xi}) &= -(\vec{n}\times\nabla)\cdot\vec{x}\phi_t\vec{\Xi} + [(\vec{n}\times\nabla)\vec{x}]\cdot\phi_t\vec{\Xi} \\
&= -(\vec{n}\times\nabla)\cdot\vec{x}\phi_t\vec{\Xi} + \phi_t\vec{\Xi}\times\vec{n}
\end{aligned} \tag{38}$$

In the last equation a single vector relation in place of 3 separate ones for each components of $\vec{x}$ is used.

Combining the last terms in the equations (34) and (38)

$$\begin{aligned}
\phi_t\vec{\Xi}\times\vec{n} - \vec{x}\times[\phi_t(\vec{n}\times\nabla)\times\vec{\Xi}] &= \phi_t(\vec{\xi}\times\vec{n}) + \phi_t[(\vec{\alpha}\times\vec{x})\times\vec{n} - \vec{x}\times(\vec{n}\times\vec{\alpha})] \\
&= \phi_t(\vec{\xi}\times\vec{n}) + \phi_t[\vec{\alpha}\times(\vec{x}\times\vec{n})]
\end{aligned} \tag{39}$$

Using relations (35-39), (34) can be written

$$\begin{aligned}
\iint_{S_b} & [(\vec{x}\times\vec{n})(\vec{\Xi}\cdot\nabla\phi_t) - (\Xi\cdot\vec{n})(\vec{x}\times\nabla\phi_t)]ds \\
= & -\iint_{S_b}(\vec{n}\times\nabla)(\vec{x}\cdot\phi_t\vec{\Xi})ds - \iint_{S_b}(\vec{n}\times\nabla)\times(\vec{x}\times\phi_t\vec{\Xi})ds + \iint_{S_b}(\vec{n}\times\nabla)\cdot\vec{x}\phi_t\vec{\Xi}ds \\
& - \vec{\xi}\times\iint_{S_b}\phi_t ds - \vec{\alpha}\times\iint_{S_b}(\vec{x}\times\vec{n})\phi_t ds \\
= & -\int_{WL}(\vec{x}\cdot\phi_t\vec{\Xi})\vec{t}dl - \int_{WL}\vec{t}\times(\vec{x}\times\phi_t\vec{\Xi})dl + \int_{WL}\vec{x}(\phi_t\vec{\Xi}\cdot\vec{t})dl \\
& - \vec{\xi}\times\iint_{S_b}\phi_t ds - \vec{\alpha}\times\iint_{S_b}(\vec{x}\times\vec{n})\phi_t ds \\
= & -\int_{WL}\vec{x}\times(\vec{t}\times\phi_t\vec{\Xi})dl - \vec{\xi}\times\iint_{S_b}\phi_t ds - \vec{\alpha}\times\iint_{S_b}(\vec{x}\times\vec{n})\phi_t ds \\
= & -g\int_{WL}\zeta\vec{x}\times[\Xi_3\vec{n}' - (\vec{\Xi}\cdot\vec{n}')\hat{k}]dl - \vec{\xi}\times\iint_{S_b}\phi_t ds - \vec{\alpha}\times\iint_{S_b}(\vec{x}\times\vec{n})\phi_t ds
\end{aligned} \tag{40}$$

The first three surface integrals on the right-hand side are converted to line interals by making use of variants of Stoke's theorem (cf Arfken 1.109,1.110, 1.111).

$$\begin{aligned}
\iint_{S_b}\frac{1}{2}\vec{n}(\nabla\phi\cdot\nabla\phi) + \vec{n}(\vec{\Xi}\cdot\nabla\phi_t)ds &= \iint_{S_b}[\nabla\phi(\frac{d\vec{\Xi}}{dt}\cdot\vec{n}) + (\Xi\cdot\vec{n})\nabla\phi_t]ds \\
&+ \iint_{S_{c+f}}[\nabla\phi\frac{\partial\phi}{\partial n} - \frac{1}{2}\vec{n}(\nabla\phi\cdot\nabla\phi)]ds \\
&- g\int_{WL}\zeta[(\Xi_3\vec{n}' - (\vec{\Xi}\cdot\vec{n}')\hat{k}]dl - \alpha\times\iint_{S_b}\phi_t\vec{n}ds
\end{aligned} \tag{41}$$

and thus

$$\begin{aligned}
\iint_{S_b}[\frac{1}{2}(\vec{x}\times\vec{n})(\nabla\phi\cdot\nabla\phi)+(\vec{x}\times\vec{n})(\vec{\Xi}\cdot\nabla\phi_t)]ds &= \iint_{S_b}[(\vec{x}\times\nabla\phi)(\frac{d\vec{\Xi}}{dt}\cdot\vec{n})+(\Xi\cdot\vec{n})(\vec{x}\times\nabla\phi_t)]ds \\
&+ \iint_{S_{c+f}}[(\vec{x}\times\nabla\phi)\frac{\partial\phi}{\partial n}-\frac{1}{2}(\vec{x}\times\vec{n})(\nabla\phi\cdot\nabla\phi)]ds \\
&- g\int_{WL}\zeta\vec{x}\times[\Xi_3\vec{n}'-(\vec{\Xi}\cdot\vec{n}')\hat{k}]dl \\
&- \vec{\xi}\times\iint_{S_b}\phi_t ds-\vec{\alpha}\times\iint_{S_b}(\vec{x}\times\vec{n})\phi_t ds \qquad (42)
\end{aligned}$$

5 Appendix C

The first terms of equations (10) and (11)

$$\begin{aligned}
F_W &= \frac{1}{2}\rho g\int_{WL}\vec{n}'\zeta^2 dl \\
M_W &= \frac{1}{2}\rho g\int_{WL}(\vec{x}\times\vec{n}')\zeta^2 dl \qquad (43)
\end{aligned}$$

can be transfered to the integrals over free surface and the intersection of the free surface and control surface as shown below. We denote the force on the intersection of the control surfaces as

$$\begin{aligned}
F_C &= \frac{1}{2}\rho g\int_{CL}\vec{n}'\zeta^2 dl=\frac{1}{2}\frac{\rho}{g}\int_{CL}\vec{n}'\phi_t^2 dl \\
M_C &= \frac{1}{2}\rho g\int_{CL}(\vec{x}\times\vec{n}')\zeta^2 dl=\frac{1}{2}\frac{\rho}{g}\int_{CL}(\vec{x}\times\vec{n}')\phi_t^2 dl \qquad (44)
\end{aligned}$$

Define a vector $V=(0,0,\zeta_3^2)$. Since $V\cdot\vec{n}'=0$, we have

$$\begin{aligned}
F_{W+C} &= \frac{1}{2}\rho g\int_{WL+CL}\vec{n}'V_3-(V\cdot\vec{n}')\hat{k}dl=-\frac{1}{2}\rho g\int_{WL+CL}\vec{t}\times V dl \\
M_{W+C} &= \frac{1}{2}\rho g\int_{WL+CL}\vec{x}\times[V_3\vec{n}'-(V\cdot n)\hat{k}]dl=-\frac{1}{2}\rho g\int_{WL+CL}\vec{x}\times(\vec{t}\times V)dl \qquad (45)
\end{aligned}$$

Again Stoke's theorem is applied as in equations (31) and (40). Here, however, in order to let the free surface be on the left side of the trace following $\vec{t}$, the normal vector on the free surface should be pointing downward and thus

$$\begin{aligned}
F_W &= -F_C+\frac{1}{2}\rho g\iint_{Sf}(\hat{k}\times\nabla)\times(\zeta^2\hat{k})ds=-F_C+\rho g\iint_{Sf}\zeta\nabla'\zeta ds \\
&= -F_C+\frac{\rho}{g}\iint_{Sf}\phi_t\nabla'\phi_t ds \qquad (46)
\end{aligned}$$

$$\begin{aligned}
M_W &= -M_C+\frac{1}{2}\rho g\iint_{Sf}(\hat{k}\times\nabla)(\vec{x}\cdot(\zeta^2\hat{k}))ds+\frac{1}{2}\rho g\iint_{Sf}(\hat{k}\times\nabla)\times(\vec{x}\times(\zeta^2\hat{k}))ds \\
&= -M_C+\rho g\iint_{Sf}\zeta(\vec{x}\times\nabla'\zeta)ds=-M_C+\frac{\rho}{g}\iint_{Sf}\phi_t(\vec{x}\times\nabla'\phi_t)ds \qquad (47)
\end{aligned}$$

Summing linear and 2nd-order wave elevations using FS_ELV

C-H Lee

October 7, 2005

Assuming a discrete spectrum, the linear incident wave elevation in the time domain, $\boldsymbol{\zeta}_I^1$ (note that it is in boldface), can be expressed as a sum of frequency domain components ζ_I^1 as follows.

$$
\begin{aligned}
\boldsymbol{\zeta}_I^1(\mathbf{x},t) &= Real[\sum_i^{N_P}\sum_k^{N_B}\zeta_I^1(\omega_i,\beta_k)] \\
&= Real[\sum_i^{N_P}\sum_k^{N_B}A(\omega_i,\beta_k)\bar{\zeta}_I^1(\omega_i,\beta_k)] \\
&= Real[\sum_i^{N_P}\sum_k^{N_B}A(\omega_i,\beta_k)e^{i(\omega_i t-\mathbf{K}_k\cdot\mathbf{x})}] \qquad (1)
\end{aligned}
$$

Here N_P is the number of frequencies (or periods) and N_B is the number of wave headings. ω_i denotes wave frequency. $\mathbf{K}_k = (\kappa\cos\beta_k, \kappa\sin\beta_k)$ denotes wave-number vector where β_k is the wave heading angle (the direction of the wave with respect to the positive x-axis). κ(kappa) is the finite depth wave number (this should be distinguished from the subscript k to β which is wave heading index), satisfying the dispersion relation (equation (2.4), WAMIT Theory Manual). $\mathbf{x} = (x,y,0)$ is the coordinates of the field point on the free surface. $\bar{\zeta}_I^1(\omega_i,\beta_k)$ represents the unit amplitude sinusoidal wave and $A(\omega_i,\beta_k)$ is the amplitude of that wave.

In the presence of the bodies, the total linear wave elevation includes the component due to scattering wave field in addition to the incident wave (1). Let the total linear wave elevation in the time domain be denoted by $\boldsymbol{\zeta}^1$ and those due to second-order wave fields at sum- and difference-frequency by $\boldsymbol{\zeta}^+$ and $\boldsymbol{\zeta}^-$, respectively. The total wave elevation, up to the second-order, is a sum of these components in the following form.

$$
\begin{aligned}
\boldsymbol{\zeta}(\mathbf{x},t) &= \boldsymbol{\zeta}^1(\mathbf{x},t)+\boldsymbol{\zeta}^+(\mathbf{x},t)+\boldsymbol{\zeta}^-(\mathbf{x},t) \\
&= Real[\sum_{i=1}^{N_P}\sum_{k=1}^{N_B}\zeta^1(\mathbf{x},\omega_i,\beta_k)e^{i\omega_i t} \\
&+ \sum_{i=1}^{N_P}\sum_{j=1}^{N_P}\sum_{k=1}^{N_B}\sum_{l=1}^{N_B}\zeta^+(\mathbf{x},\omega_i,\omega_j,\beta_k,\beta_l)e^{i(\omega_i+\omega_j)t} \\
&+ \sum_{i=1}^{N_P}\sum_{j=1}^{N_P}\sum_{k=1}^{N_B}\sum_{l=1}^{N_B}\zeta^-(\mathbf{x},\omega_i,\omega_j,\beta_k,\beta_l)e^{i(\omega_i-\omega_j)t}] \qquad (2)
\end{aligned}
$$

$\zeta^1(\mathbf{x},\omega_i,\beta_k)$ represents the linear wave elevation in the frequency domain, in the presence of an incident wave of frequency ω_i, wave heading β_k and amplitude $A(\omega_i,\beta_k)$. $\zeta^\pm(\mathbf{x},\omega_i,\omega_j,\beta_k,\beta_l)$ represent the sum and difference frequency wave elevation in the frequency domian in the presence of two linear incident waves: one with frequency ω_i, wave heading β_k and amplitude $A(\omega_i, \beta_k)$ and the other with frequency ω_j, wave heading β_l and amplitude $A(\omega_j, \beta_l)$.

The wave elevations, ζ_1, ζ^+ and ζ^- are related to the corresponding WAMIT's normalized wave elevations, $\bar{\zeta}_1$, $\bar{\zeta}^+$ and $\bar{\zeta}^-$, as follows.

$$
\begin{aligned}
&\zeta^1(\mathbf{x}, \omega_i, \beta_k) = A(\omega_i, \beta_k)\bar{\zeta}^1(\mathbf{x}, \omega_i, \beta_k) \\
&\zeta^+(\mathbf{x}, \omega_i, \omega_j, \beta_k, \beta_l) = (A(\omega_i, \beta_k)A(\omega_j, \beta_l)/L)\bar{\zeta}^+(\mathbf{x}, \omega_i, \omega_j, \beta_k, \beta_l) \\
&\zeta^-(\mathbf{x}, \omega_i, \omega_j, \beta_k, \beta_l) = (A(\omega_i, \beta_k)A^*(\omega_j, \beta_l)/L)\bar{\zeta}^-(\mathbf{x}, \omega_i, \omega_j, \beta_k, \beta_l)
\end{aligned} \tag{3}
$$

L is the character length specified and is the same as ULEN in GDF file. A^* denotes the complex conjugate of A.

$\bar{\zeta}^{\pm}$, on the right-hand side of of (3), have the following symmetry property with respect to two wave frequencies (see equation (3.7), WAMIT Theory Manual).

$$
\begin{aligned}
\bar{\zeta}^+(\mathbf{x}, \omega_i, \omega_j, \beta_k, \beta_l) &= \bar{\zeta}^+(\mathbf{x}, \omega_j, \omega_i, \beta_k, \beta_l) \\
&\text{and} \\
\bar{\zeta}^-(\mathbf{x}, \omega_i, \omega_j, \beta_k, \beta_l) &= \bar{\zeta}^{-*}(\mathbf{x}, \omega_j, \omega_i, \beta_k, \beta_l)
\end{aligned} \tag{4}
$$

Using the symmetry relation, a half of the off-diagonal terms can be removed in double summation over frequency index in (2). Also using the normalization convention in (ref eq:normal), $\boldsymbol{\zeta}$can be evaluated from the following expression.

$$
\begin{aligned}
\boldsymbol{\zeta}(\mathbf{x}, t) \;=\;& Real[\sum_{i=1}^{N_P}\sum_{k=1}^{N_B} A(\omega_i, \beta_k)\bar{\zeta}^1(\mathbf{x}, \omega_i, \beta_k)e^{i\omega_i t} \\
+\;& \sum_{i=1}^{N_P}\sum_{k=1}^{N_B}\sum_{l=1}^{N_B}(A^2(\omega_i, \beta_k)/L)\bar{\zeta}^+(\mathbf{x}, \omega_i, \omega_i, \beta_k, \beta_l)e^{i(\omega_i+\omega_j)t} \\
+\;& 2\sum_{i=1}^{N_P}\sum_{j=1}^{i-1}\sum_{k=1}^{N_B}\sum_{l=1}^{N_B}(A(\omega_i, \beta_k)A(\omega_j, \beta_l)/L)\bar{\zeta}^+(\mathbf{x}, \omega_i, \omega_j, \beta_k, \beta_l)e^{i(\omega_i+\omega_j)t} \\
+\;& \sum_{i=1}^{N_P}\sum_{k=1}^{N_B}\sum_{l=1}^{N_B}(|A(\omega_i, \beta_k)|^2/L)\bar{\zeta}^-(\mathbf{x}, \omega_i, \omega_i, \beta_k, \beta_l) \\
+\;& 2\sum_{i=1}^{N_P}\sum_{j=1}^{i-1}\sum_{k=1}^{N_B}\sum_{l=1}^{N_B}(A(\omega_i, \beta_k)A^*(\omega_j, \beta_l)/L)\bar{\zeta}^-(\mathbf{x}, \omega_i, \omega_j, \beta_k, \beta_l)e^{i(\omega_i-\omega_j)t}]
\end{aligned} \tag{5}
$$

It is assumed that $\omega_i - \omega_j \geq 0$ without loss of generality in the above equation.

In general, $A(\omega_i, \beta_k)$ is complex quantity and it is convenient to specify it in the form of $|A_{i,k}|e^{iP_{i,k}}$ where $|A_{i,k}|$ is the modulus and $P_{i,k}$ is the phase angle. As an example, if the incident wave component has its crest at $\mathbf{x} = 0$ when $t = 0$, $P_{i,k} = 0$.

FS_ELV

The program FS_ELV computes the wave elevation in the time domain based on the equation 5. The normalized linear wave elevations (ie. due to unit amplitude of the incident waves) $\bar{\zeta}^1$ is read from numeric output *frc*.6 files and normalized second-order wave elevation $\bar{\zeta}^{\pm}$ is read from *frc*.15s and *frc*.15d.

In addition to these files, *frc*.fpt file should be available as an input to FS_ELV. *frc*.fpt is a standard WAMIT output file and contains the coordinates of the field points. (*Note 1: .6 contains normalized linear hydrodynamic pressure for all field points specified in .fpt (and .frc) file. The normalized linear pressure has the same numerical value as the normalized linear wave elevation when the points are on the free surface (ie z=0 in global coordinates system). On the other hand, .15s and .15d contain the 2nd-order wave elevation only for the field points on the free surface only. The linear wave elevations are read only for the free surface points*)

An additional input file with an extension '**.FEI**' must be prepared. If the filename of .FEI file is the same as that of WAMIT output file, i.e. *frc*.FEI, FS_ELV reads the input parameters from this file. Otherwise FS_ELV prompts to enter a filename without the extension .FEI.

FS_ELV outputs wave elevations over specified time instances at specified free surface point(s). The incident wave amplitudes for NP times NB components are also specified in .FEI. The default output filename of FS_ELV is same as .FEI file. The extension of the output file is '**.FEO**' The parameters in .FEI and the output in .FEO are explained next. (Program writes data in .FEO file in Techplot output format to a file _FEO.DAT. The only difference from .FEO is the lines for IF(i). This is written as ZONE T="IF(i)", to group the elevation for each field point into a ZONE.)

Input parameters in .FEI:

NUMHDR
ULEN
NT
T1, DT
NF
IF(1),IF(2),...,IF(NF) (do not specify when NF ¡ 0)
NP
IP(1),IP(2),...,IP(NP) (do not specify when NF ¡ 0)
NB
IB(1),IB(2),...,IB(NB) (do not specify when NF ¡ 0)
ABSA(1,1),ABSA(2,1),...,ABSA(NB,1)
ABSA(2,1),...
...
ABSA(1,NP),ABSA(2,NP),...,ABSA(NB,NP)
PHSA(1,1),PHSA(2,1),...,PHSA(NB,1)
PHSA(2,1),...
...
PHSA(1,NP),PHSA(2,NP),...,PHSA(NB,NP)
NUNHDR can be 0 or 1 and it should have the same value as that specified .cfg file. If NUMHDR=1, WAMIT output files .fpt, .6, .15s and .15d have a header line.

ULEN characteristic length. It should have the same value as that specified .gdf file.

NT is number of time steps.

T1 is initial time.

DT is time inverval between time steps.

NF is the number of field points for which the wave elevations are output. NF should be less or equal to the total number of field points on the free surface.

If NF $\leq$ 0, IF array below should not be specified. The program outputs free surface elevation at all points on the free surface among the field points specified in .fpt file.

IF is an integer array for the indices of free surface points. IF $\leq$ NFIELD. The latter is specified in FRC file. IF **should not** be specified, if NF $\leq$ 0.

NP is number of periods to be included in the summation. NP $\leq$ NPER. The latter is specified in POT file.

If NP $\leq$ 0, IP array below should not be specified. The program includes all wave periods in .6 file for the evaluation of the free surface elevation.

IP is an integer array of dimension NP. It contains period indices. This **should not** be specified if NP $\leq$ 0.

NB is number of headings to be included in the summation. NB $\leq$ NBETA. The latter is specified in POT file.

If NB $\leq$ 0, IB array below should not be specified. The program includes all wave headings in .6 file for the evaluation of the free surface elevation.

IB is an integer array of dimension NB. It contains heading indices. This **should not** be specified if NB $\leq$ 0.

ABSA is a real matrix of dimension NP×NB. It contains the modulus of the incident wave amplitude.

PHSA is a real matrix of dimension NP×NB. It contains the phase angle, in degrees, of the incident wave amplitude. **Output quantities in .FEO:**

IF(1)					
T1	ELV(T1)	ELV1(T1)	ELVS(T1)	ELVD(T1)	
T2	ELV(T2)	ELV1(T2)	ELVS(T2)	ELVD(T2)	
.					
.					
Ti	ELV(Ti)	ELV1(Ti)	ELVS(Ti)	ELVD(Ti)	**IF** field point index.
.					
.					
TN	ELV(TN)	ELV1(TN)	ELVS(TN)	ELVD(TN)	
IF(2)					
.					
.					

TN Time. TN=T1+(N-1)·DT

ELV Total wave elevation. ELV1, ELVS and ELVD are linear, sum and difference frequency component of the wave elevation.

Note2: NFIELD, NPER and NBETA are estimated from .fpt and .6 files. FS_ELV reads .fpt and *finds total number of field points. It also finds the number of field points on the free surface and their sequential index among all field points. It then reads .6 and finds NPER and NBETA. It reads in linear pressure corresponding to selected points, periods, headings (specified by* IF, IP *and* IB *in .FEI file).*